Investigation of Dynamical Brain Networks

A closer look at brain flexibility and its applications

vorgelegt von
M. Sc.
Narges Chinichian
ORCID: 0000-0001-8444-4802

an der Fakultät II – Mathematik und Naturwissenschaften
der Technischen Universität Berlin
zur Erlangung des akademischen Grades

Doktorin der Naturwissenschaften
- Dr. rer. nat. -
genehmigte Dissertation
Promotionsausschuss:
Vorsitzender: Prof. Michael Lehmann (Chair of Committee)
Gutachter: Prof. Eckehard Schöll
Gutachter: Prof. Alessandro Treves
Tag der wissenschaftlichen Aussprache: 27. Oktober 2022
Berlin 2022

Technische Universität Berlin

Investigation of Dynamical Brain Networks

A closer look at brain flexibility and its applications

Narges Chinichian
ORCID: 0000-0001-8444-4802

Technical University of Berlin (Technische Universität Berlin)
Faculty II - Mathematics and Natural Sciences (Mathematik und Naturwissenschaften)
Institute for Theoretical Physics (Institut für Theoretische Physik)
Thesis for the degree **Doctor rerum naturalium**

Submission Date: 23.08.2022
Approved on: 27.10.2022
Assessment Committee (Promotionausschuss)
Prof. Michael Lehmann (Chair of Committee)
Prof. Eckehard Schöll
Prof. Alessandro Treves
Date of defense: 27.10.2022; Room MA 415| 13:30
Berlin 2022

Technische Universität Berlin

TUB
Technische Universität Berlin
Technical University of Berlin

Thesis for the Degree of Dr. rer. nat.
Faculty II - Mathematics and Natural Sciences
Institute for Theoretical Physics

Supervisors
Prof. Eckehard Schöll
Prof. Tilo Schwalger
Prof. Henrik Walter

Investigation of Dynamical Brain Networks

Doctoral thesis at TUB

Dedicated to,
The kind friend who slept on the sofa behind my working desk to motivate me continue writing these lines for countless nights.

And to,
My parents
For their planting of love for science in my young brain.

The fifth planet was very strange. It was the smallest of all. There was just enough room on it for a street lamp and a lamplighter. The little prince was not able to reach any explanation of the use of a street lamp and a lamplighter, somewhere in the heavens, on a planet, which had no people, and not one house. But he said to himself, nevertheless:

"It may well be that this man is absurd. But he is not so absurd as the king, the conceited man, the businessman, and the tippler. For at least his work has some meaning. When he lights his street lamp, it is as if he brought one more star to life, or one flower. When he puts out his lamp, he sends the flower, or the star, to sleep. That is a beautiful occupation. And since it is beautiful, it is truly useful."

When he arrived on the planet he respectfully saluted the lamplighter. "Good morning. Why have you just put out your lamp?"

"Those are the orders," replied the lamplighter. "Good morning."

"What are the orders?"

"The orders are that I put out my lamp. Good evening." And he lighted his lamp again.

"But why have you just lighted it again?"

"Those are the orders," replied the lamplighter.

"I do not understand," said the little prince.

"There is nothing to understand," said the lamplighter. "Orders are orders. Good morning." And he put out his lamp. Then he mopped his forehead with a handkerchief decorated with red squares.

"I follow a terrible profession. In the old days it was reasonable. I put the lamp out in the morning, and in the evening I lighted it again. I had the rest of the day for relaxation and the rest of the night for sleep."

"And the orders have been changed since that time?"

"The orders have not been changed," said the lamplighter. "That is the tragedy! From year to year the planet has turned more rapidly and the orders have not been changed!"

"Then what?" asked the little prince.

"Then the planet now makes a complete turn every minute, and I no longer have a single second for repose. Once every minute I have to light my lamp and put it out!"

"That is very funny! A day lasts only one minute, here where you live!"

"It is not funny at all!" said the lamplighter. "While we have been talking together a month has gone by."

"A month?"

"Yes, a month. Thirty minutes. Thirty days. Good evening." And he lighted his lamp again. As the little prince watched him, he felt that he loved this

lamplighter who was so faithful to his orders. He remembered the sunsets, which he himself had gone to seek, in other days, merely by pulling up his chair; and he wanted to help his friend.

"You know," he said, "I can tell you a way you can rest whenever you want to..."

"I always want to rest," said the lamplighter. For it is possible for a man to be faithful and lazy at the same time. The little prince went on with his explanation:

"Your planet is so small that three strides will take you all the way around it. To be always in the sunshine, you need only walk along rather slowly. When you want to rest, you will walk and the day will last as long as you like."

"That doesn't do me much good," said the lamplighter. "The one thing I love in life is to sleep."

"Then you're unlucky," said the little prince.

"I am unlucky," said the lamplighter. "Good morning." And he put out his lamp.

"That man," said the little prince to himself, as he continued farther on his journey, "that man would be scorned by all the others: by the king, by the conceited man, by the tippler, by the businessman. Nevertheless he is the only one of them all who does not seem to me ridiculous. Perhaps that is because he is thinking of something else besides himself."

He breathed a sigh of regret, and said to himself, again: "That man is the only one of them all whom I could have made my friend. But his planet is indeed too small. There is no room on it for two people..." What the little prince did not dare confess was that he was sorry most of all to leave this planet, because it was blest every day with 1440 sunsets!

- Antoine de Saint-Exupéry

در ساحت حضور نسیم و
نماز نور،
در ساحت وقوف به زیبایی حیات،
در آفتاب از پس باران، کنار راه،
مرد ایستاده است.
مرد ایستاده است و
نمی خواهد،
در رهگذار خویش،
برهم زند،
آرامش موقر سنجاب را،
که،
با خوشه ی اقاقی یا ساقه ی علف،
دم لرزه میکند.
می دانم،
آه!
هرگز،
باور نمی کند کسی از من،
کین مرد،
تا چند روز پیش چه می کرد،
در شرق دوردست.
در آفتاب از پس باران،
کنار راه،
مرد ایستاده است.

«شفیعی کدکنی»

Acknowledgements

I thank my parents, Parvin and Amir, for their constant help and support through my life. For providing me with all the encouragements I needed to build up my current state step by step. My partner, Maximilian Palm, was the person who made me feel home in Germany and helped me through days and nights of thesis work. He slept on the sofa behind my working desk in the living room countless nights to motivate me to continue writing after midnights. Katharina, for her amazing company and the great Sunday cake meetings with Anna, Noah and Gabriela which gave me some anchor in the stressful times. Martin, for caring so deeply about us and for being the always dependable father for Max.

My brother, Mahdi, the best childhood enemy and adulthood friend one can wish for. His wife, Narges, the encouraging kind sister-in-law and the soon-to-be 3 sweet kids (Meysam, Sobhan and X) who made me experience the unexpected world of childhood again.

I would like to thank my supervisors for their time, energy and patience. Eckehard, for if it was not for his fatherly kind supports, I would have not passed the pandemic time continuing my research projects. He spent many hours guiding me through the first steps of becoming a good researcher and taught me countless valuable lessons with his to-the-point but always encouraging feedback. I recall attending a graduation ceremony at the TU Physics department in 2019, while we were discussing the possibility of a supervisor-student relationship. I could see Eckehard's pride in his clapping and happy expression as the presenters read the names of Eckehard's students to receive their certificates. This memory stuck with me, and I personally felt the depth of that care and supportive nice feelings throughout my PhD studies. Henrik, for his invaluable feedbacks to my research. Tilo, for his clear advises and honest criticisms and his extended spending of time and energy every time I needed to discuss something in details. I thank Serhiy, for his always calming yet active participation in the projects and for his amazing insights in our meetings for the simulation project. For being patient and help me learn more.

I thank Rico and Micha, for they spent hours discussing the outputs in the

meetings and helped me forge the path, they helped me learn new topics and extend my horizons during the PhD. Their presence was a hopeful light in my social life as an expat.

I thank Ilya Veer, for his always in-time, always helpful feedback. For the time he spent showing me how to network in a conference and for his valuing of my efforts.

My masters supervisors, Dr. Hosseini and Dr. Jafari, they still supported me through my PhD with their kind inputs and great company.

I thank my bachelor university friends in Yooogi group. They were always with me when I needed them. Some of them even travelled to Berlin frequently and gifted me some delightful moments of kinship.

My climbing meetup members, they made the best social weekend crew I could wish for. If it was not for the regular climbing and belayings with them, I was having a way unhealthier PhD life.

I thank the members of my Charite group, Sabine, Lea, Pablo, Sarah, Anna, Wladimir, Antje, Susanne, Johann and Tris.

BCCN Berlin organizers, Lisa and Margret, they helped me with countless bureaucratic procedures and made me feel a member of BCCN family. I asked for their helps in many cases and was never disappointed.

The CJS center at TU Berlin for their support with the 6 months of scholarship at the final phase and their nice workshops and meetings. They provided me with the opportunity to connect with other PhD students at the same stage with whom I still kept the connection. Leila and Najmeh, my scholarship sisters whom I found through this grant.

I thank Eckehard's group members, Anna, Max, Jan, Fenja, Jakub and the others. The short time before pandemic when we could meet for the weekly meetings were really enjoyable. Tilo's group at the Math department were always fun to hang out with, Basti, Veronika, Melissa and Alex. Abbas, my friend who sent some occasional messages and made me laugh laud at some Isfahanian jokes. Another special thanks to Ronan, Lea, Micha, Quentin and Max who proofread my thesis in the final days before its submission.

I am sure that this list can be way longer and it's only my imperfect memory stopping me from writing more. I thank everyone who helped me concentrate on my research and learn the most valuable lessons one can learn during the initial years of research in academia.

Contents

Chapter 1: INTRODUCTION

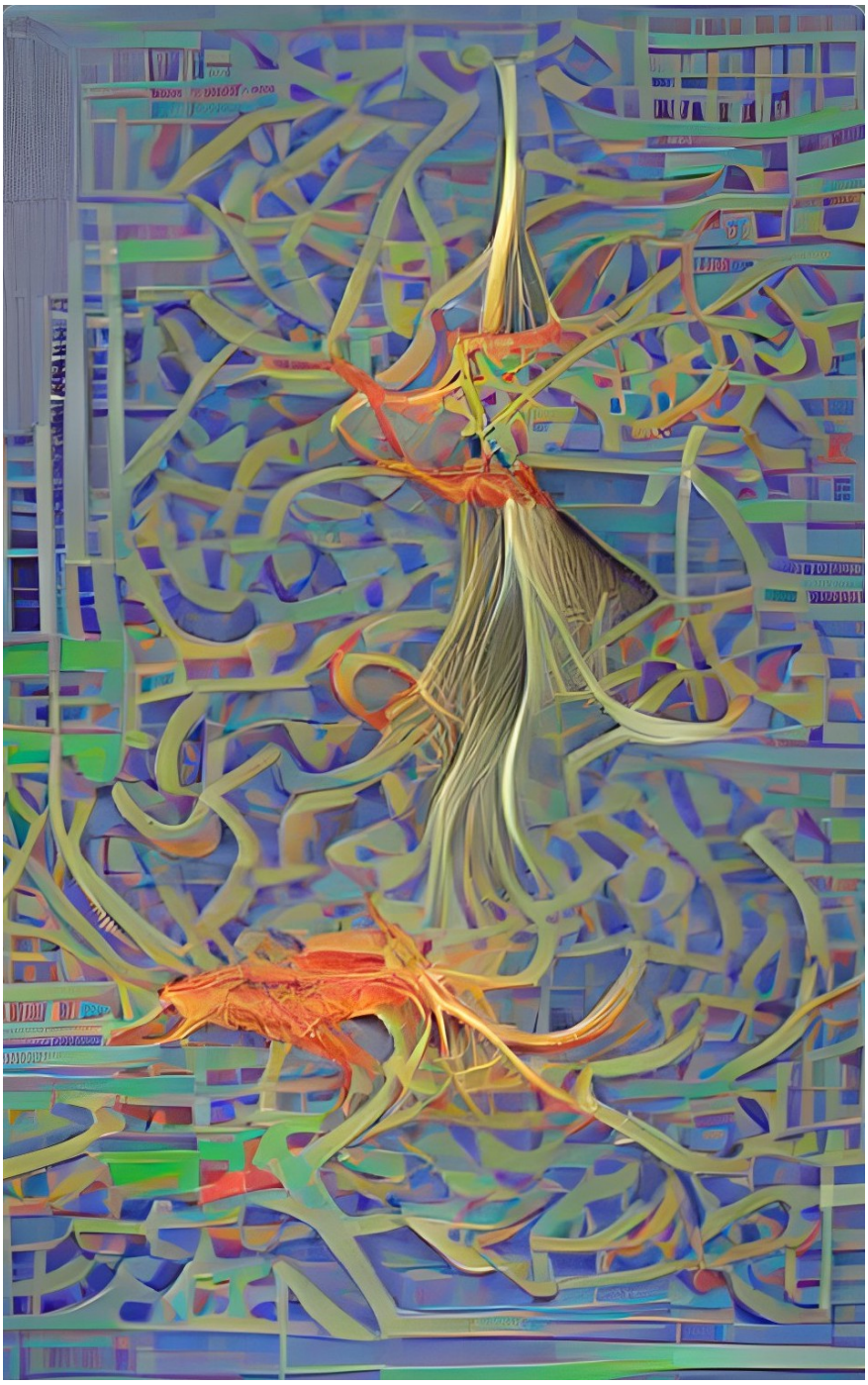

AI powered painting created by Wombo art [tea] using chapter 1 keywords.

Chapter 1

Introduction

"If our brains were simple enough for us to understand them, we'd be so simple that we couldn't."

- Ian Stewart

The mystery of the human brain and the control center of emotions and thoughts in people have occupied many great minds from ancient times to this very day.
As early as 3000 B.C., ancient Egyptians knew the relationship between the symptoms of patients with brain injury and the site of their injury.
Greek philosopher Alcmaeon (5th. century B.C) is believed to be the first to regard the brain as the seat of mind while distinguishing between understanding and perception. He discovered that the sensory organs reach the brain through channels (poroi) and performed actual experiments on animal brains [Ade+87; Huf03].

Through the advancement of science, humans learnt much more about the brain and its role as a processing unit. Meanwhile, the question of whether localized or non-localized (distributed) contributions of brain regions result in functions remains an interesting and partially obscure one.

Are the functions expected from the brain processed locally at a specific location that is highly specialized for that function or are they processed in a distributed fashion using the capacity of many distant regions?
Putting aside the two extreme answers of "highly localized" or "highly distributed" [OHK08; MBK09; Kan10; Sch+17], the popular view among modern neuroscientists lies somewhere in between [Bor+10; Coc+22]. There are spatial

regions (differing in scale from single neurons to whole regions and areas) that are responsible for very specific tasks. For example, the visual response to bodies, places or faces [KMC97; Dow+01; KY06; TWD07; PC09; Iid14; Wei+18] all support the localizationists theory. From 1950, localization was supported by observations of lesions and their consequences, for example a lesion in inferotemporal cortex area 21 (affecting the visual discrimination learning) or premotor cortex area 6 (visuomotor associative learning) [MUM83; Pas85; HP85].
There is however, a logical limitation when we infer the local functions from the lesions; even if the region is only a part of a group or chain that is needed to perform a certain cognitive task, its malfunction or loss will result in a measurable impairment and therefore these studies do not effectively reject the distributed performance of functions concept.

With the development of new techniques which allow scientists to measure the brain activity in vivo non-invasively, the importance of distributed process and connections and connectivity patterns between brain regions strengthened. In 2002, Passingham et al [PSK02] proposed the concept of a "connectivity fingerprint" for brain regions. They claimed that the function of each region is determined by its collection of connections to the other brain regions [PSK02; MPJ18].

In parallel, the interdisciplinary field of "Complex Networks" [New10] emerged and thrived in the late 1990s. It has its roots in the traditional study of graphs (first named so by Sylvester [Syl78]) in mathematics since at least 1736, when Euler used it to solve the Seven Bridges of Königsberg problem [Eul41]. See Table 1.1 for an overview of groundbreaking works in network science.

In addition to the existing list[1] in Table 1.1, the author would like to highlight a number of other works which might be of interest [2]:

- the 2007 work of Palla, Barabasi, and Vicsek which focuses on time dependence of overlapping communities characterizing community evolution [PBV07]. - the 2009 study by Opsahl and Panzarasa on clustering in weighted networks that proposes a generalization of clustering coefficient which preserves the information from the weights of network links [OP09]. - The 2010 paper by Mucha et al on the generalization of community detection trend in time-dependent (multiscale and multiplex) networks [Muc+10] and the paper (also published in 2010) by Olaf Sporns on networks of the brain [Spo10]. - The

[1] Following the discussions with Morteza Eftekhar and Abbas Rizi and with some kind input from Stefano Bocalleti

[2] The list contains only a few studies that the author subjectively found interesting to mention. It is by no means close to a complete network science studies list of all highly cited or well-known works.

review of multiplex and multilayer networks studies conducted by Boccaletti et al in 2014 [Boc+14].

More recent publications have focused on ever growing high quality big datasets that became more significant due to the Covid-19 pandemic and the supply chain crisis that should also be noted:

- The 2018 study on how a pandemic may spread in the United Kingdom based on volunteers recorded movement and self reported contacts by Klepac, Kissler and Gog [KKG18]. - A 2020 paper by Galloti et al assessing the risks of what they call 'infodemics' in response to the COVID-19 epidemic, which analyzed over 100 million Tweets to develop an Infodemic Risk Index capturing the extent of exposure to unreliable news across nations [Gal+20]. - Inoue and Todo's 2020 study is also of particular value in relation to supply chain management. They use an agent-based model to simulate the economic effects of shutdowns on the actual supply chains of approximately 1,6 Million Japanese firms [IT20].

Remarkably, network science, provided the scientists with new tools to study and analyze the interconnected systems they observed in the nature [Lew11]. A graph (or network) is a mathematical structure made up of vertices (or nodes) which are connected by edges (or links) [BM+76]. A brain can be seen as such a structure.

In the following sections, a short introduction to networks in general and "Network Neuroscience" in particular is presented.

1.1 GRAPHS

As mentioned above, Graphs are mathematical structures consisting of vertices and edges. A graph G can be shown as:

$$\begin{aligned} G &= (V(G), E(G)), \\ V(G) &= \{v_1, v_2, v_3, v_4, ..., v_n\}, \\ E(G) &= \{e_1, e_2, e_3, ..., e_{n'}\} \end{aligned} \tag{1.1}$$

where V is the set of vertices and E is the set of edges [BM+76].

TABLE 1.1. Historical timeline of a few significant contributions to network science Original table until 2009 from Ted Lewis' book "Network Science: Theory and Applications"[Lew11]. Re-used with permission from the publisher.

Date	Who	Contribution
1736	Euler	Bridges of Koenigsberg
1925	G. Yule	Preferential attachment, Yule–Simon distribution
1927	Kermack, McKendrick	First epidemic model
1951	Solomonoff, Rappaport	Spread of infection in random networks
1955	Simon	Power law observed in word analysis
1959	Gilbert	First generative procedure for random graph
1960	Erdos, Renyi	Random graphs
1967	Milgram	Small-world experiment
1969	Bass	Diffusion of innovation in populations—nonnetwork model
1971	Fisher, Pry	Diffusion by product substitution—nonnetwork model
1972	Bollobas	Complex graphs
1972	Bonacich	Idea of influence in social networks leading to influence diagrams
1973	Granovetter	Job-seeking networks formed clusters with "weak links" between them
1978	Pool, Kochen	First theoretical examination of small worlds
1984	Kuramoto	Synchronization of linear systems
1985	Bollobas	Publishes book on "random graphs"
1988	Waxman	First graph model of the Internet
1989	Bristor, Ryan	"Buying networks" = application of network science to model economic system
1990	Guare	Coined phrase, "six degrees of separation" = name of his Broadway play
1995	Molloy, Reed	Generation of networks with arbitrary degree sequence distribution
1996	Kretschmar, Morris	Early application of network science to spread of infectious disease contagion driven by largest connected component
1998	Holland	Introduction of emergence in complex adaptive systems
1998	Watts, Strogatz, Faloutsos, Faloutsos	Renewed interest in Milgram's original work on small worlds, examples of clustering; first generative procedure for small world
1999	Faloutsos	Power law observed in Internet
1999	Albert, Jeong, Barabasi	Power law observed in WWW
1999	Dorogovtsev, Mendes	Small-world properties
1999	Barabasi, Albert	Scale-free network model
1999	Dorogovtsev, Mendes, Samukhim, Krapivsky, Redner	Exact solution to scale-free network degree sequence
1999	Watts	Explanation of "small-world dilemma": high clustering, low path length
1999	Adamic	Distance between .edu sites shown to be small-world
1999	Kleinberg, Kumar, Raghavan, Rajagopalan, Tomkins	Distance between .edu sites shown to be small-world Formalized model of WWW as "Webgraph"
1999	Walsh	Difficulty of search in small worlds using local properties
2000	Marchiori, Latora	Harmonic distance replaces path length: works for disconnected networks
2000	Broder, Kumar, Maghoul, Raghavan, Rajagopalan, Stata, Tomkins, Wiener	Full Webgraph map of the WWW
2000	Kleinberg	Shows O(n) search in small world using "Manhattan distance"
2000	Albert, Jeong, Barabasi	Scale-free networks are resilient if hubs are protected (Internet's "Achilles heel")
2001	Yung	Taxonomy of applications of small-world theory to: SNA, collaboration, Internet, business, life sciences
2001	Pastor-Satorras, Vespignani	Claim no epidemic threshold in scale-free networks; Internet susceptible to SIS viruses
2001	Tadic, Adamic	Use of local information can speed search on scale-free networks
2002	Levene, Fenner, Loizou, Wheeldon	Enhanced Webgraph model concluded structure of the WWW couldn't be explained by preferential attachment alone
2002	Kleinfeld	Claims Milgram experiments not well founded: small-world social network is an "urban myth"
2002	Wang, Chen, Barahona, Pecora, Liu, Hong, Choi, Kim, Jost, Joy	Sync in small worlds equivalent to stability in coupled system
2003	Wang, Chakrabarti, Wang, Faloutsos	Showed spread of epidemics determined by network's spectral radius, largest eigenvalue of connection matrix
2003	Virtanen	Complete survey of network science results up to 2003
2003	Strogatz	Synchronization of crickets, heartbeats
2005	NRC	Definition of network science
2006	Atay	Synchronization in networks with degree sequence distribution —application to networks
2007	Gabbay	Consensus in influence networks—linear and nonlinear models

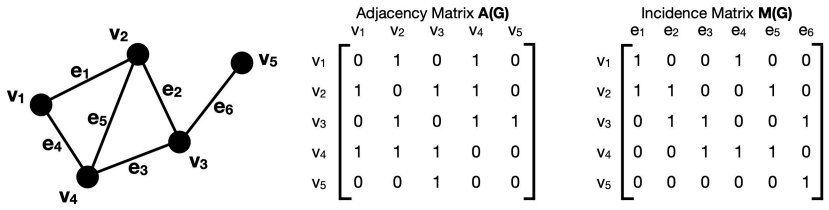

FIGURE 1.1. An example graph with adjacency and incidence matrices
Adjacency matrix elements are showing if there are connections between vertices and incidence matrix elements are showing how many times an edge and a vertex are incident. Both of these matrices are used to specify a graph. In this work, we focus more on adjacency matrix representations.
For the example graph above:
V(G) = $\{v_1, v_2, v_3, v_4, v_5\}$,
$E(G) = \{e_1, e_2, e_3, e_4, e_5, e_6\}$

1.1.1 *Adjacency vs Incidence Matrices*

For any given graph G, the corresponding two matrices (called the "incidence" and "adjacency" matrix respectively) can be used for specification.

- **Incidence Matrix**: An incidence matrix $M(G) = [m_{i,j}]$ is a $n \times n'$ matrix with elements $m_{i,j}$ showing how many times an edge and a vertex are incident.

- **Adjacency Matrix**: An adjacency matrix $A(G) = [m_{i,j}]$ is a $n \times n$ matrix with its elements $a_{i,j}$ showing if vertex i is connected by an edge or more to vertex j. If there is no self-loop in the graph, the diagonal elements of adjacency matrix are all 0. If the edges have no preferred direction, the graph is undirected and the adjacency matrix is symmetric.

An example of an undirected matrix with its two adjacency and incidence matrices is shown in Figure 1.1.
The adjacency matrix is generally significantly smaller than the incidence matrix and is therefore used more often. In the following chapters of this work, we mainly use the adjacency matrix.

1.1.2 *Weighted Graphs*

If there is a weight $w(e)$, associated to each edge, then our graph G is called a "weighted graph" [BM+76] [to be more precise, it is an "edge-weighted graph"

in contrast to a "vertex-weighted graph" but the name "weighted graph" usually refers automatically to "edge-weighted graph"]. To show the weighted graphs, we use the "weighted adjacency matrices" where the elements $a_{i,j}$ show the weight of edge/link between two vertices i and j instead of the number of connections between them.

1.2 Scales and Dimensions

The Brain can be investigated as a network in various dimensions and scales. Figure Figure 1.3 from Betzel and Bassett [BB17a] introduces the three axes of study for brain networks; spatial, temporal and topological. Spatially, single neurons, populations of neurons and bigger regions or areas of the brain can be defined as network nodes. In the temporal dimension, networks can be analyzed from an approximately a single point in time to the millennia underpinning evolutionary changes. Finally, in the topological dimension, studies can focus on local node/link scale, meso-scale motifs, clusters, groups, components or global aspects of a network. The majority of studies on brain networks exist as points in this space, focusing on networks defined at a single spatial, temporal, and topological scale. While such research has indeed been insightful, Betzel and Bassett [BB17a] suggest that in order to better comprehend the brain's real multi-scale nature, it is imperative that further network analyses begin to build bridges between different dimensions.

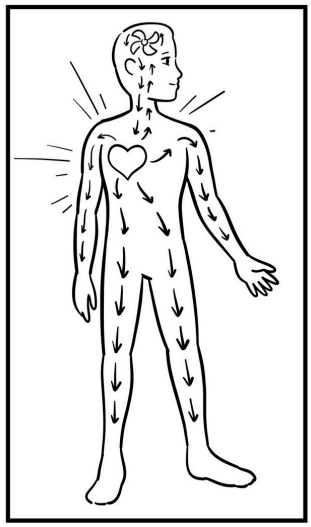

Figure 1.2. Aristotle idea of the role of brain vs heart Aristotle believed that the brain serves to cool down the blood from the heart, the central organ.

1.3 Brain Data

Aristotle (384 - 322 B.C.) believed that the brain is an organ which helps to cool down the blood coming from the heart, similar to a car radiator, while the heart is the seat of intelligence[3][Ole18]. If that sounds absurd to a modern scientist,

[3] In his work "De Partibus Animalium", Aristotle discusses first the function of the heart and then the brain.

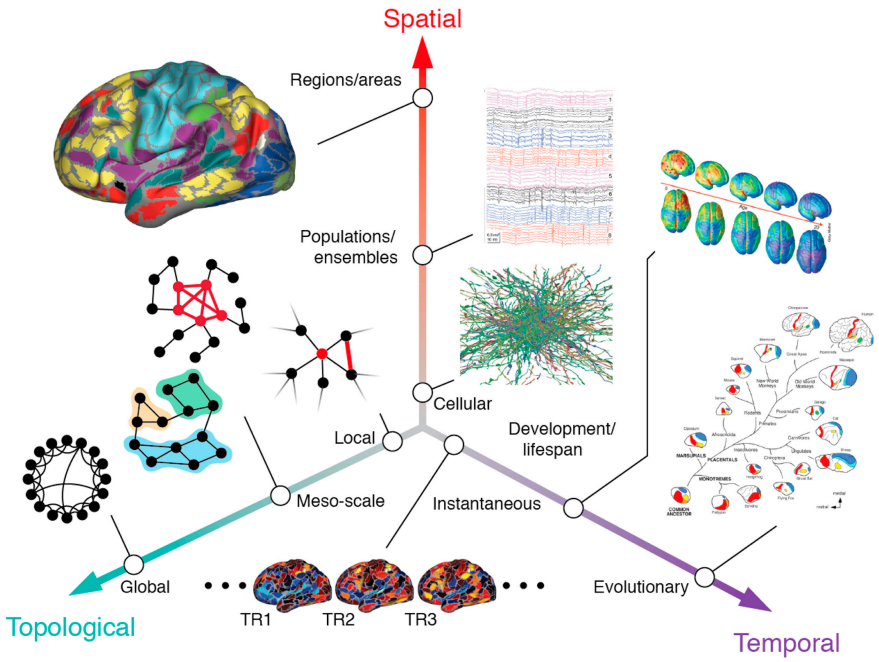

FIGURE 1.3. 3 different dimensions to study the brain network in different scales
Brain network can be studied in different scales and along different axes. The figure is re-used from Betzel and Bassett [BB17a] under the open licence adopted with permission from [Bey+13; Buz04; Gog+04; Kru09].

it is helpful to consider the limitations of gathering data from living humans without harming them. How might one methodically examine the interior structure or function of the body without opening it or causing it harm?
The invention of X-Ray imaging by Röntgen in 1895 opened the door to investigate the state of bones in depth without requiring surgery [NS04].
However, X-Ray imaging is not helpful in the study of soft internal tissues.

Around the same time, the first attempts to study the function of brain in a non-invasive way were performed by Angelo Mosso (1880) [Mos81; San+14]. Mosso hypothesized that demanding cognitive tasks need extra blood to reach the brain; therefore, if one places human subjects on a carefully balanced plate while they performed heavily demanding cognitive tasks, the plate would eventually tilt towards their heads. Following these first steps in the study of internal structures and functions, several other methods were proposed during the 20th century.
Xenon inhalation in 1960s and 1970 for example produced the first 2D map of the brain on the colored screen. In their 1978 paper, Lassen and colleagues [LIS78] measured the brain during rest, sensory perception, voluntary movement, speaking and reading. A figure from their reading experiment is included

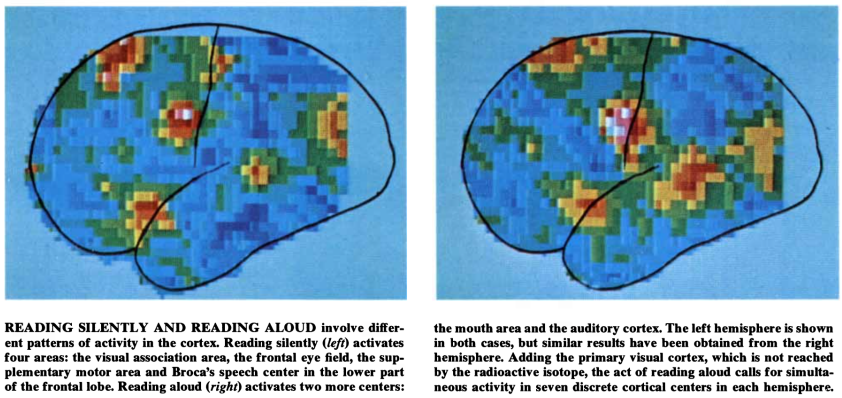

READING SILENTLY AND READING ALOUD involve different patterns of activity in the cortex. Reading silently (*left*) activates four areas: the visual association area, the frontal eye field, the supplementary motor area and Broca's speech center in the lower part of the frontal lobe. Reading aloud (*right*) activates two more centers: the mouth area and the auditory cortex. The left hemisphere is shown in both cases, but similar results have been obtained from the right hemisphere. Adding the primary visual cortex, which is not reached by the radioactive isotope, the act of reading aloud calls for simultaneous activity in seven discrete cortical centers in each hemisphere.

FIGURE 1.4. Brain image from Lassen et al in 1978 [LIS78]
Colored brain image recorded using Xenon inhalation method. Reused with permission from the publisher.

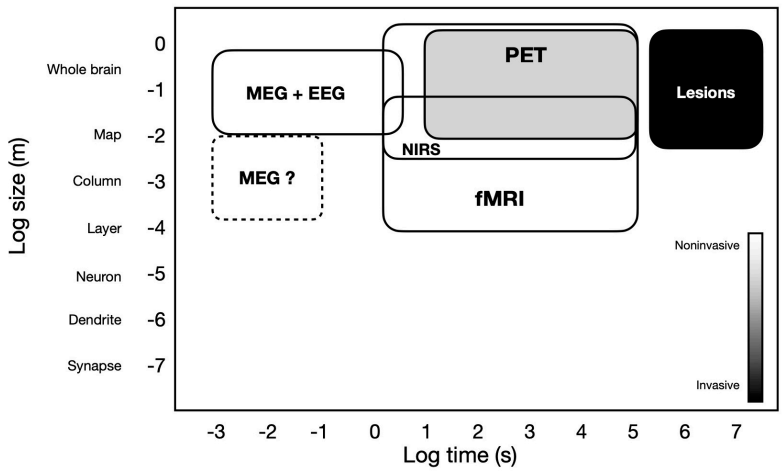

FIGURE 1.5. Comparing different imaging techniques
Each of the imaging techniques cover different spatial and temporal scales. A summary of some techniques is presented here. Plot re-created from [Ban20]

here with the permission from the publisher [Figure 1.4]. Positron Emission Tomography (PET) and Near-InfraRed Spectroscopy (NIRS) then appeared in the 1970s, they each contributed significantly to our understanding of the human brain.

The well known electroencephalography (EEG) method was first introduced in 1924 by Hans Berger [TTT05] but it was not up until 1938 that it

became widely accepted and utilised. EEG signals are measured using small electrodes placed on the skull that mainly detect the electrical activity of pyramidal cells, which make up about 70% of the brain cortex. EEG signals have an excellent time resolution but lack a good spatial resolution. Collecting data from the 2D surface of the head after the internal effects of different conductivities in various tissues and individually shaped skulls makes the locating of signal sources difficult [NS05].

However, the most dominant functional brain imaging method in current brain research is functional Magnetic Resonance Imagine (fMRI)[4] [ZY15] initially discovered by Seiji Ogawa in 1990 [Ban20].
In the next subsection, a short introduction to fMRI is presented.

1.3.1 *Functional Magnetic Resonance Imaging (fMRI)*

Functional Magnetic Resonance Imaging (fMRI) works based on the blood-oxygen-level-dependent (BOLD) contrast. It detects where the blood is utilized in the brain. The assumption is that the higher neural activity in a region results in higher blood consumption there. Peter Bandettini counts five main advantages that caused the success of fMRI in his work [Ban20] as follows:

1. MRI scanners were already available and accessible in hospitals and therefore there is no need for the installation of a totally new device.

2. As far as research shows, this method is safe and non-invasive

3. The spatial resolution of this method is very high, voxels as small as $0.5mm \times 0.5mm \times 0.5mm$ can fall into the resolution range of fMRI scans

4. Acquisition speed is high. The period between two imaging volumes can be as short as 200ms

5. The High sensitivity of fMRI allows it to be useful in generating functional maps of subjects brains in a considerably short period of time (order of minutes). A subject can perform then several tasks in an hour while being scanned.

[4] Some interesting statistics can be seen here: https://sapienlabs.org/lab-talk/500000-human-neuroscience-papers/

1.3.2 *Diffusion Tensor Imaging (DTI)*

Diffusion Tensor Imaging (DTI) is an MRI technique to generate a map of white matter tracts in the central nervous system (CNS) [Lop18]. If water molecules are diffusing through an isotropic environment, they will diffuse as spheres. Any boundary condition that affects the diffusion will result in a non-sphere ellipsoidal diffusion. DTI uses this principle to locate the white matter (axons) tracts boundary conditions in the scanned brain. DTI indices such as the "apparent diffusion coefficient" (ADC), "functional anisotropy", "mean", "radial" and "axial-diffusivity" are the quantities that provide the needed information to extract a map of axonal organization [Win22]. A map of weighted connections given by DTI can serve as an adequate depiction of the brain's structural organization.

1.4 Building Networks from Brain Data

In neuroimaging-based network neuroscience, brain regions identified by any given method of parcellation are considered the network's nodes, while links can be defined either as white matter connections between brain regions (structural networks) or as statistical interdependencies between the time series of brain regions (functional networks)[5] [BM08; Fai+09; FZB16; Pow+10; RS10; Spo10; Spo12]. Figure 1.6 shows how fMRI and dMRI can result in the functional and structural network weighted adjacency matrices. In the next section, a common approach to construct functional network is explained.

1.5 Functional Network

Time series for each node (from optional parcellation of the brain) are extracted from the preprocessed fMRI images. A commonly used approach to build an adjacency matrix from these time series is to calculate a co-activity measure between pairs. Co-activation can be quantified using a wide variety of measures such as Pearson's correlation and partial correlation [Buc+09; He+09; Wan+09; Egu+05; Liu+08; NHB09; Zha+11; Lia+12] between two nodes time series. Pearson's correlation assesses the broad dependency between variables, while partial correlation evaluates the direct interdependence after excluding the impacts of third parties [PQB05; SMD04]. Smith et al. [Smi+11] proved that both correlation approaches provide outstanding performance when estimating

[5] A third category, "effective" network is also used in some studies. Interested readers will find useful explanations in [Fri11]

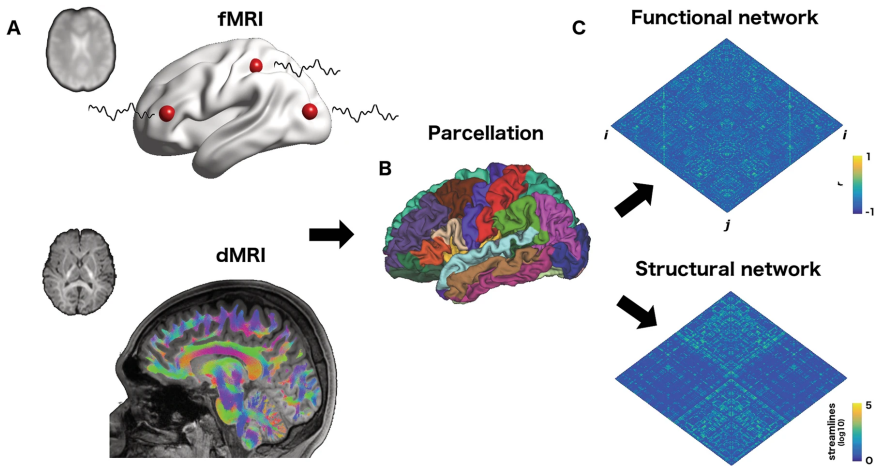

Figure 1.6. Structural and functional brain network schematic for fMRI and DTI
brain regions identified by any given method of parcellation are considered the network's nodes, while links can be defined either as white matter connections between brain regions (structural networks) or as statistical interdependencies between the time series of brain regions (functional networks). fMRI: functional MRI/ dMRI: Diffusion MRI. A) time series from fMRI and white matter tracts from dMRI are extracted. B) A target parcellation is chosen. C) Structural and functional weighted adjacency matrices are calculated in that parcellation. Figure reused from Fig 1 in [Per+19] under Creative Commons Attribution 4.0 International License.

functional connections; however, when the number of nodes in brain networks increased substantially, Pearson's correlation surpassed partial correlation. In this work, we focus on Pearson's correlation coefficient. Pearson's correlation coefficient between the two time series x and y is calculated as

$$r = \frac{\sum_{\eta=1}^{t}(x_\eta - \overline{x})(y_\eta - \overline{y})}{\sqrt{\sum_{\eta=1}^{t}(x_\eta - \overline{x})^2}\sqrt{\sum_{\eta=1}^{t}(y_\eta - \overline{y})^2}} \tag{1.2}$$

where r is the Pearson's correlation coefficient. x_η is the η-th element of time serie x. y_η is the η-th element of time serie y. $\overline{x}$ is the average of time serie x elements and $\overline{y}$ is the average of elements in time serie y.

For each pair of time series for N nodes, the r coefficient can be determined. The end result is an N by N matrix of Pearson correlation coefficients. This matrix is the weighted adjacency matrix of a functional network.

1.6 Structural Network

Diffusion MRI (dMRI) data can be analyzed in a variety of ways to infer the features of structural brain networks. Estimates of local "white matter in-

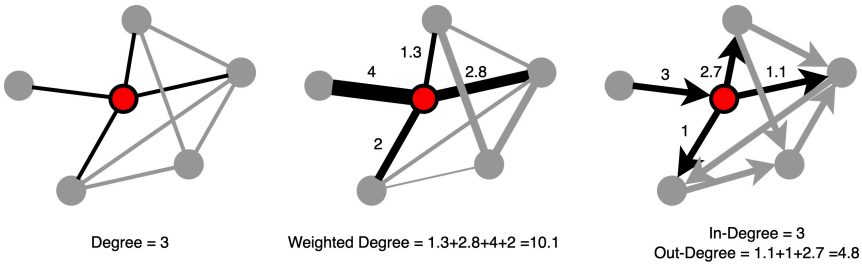

FIGURE 1.7. Three different degree variations
Simple illustrations of degree, weighted degree and weighted in/out degrees.

tegrity" can be obtained using voxel-wise diffusion measures such as fractional anisotropy (FA) and mean diffusivity (MD), or by employing tractographic techniques to reconstruct whole-brain structural networks and then subjecting these to graph theoretical analyses. FA and MD have been the most widely used of the aforementioned methods, employing either a voxel-based approach or tract-based spatial statistics (TBSS)[6] [Per+19].

1.7 QUANTIFYING BRAIN DYNAMICS

The reliance of network science on graph theory gives the researcher access to the rich history of graphs in mathematics. To investigate and compare networks, we describe the measures degree and module or clusters here in later subsections. A more detailed list of several well-known network measures together with their mathematical definitions is presented in pages 1066 to 1068 of Rubinov and Sporn's review [RS10]. In addition, an in-depth review of graph theory as a tool for identifying connectivity patterns in the human brain can be found in Farahani et al review in 2019 [FKL19]

1.7.1 Degree

The degree of a node in a non-weighted, undirected network is the number of connections that node has to the rest of nodes in the network. This definition can be extended to the weighted network case as the sum of weighted connections a node has [weighted degree] or the sum of incoming connections as in-degree and the sum of outgoing connections as out-degree. See Figure 1.7 for an illustration.

[6] TBSS is an automated, observer-independent method for measuring fractional anisotropy in the major white matter tracts on a voxel-by-voxel basis across subject groups[Smi+06]

1.7.2 *Clusters/Modules*

Densely interconnected groups of nodes or nodes that share a specific feature can form distinct meso-scale structures [along topological axis of Figure 1.3] within the network. A network that includes a lot of densely interconnected groups of nodes reacts differently to external stimulation in comparison to a random network with uniform connections all over the network. Within anatomical and functional networks, segregation measures have straightforward interpretations. The presence of clusters in anatomical networks indicates the possibility of functional segregation in these networks, whereas the presence of clusters in functional networks indicates an organization of statistical dependencies that is indicative of segregated neural processing[RS10]. There are numerous methods to detect cluster or modules in a networks, which will be discussed in the later chapters of this thesis. For a more general overview of algorithms (both graphs-based and non graph based , see Xu and Tian's 2015 publication [XT15].

1.8 Brain Simulation

The last introductory topic in this chapter is "brain simulation". Simulations of the human brain on a computer are one of the more modern techniques employed by scientists. They are also low-cost opportunity to test hypotheses that may not be ethically or practically applicable to the real brain.

With simulations and computational models, we can now predict the optimal targets of deep brain stimulation [FDK22; Tre+20], explain changes in brain connectivity during the progression of Alzheimer's disease [Dem+17] and epileptic seizures or find a patient-specific epileptogenicity of the brain regions to improve epilepsy surgeries in hospitals [Has+20; Ger+20; Olm+19; Pro+18].

1.9 Outline of the Thesis

This work consists of 7 chapters:
The current chapter, chapter 1, focuses on the fundamental principles required by the reader to understand the basic concepts used in this thesis. The reader is introduced to graphs, their adjacency matrices, weights, and representations. Section 2 introduces the scales in which the brain networks are commonly studied. The next section, section 3, addresses brain data types and the methods used to obtain this data. Section 4 discusses the construction of a network based on the brain data. "Functional" and "structural" brain networks are explained in

the 5th and 6th sections. Some well-known measures to investigate the brain network are described in section 7. The final section highlights the advantages of brain simulations for our understanding of brain mechanism.

Chapter 2, re-introduces brain flexibility and its applications. A novel "template/a-priori flexibility" measure is proposed in section 2, followed by the step by step calculation detailed in section 3. The investigation of module population is presented as a side advantage of the flexibility method. Section 5 describes the advantages and limitations of the newly proposed method and the chapter ends in a short summary section.

In chapter 3, a fMRI dataset of over 300 participants is studied using the method presented in chapter 2. The fMRI scans are collected during the performance of a block-designed working memory task called n-back. The fist section of this chapter details the method and data. A selection case for a-priori modules is introduced in subsection 3.1.3. An integration measure is used as a complementary method together with our flexibility information (subsection 3.1.4). The 2 final sections of chapter 3 explain the findings and compare the results of new method with a previously used one. Finally come the discussion on the findings, similarities and differences.

Chapter 4 expands the usage of flexibility-based measures to patients after it was tested on healthy participants (in chapter 3). A total of 64 schizophrenia patients and 64 healthy controls are compared based on their brain template flexibility on the three [topological axis] scales of nodes, modules and whole-brain. These participants were scanned during a "theory of mind" task [7]. The significantly different features of flexibility are explained and shown in sections 5 to 7. On the 9th section, a simple GLM classifier is applied on the flexibility based measures of the two groups to determine whether it is possible to identify patients based on their brain flexibility.

Mini-chapter 5 is a report on the findings of a group of our collaborators who investigated the influence of suicidality on the brain network using the template flexibility method as a tool. The implementation of the method on their dataset was done by the author of this thesis.

The 6th chapter is a theoretical approach to reconstruct the flexibility pattern (observed in empirical data from chapter 3) on a simplified oscillator model in physics. To this end, a computer simulation of the brain time series is performed. This simulation is based on the dynamics of FitzHughNagumo

[7] Read more about the theory of mind task in chapter 4

oscillators as nodes, Balloon model to generate fMRI-like signals and an averaged empirical structural brain network extracted from DTI data.

The final chapter, chapter 7, concludes the thesis with a review on the findings, limitations and future research opportunities.

Chapter 2: A NOVEL FLEXIBILITY MEASURE

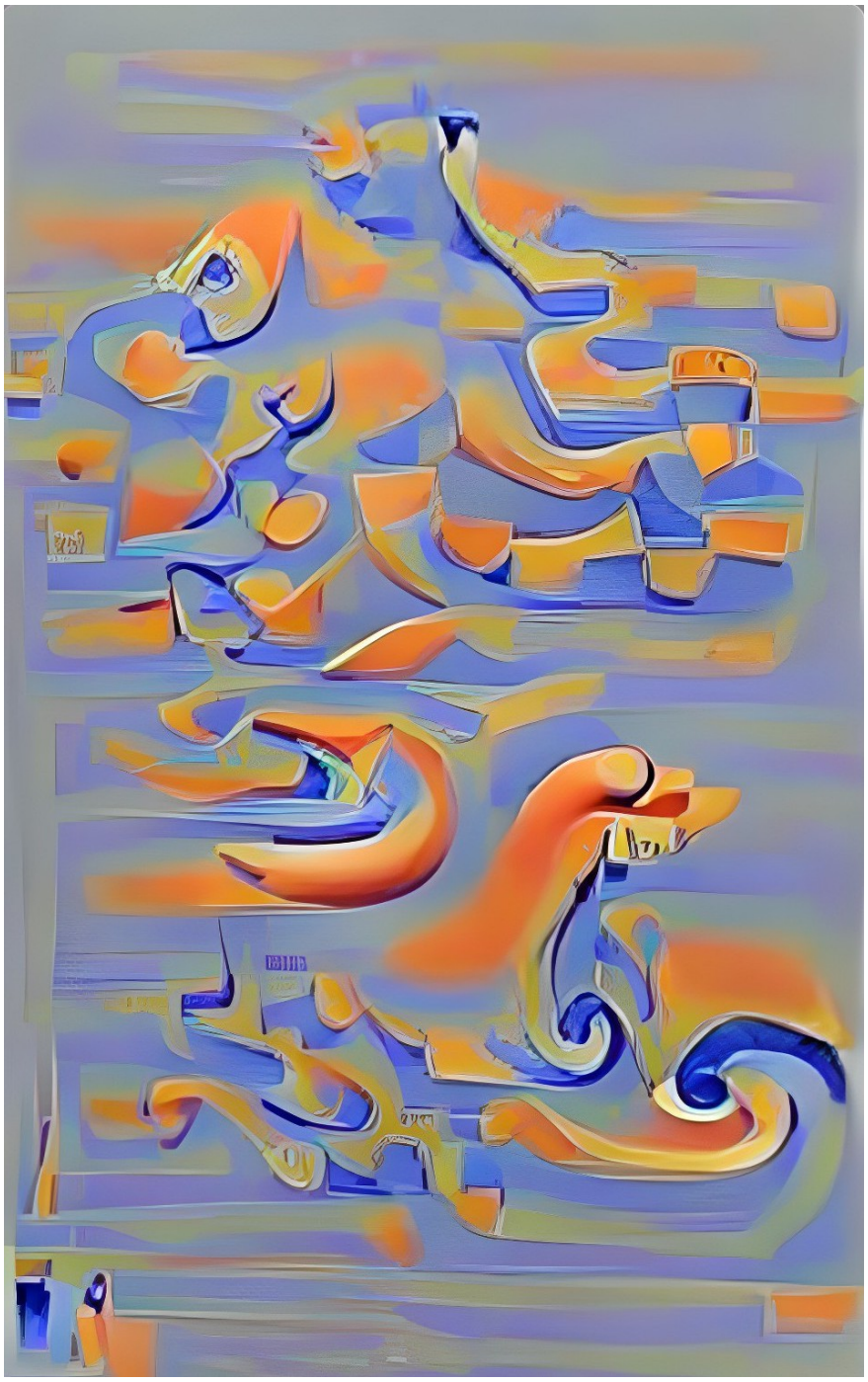

AI powered painting created by Wombo art [tea] using chapter 2 keywords.

Chapter 2

Template Flexibility

"The map had been the first form of misdirection, for what is a map but a way of emphasizing some things and making other things invisible?"

- Jeff VanderMeer

The material discussed in this chapter has overlap with the content of the below mentioned paper. Due to the differences in the nature of papers and thesis, some results are discussed more extensively here in the thesis.

A fast and intuitive method for calculating dynamic network reconfiguration and node flexibility

Narges Chinichian[1,2,3,*], Johann D. Kruschwitz[2], Pablo Reinhardt[2], Sarah A. Wellan[2,4], Susanne Erk[2], Andreas Heinz[2], Henrik Walter[2,#] and Ilya M. Veer[5,#]

First published in: *bioRXiv* (2022).
DOI: 10.1101/2022.02.06.479287
Currently in peer review process

In this chapter we introduce a novel measure to assess brain flexibility using

[1]Institut for Theoretical Physics, Technical University of Berlin, Berlin, Germany. [2]Department of Psychiatriy and Psychotheray, CCM, Charité-Universitätsmedizin Berlin, corporate member of Freie Universität Berlin and Humboldt-Universität zu Berlin, Germany. [3]Bernstein Center for Computational Neuroscience, Berlin, Germany. [4]Faculty of Philosophy, Berlin School of Mind and Brain, Humboldt-Universität zu Berlin, Berlin, Germany. [5]Department of Developmental Psychology, University of Amsterdam, Amsterdam, The Netherlands.

[#]shared senior authorship.

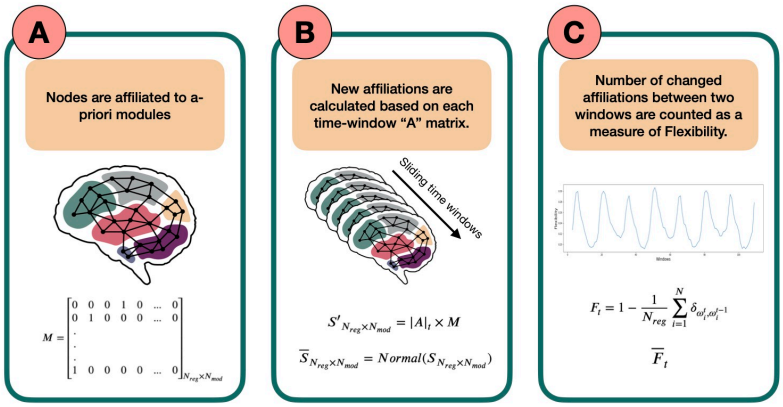

FIGURE 2.1. Schematic overview of the template-based flexibility method. A) Each node has an a-priori affiliation to a template module, not allowing overlap. Importantly, matrix M, describing the a-priori module affiliation for each node, is predetermined and serves as a reference. B) Using a sliding-window approach, a weighted adjacency matrix is constructed for each time window by calculating Pearson's correlation coefficients between the time series of all possible pairs of nodes. Then, for each node and time window the reference module receiving the highest normalized connection weight will serve as the new modular affiliation for that node in that time window. C) Last, the number of affiliation changes between affiliation vector in t and its successive vector in $t+1$ is defined as the flexibility F_t of the network between two time points. The average of F_t across participants (called $\overline{F_t}$) can be plotted for all consecutive time points (an example is presented later in chapter 3).

the deformation of sub-networks found in the brain connectivity matrices.

2.1 BRAIN FLEXIBILITY

Mesoscopic structures or groups formed by interactions between nodes of a network, called modules, clusters or communities, can be quantified by a variety of detection methods [For10]. Nodal interactions are typically represented by a weighted adjacency matrix A of the network, where each element $a_{i,j}$ of A (called a_{ij}) is the weight of the connection or strength of interaction between nodes i and j (undirected). Modules are usually determined based on the general idea of maximizing the number/weight of within-group and minimizing the number/weight of between-group links. Modules can then be considered as entities in the network that can be modified individually without affecting the rest of the network. Modularity measures have been shown to be useful as a biomarker of disease, including epilepsy [Cha+10], Alzheimer's disease [Bri+14], schizophrenia, bipolar, and major depressive disorder [Ma+20]. However, brain modularity has also been associated with normal variation in cognition:

Individuals with lower whole-brain modularity performed better in complex tasks, while those with higher modularity showed an advantage in simple tasks [Yue+17]. Whereas the 'static' community detection methods employed in the above-mentioned studies consider the brain's connectivity averaged over time (based on only one adjacency matrix per subject as a single-layer network), other methods have assessed changes in community structure over time [New+09; Meu+09; Bas+11; Cal+14; Ala+15; SB16]. These dynamic approaches take into account that a node can frequently change its connections depending on which state the brain is in, both during resting-state (RS) and during the performance of tasks. Here, changes in modular structure are captured by a sequence of adjacency matrices (A_t), thus creating multi-layer networks. The adjacency matrices are typically calculated using a sliding-window approach on nodal time series, in which the window length reflects the time scale of interest [FZB16]. Subsequently, dynamic module detection methods can be applied to these time-dependent multi-layer networks to not only characterize changes of modules over time, but also to determine how nodes change their affiliation [the module/group they belong to] as a function of time. The latter can be thought of as the flexibility of a node [Bas+11; BB17b] and is defined based on the consecutive presence of nodes in different modules over time [MLB10; Cal+14]. These measures of flexibility enable us to track time-dependent changes and thereby track phenomena of both integration and segregation in the brain [Bas+11; Bra+15]. It offers the opportunity to study which brain nodes are more likely to change their affiliation over time and thereby which brain regions are rather consistently associated with a certain brain module, forming a backbone for the constantly changing network. For example, a recent study by Harlalka et al [Har+19] suggested higher symptom severity in autism spectrum disorder to be associated with more connectivity flexibility in visual and sensorimotor areas during rest. [Bra+15] demonstrated that individuals with more connectivity flexibility in frontal cortices have enhanced memory performance and score better on neuropsychological tests measuring cognitive flexibility, suggesting that dynamic network reconfiguration may form a fundamental mechanism underlying executive function. For a broader discussion on modularity and flexibility findings, see [KVL19].

A data driven widely used method to calculate brain network flexibility is based on the Louvain community detection algorithm by Blondel et al [Blo+08]. This algorithm aims to optimize the "Modularity" variable Q, initially introduced for a single layer network in [New06] by Newman, and later modified for multi-layer networks by others [Muc+10; VM18; Baz+16].

$$Q = \frac{1}{\mu} \sum_{ijsr} \left[\left(A_{ijs} - \gamma_s \frac{k_{is} k_{js}}{2m_s} \right) \delta_{sr} + \delta_{ij} C_{jsr} \right] \delta(c_{is}, c_{jr}) \tag{2.1}$$

Where A is the weighted adjacency matrix of the network, A_{ijs} is the weight of connection between nodes i and j in layer s. γ_s is the resolution parameter (a parameter to tune for the size of captures modules) for layer s, i and j are indices of nodes, and s and r indices of layers. k_{is} is the degree of node i in layer s. m_s is proportional to the sum of weights in layer s. C_{jsr} refers to the connection of node j to itself in different layers. c_{is} is the defined module/cluster of node i in layer s. Finally, Q captures how good the grouping is compared to a null-model (here random).

Although, this and similar methods have undoubtedly contributed to our understanding of brain dynamics, these come with a cost: Given the random nature of algorithms like Louvain, the resulting clusters may differ each time the algorithm is run on the same adjacency matrix. As such, brain modules show variation within and across participants, which is overcome by running the algorithm multiple times to reach a consensus on the modular structure [LF12]. However, this can be a computationally expensive process, while the identified modules may in the end have low biological plausibility or at least can not be interpreted straightforwardly.

2.2 A Novel Flexibility Measure

Here, we introduce a new method to capture nodal flexibility and brain network reconfiguration using a fast and intuitive method based on a set of template modules. This offers three main advantages over the existing methods:

1. It is computationally more efficient and deterministic compared to the Louvain (and similar) algorithm.

2. It offers high replicability, as it uses the same set of module templates for all subjects and time scales. This ensures comparability between subjects and studies, which is one of the current concerns in the field [HH18].

3. It gives researchers the opportunity to choose the best-fitting, or biologically most relevant module templates for each study.

In this chapter, the proposed method is described in detail and step by step. Later in chapter 3, this method is applied to a real-life dataset that was previously assessed using a Louvain-like locally greedy heuristic algorithm [Bra+15; Blo+08]. Compared to the previous work, this method is equally successful in capturing a brain reconfiguration pattern that mimics the stimulation periods of an externally-cued working memory task, yet it can be directly related to well-known functional brain networks as well.

2.3 METHOD

2.3.1 *Concept and Steps*

Before going into mathematical detail, let us first explain the concept behind the method. Consider the brain as a network, in which each region of the brain (defined by any arbitrary parcellation) is a node, each co-activation between any two nodes is an edge, and each node belongs to an a-priori defined set of nodes, termed a module. As a first step, we consider that each node has an a-priori affiliation to one of the predefined [template] modules or in other words, belongs to an a-prioiri module. The affiliation is determined as the template module with which each node of the selected brain atlas has the largest spatial overlap. Next, the strengths of all edges between each node and all members of every module are summed. When a node is more strongly connected to nodes affiliated with another module than to nodes of its own predefined module, then this node will receive another affiliation than its a-priori one. This can now be extended to a dynamic scenario, in which node affiliations can be determined for a range of consecutive time points. Some nodes might change their affiliation over time, while others do not. The ratio of nodes changing affiliation with respect to all is what we are interested in. We understand this ratio as a measure of flexibility of the brain. In other words, the more nodes switch affiliation between consecutive time points, the more flexible the network dynamics are. See Figure 2.1 for a summary of these steps.

The steps to calculate the template (aka a-priori) flexibility measure are listed below in detail:

1. An a-priori affiliation is assigned to each node to form the following matrix M:

$$M = \begin{bmatrix} 0 & 0 & 0 & 1 & 0 & \dots & 0 \\ 0 & 1 & 0 & 0 & 0 & \dots & 0 \\ \vdots & & & & & & \\ 1 & 0 & 0 & 0 & 0 & \dots & 0 \end{bmatrix}_{N_{reg} \times N_{mod}} \tag{2.2}$$

   Where N_{reg} is the number of regions (nodes) and N_{mod} number of a-priori modules. Each row of this matrix belongs to a node and, in the first-approximation case in this study, has only one non-zero element that indicates the a-priori modular affiliation of the node. For example, in row 1 the fourth column is 1, which means that the first node has an

a-priori affiliation to template module 4.
Note that we assign all nodes that do not show any overlap with the template modules to a last, artificial module to not exclude these nodes in calculating the flexibility metric. To add to the interpretability of the process, it is better if we chose template modules that span the whole brain or leave out only a small number of regions.

2. Next, for each node we extract the mean time series across all volumes of the fMRI scan. We then divide our time-series into smaller windows using a sliding-window approach. For each time window, a weighted adjacency matrix is constructed using Pearson's correlation coefficients between all possible node pairs. The weighted adjacency matrix at time-window t is defined as A_t of shape $N_{reg} \times N_{reg}$:

$$A_t = \begin{bmatrix} Weighted & Adjacency & Matrix & \\ of & Time & Window & t \end{bmatrix} \tag{2.3}$$

3. Now, we want to calculate how each node is connected to the nodes that are the predefined members of each of the template modules, as defined in M. To this end, we sum the absolute values of all the weights from one node to all the nodes affiliated to each of the modules, so that each node has N_{mod} [in our subsection chapter 3 analysis: 15] different values (one weighted sum for links to each module), indicating the strength of its links with the predefined members of each of the template modules. In mathematical terms, we calculate the $N_{reg} \times N_{mod}$ matrix S' as follows:

$$S' = |A|_t \times M \tag{2.4}$$

where $|A|_t$ matrix elements are the absolute values of A_t elements and the matrix has the dimension $N_{reg} \times N_{reg}$. Row i of S' belongs to the region i and each column j shows the sum of absolute connection weights of i to the members of j-th module. As the predefined modules differ in size, the S' matrix elements are then normalized to the number of regions affiliated by template definition to the modules, creating a new matrix called S [dividing each matrix element S'_{ij} by the number of regions affiliated to the jth template module.] Importantly, to be able to compare the elements of S, we normalize it in a way that the sum of each row is one. This normalization step has no effect on the output of the next steps but is rather to increase the interpretability at this stage. The normalized numbers represent which portion of each node's connections is to which module. We call this new matrix, $\overline{S}$.

$$\overline{S}_{N_{reg} \times N_{mod}} = rowNormalized(S_{N_{reg} \times N_{mod}}) \tag{2.5}$$

4. With $\overline{S}$, we have the ratio of affiliations to each module calculated for all nodes. From these, the strongest affiliation per node is chosen as the winner and together form an affiliation vector for time window t, we call this vector Ω_t:

$$\Omega_t = \begin{bmatrix} ArgMax(\overline{S}_{1*}) \\ ArgMax(\overline{S}_{2*}) \\ ArgMax(\overline{S}_{3*}) \\ ArgMax(\overline{S}_{4*}) \\ .. \\ ArgMax(\overline{S}_{i*}) \\ ... \\ ArgMax(\overline{S}_{N_{reg}*}) \end{bmatrix}_{N_{reg}\times 1} \tag{2.6}$$

where $ArgMax(\overline{S}_{i*})$ points to the index (argument) of the module with the largest average connection strength to node i in matrix $\overline{S}$.

5. Following steps 2-4 for consecutive time windows, we calculate one Ω_t for each window t. The $flexibility$ of the network denoted by F is then defined as the ratio of regions that change their affiliation from one window to the next, to the network size, or:

$$F_t = 1 - \frac{1}{N_{reg}} \sum_{i=1}^{N} \delta_{\omega_i^t, \omega_i^{t-1}}, \tag{2.7}$$

where ω denotes an element of vector Ω. The Kronecker delta $\delta_{\omega_i^s, \omega_j^t}$ is 1 if $\omega_i^s = \omega_j^t$ and 0 otherwise. The $\sum$ then counts the number of nodes that did not change their affiliation between windows t and $t+1$. Note that as a side-product of calculating Ω, we can output a vector describing the affiliations over time for each node separately as well by making a vector of the same element in $\Omega_{t=1,..,N_t}$:

$$\left[\omega_i^{t=1}, \omega_i^{t=2}, \omega_i^{t=3} ..., \omega_i^{t=N_t}\right]_{1\times N_t} \tag{2.8}$$

Where N_t is the total number of time windows. This output can be used for further region-specific analysis.

6. Where we apply the method to real-life data (see subsection **??**) we also calculate the average $flexibility$ over time for a sample (cohort of subjects), $\overline{F}_t$, by simply summing the flexibility over all participants and divide it by the sample size N_{sub}.

2.4 Module Population Analysis

With Ω from all time windows [see step 4], the distribution of regions in modules can be extracted. A change in the population of one module can be a cue to interpret the level of that module's importance during the performance of cognitive task in hand. If a module is absorbing more members during the time windows of a task, that module can be associated with more cognitive load during that task. Less associated modules, on the other hand, can either lose members to the dominant modules while still actively engaged in the cognitive task or remain unchanged.

2.5 Advantages vs Limitations

We discussed above how our method could be used to assess flexibility at multiple levels of the brain. That is, on the whole-network level, module level and at the regional (node) level, thereby extending the inferential potential compared to the other widely-used algorithms. However, this method, like every method, has its own limitations that might affect the results. One possible limitation appears when the sizes of a-priori modules are very different, a module of size 1 and another of size 200 are not to be compared in such a method. The researchers who use this method should also be aware that the absolute value of correlation weights used in step 3, though widely used in the neuroscience literature, equalizes the case of correlated and anti-correlated weights. The logic behind is that the regions that are heavily anti-correlated are also responding actively to the other node by doing the reverse of what they do and only nodes with no [close to zero] correlation should be excluded from meaningful connection.

In the description of our method, we determined the modular affiliation for a particular node and window as the module with which the node demonstrated the strongest connectivity in the affiliation vector. Although this crisp algorithm is arguably the easiest and most pragmatic choice, it would also be possible to use the weighted affiliation with each of the template modules in the affiliation vector [3] as a fuzzy module detection to assess flexibility. Such a weighted approach may ultimately prove to be even more informative in characterizing brain flexibility.

On the positive side, in addition to having a much higher computational efficiency, our method also promotes replicability across different samples and studies through the use of biologically plausible template modules. We believe that our approach can be a feasible choice for researchers aiming to study dynamical reconfiguration at multiple scales of the brain, be it nodes,

modules, or the brain as a whole.

2.6 Chapter Summary

This chapter contained the detailed calculation steps of the a-priori flexibility measure together with a discussion of the advantages and limitations of it. An example application of this method is going to be presented in the next chapter.

Chapter 3: APPLICATION AND COMPARISON OF A-PRIORI FLEXIBILITY

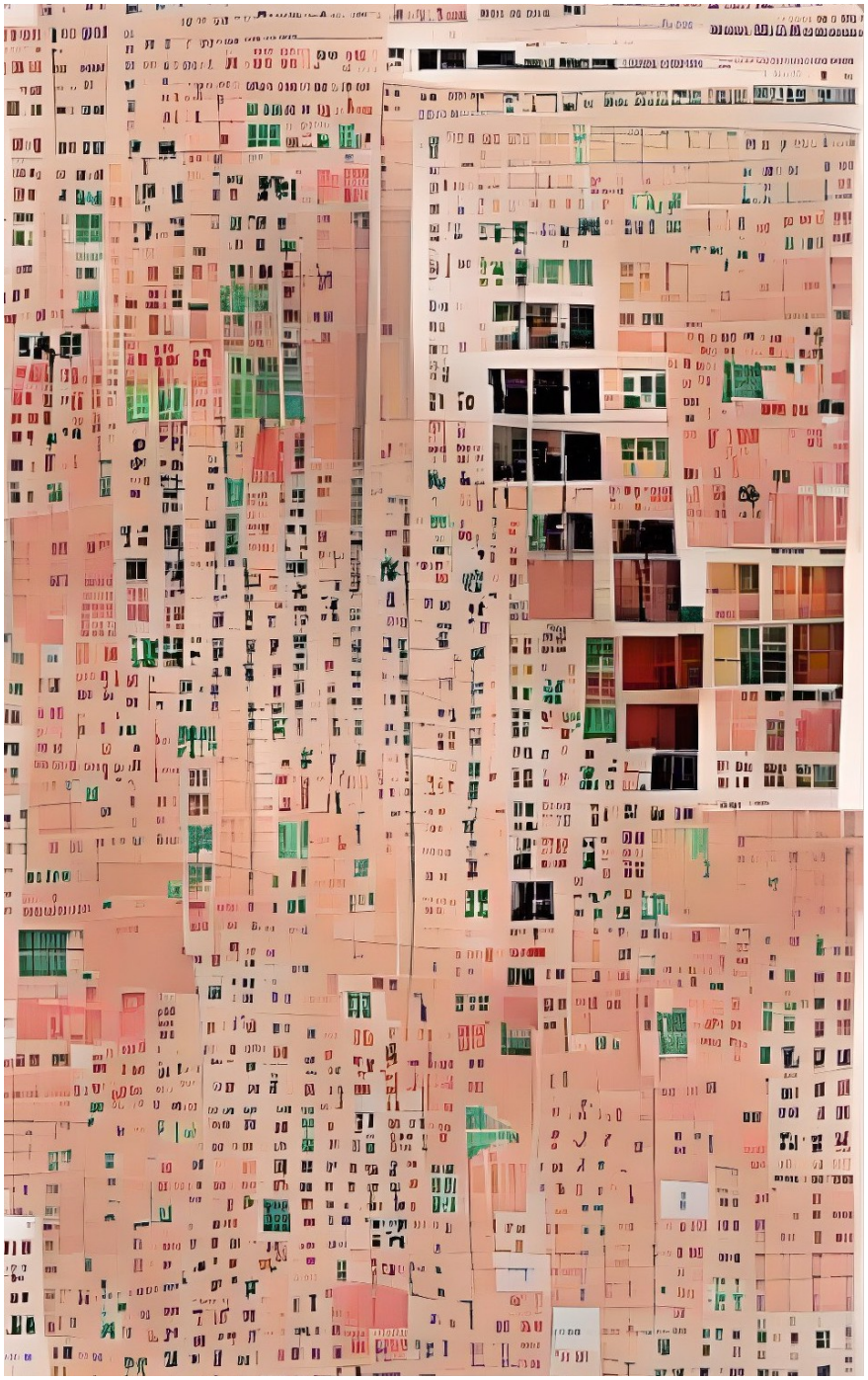

AI powered painting created by Wombo art [tea] using chapter 3 keywords.

Chapter 3

Application and Comparison

"memory is the glue that holds our mental life together. Without its unifying force, our consciousness would be broken into as many fragments as there are seconds in the day."

- Eric Kandel

The material discussed in this chapter has overlap with the content of the below mentioned paper. Due to the differences in the nature of papers and thesis, some results are discussed more extensively here in the thesis.

A fast and intuitive method for calculating dynamic network reconfiguration and node flexibility

Narges Chinichian[1,2,3,*], Johann D. Kruschwitz[2], Pablo Reinhardt[2], Sarah A. Wellan[2,4], Susanne Erk[2], Andreas Heinz[2], Henrik Walter[2,#] and Ilya M. Veer[5,#]

First published in: *bioRXiv* (2022).
DOI:10.1101/2022.02.06.479287
Currently in peer review process

In this Chapter, an application of our method introduced in the previous chap-

[1]Institut for Theoretical Physics, Technical University of Berlin, Berlin, Germany. [2]Department of Psychiatriy and Psychotheray, CCM, Charité-Universitätsmedizin Berlin, corporate member of Freie Universität Berlin and Humboldt-Universität zu Berlin, Germany. [3]Bernstein Center for Computational Neuroscience, Berlin, Germany. [4]Faculty of Philosophy, Berlin School of Mind and Brain, Humboldt-Universität zu Berlin, Berlin, Germany. [5]Department of Developmental Psychology, University of Amsterdam, Amsterdam, The Netherlands.

[#]shared senior authorship.

ter, Chapter 2, is shown.

3.1 Applying a-priori Flexibiliity Method on Empirical Brain Data

An ideal format to study the flexibility, can be found when two cognitive tasks are repeatedly performed in separated blocks of time and the brain response is recorded during and between the blocks. Such a data is used in this chapter to evaluate our method performance in capturing the brain reconfiguration.

3.1.1 Working Memory

"Working memory" is widely defined as the cognitive system that is responsible for short-term retaining and manipulating of information in the brain in order to perform tasks [CAA18; MS99; Bad92] in absence of external cues or prompts [Gol96]. Amongst the current popular paradigms to measure "working memory", the variants of "N-back" task, first introduced by Kirchner[Kir58], play a central role. Subjects are required to observe a series of stimuli and respond when the same stimulus is presented as the one in n trials back, where n can vary and is usually 0 [for the control condition],1, 2, or 3. A meta-analysis of 24 studies done by Owen et al [Owe+05], on n-back associated brain regions, finds the robustly activated (voxelwise false discovery rate = 1%) areas to be: lateral premotor cortex, dorsal cingulate and medial premotor cortex, dorsolateral and ventrolateral prefrontal cortex, frontal poles, and medial and lateral posterior parietal cortex (see also section 6.1.3 and Figure 6.7).

In the coming sections, the following variation of n-back task was performed:
The task was presented in a blocked fashion. Four blocks of 0-back and 2-back each (30s duration) were alternated, starting with the 0-back condition. Participants were asked to either press the button corresponding to the number shown on the screen (0-back) or the number that was shown 2 steps ago (2-back). See A and B panels from Figure 3.1 for more information on the task.

3.1.2 Subjects and Data

331 participants [a subset of 344 participants included in [Bra+15]] were considered for the analysis. Thirteen subjects [344-331] were excluded due to scanning artefacts, exceeding movement or insufficient image quality. Functional MRI data were acquired at three sites during performance of an N-back task: the

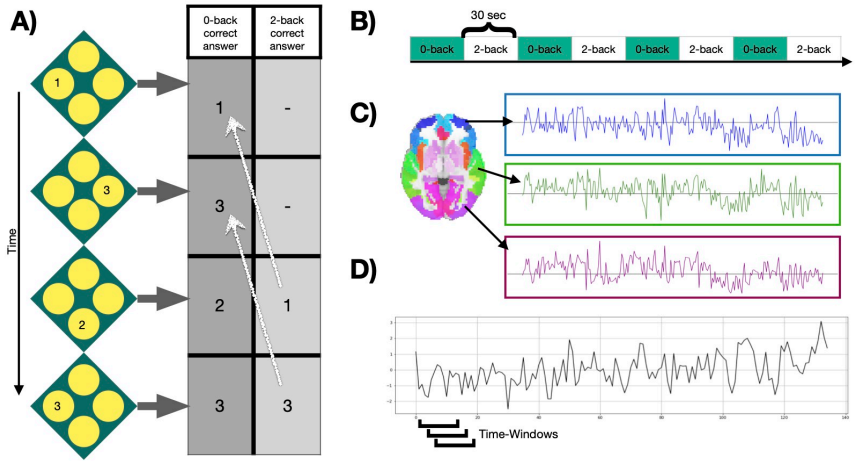

Figure 3.1. A) Example of the N-back working memory task with a 0-back and 2-back condition, during which participants were asked to choose the value that was either shown at the current step or 2 steps ago, respectively. B) Four blocks of each condition were presented in alternated fashion for 30 seconds. C) After preprocessing, mean time courses were extracted from 246 Brainnetome atlas regions [Fan+16]. D) Windowed time series were extracted using a sliding-window approach, moving a window of 15 time points over the time series one volume at a time.

Life and Brain Center of the University of Bonn, the Central Institute of Mental Health Mannheim, and Charité - Universitätsmedizin Berlin. The study was approved by the Medical Ethics Committees of the three study sites and all participants provided written informed consent. At all sites, a Siemens Trio 3T MRI scanner (Siemens Healthcare, Erlangen, Germany) was used with identical sequences: gradient-echo EPI, 28 slices, slice thickness 4mm (1mm gap), field of view 192 x 192 x 140mm, acquisition matrix 64 x 64, TR (repetition time) 2s, TE (echo time) 30ms, flip angle 80°. Standard preprocessing was conducted using SPM8 [Pen+11] and included motion correction (participants with $>$ 3mm translation and $>$ 1.7° rotation between volumes were excluded), slice-time correction, spatial smoothing with a FWHM of 9mm, high-pass temporal filtering with a 128s cutoff, and normalization to the Montreal Neurological Institute (MNI) template space with 3mm isotropic voxel size. A detailed description of data acquisition and preprocessing is provided in [Ess+09].

Mean time-courses of the 246 Brainnetome Atlas regions [Fan+16] were extracted from the preprocessed data of the 331 subjects. In line with [Bra+15], a 15-volume window length with 14 volumes overlap was chosen for the sliding-window analysis (figure Figure 3.1.C and Figure 3.1.D), generating in total 114 windows for each subject. For every window, an adjacency matrix using Pearson

correlation coefficients between all possible pairs of the 246 regions mean time series was calculated (using scipy.stats.pearsonr [Vir+20]). Considering that the N-back working memory task consisted of 30s alternating blocks of 0-back and 2-back, the 15-volume window (30s length) allows for one window purely reflecting a single condition block. For more information on selection of the window length see [Bra+15] and [LV15].

3.1.3 A-priori Modules Selection

The a-priori modules (Matrix M) were selected based on 14 well-described functional connectivity template networks (modules) in [Shi+12] by the FIND lab . As described before, a 15th (artificial) module was added comprising all atlas regions that did not overlap with any of the 14 template networks (read more about this module in the next chapter, Figure 4.13). The a-priori affiliations of all atlas regions can be found in Table Table 3.2 and the labels of the FIND lab templates in Table Table 3.1.

Table 3.1. Findlab-based modules [Shi+12] used in our application section.

Number	Name
Module 1	Anterior Salience
Module 2	Auditory
Module 3	Basal Ganglia
Module 4	Dorsal Default Mode Network (dDMN)
Module 5	High Visual
Module 6	Language
Module 7	Left Executive Control (LECN)
Module 8	Posterior Salience
Module 9	Precuneus
Module 10	Prim Visual
Module 11	Right Executive Control (RECN)
Module 12	Sensorimotor
Module 13	Ventral Default Mode Network (vDMN)
Module 14	Task Positive
Module 15	Undefined

http://findlab.stanford.edu/

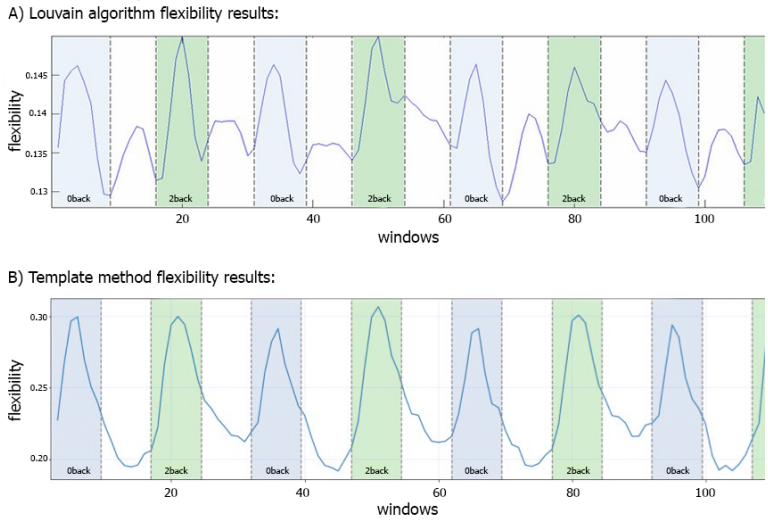

Figure 3.2. Comparison of flexibility generated by the generalized Louvain-like locally greedy heuristic algorithm [Blo+08; Jeu+] and the template-based method during an N-back working memory task. A) Flexibility plot from [Bra+15] illustrating the probability that a brain region changes its modular allegiance between two consecutive windows in a sample of 344 healthy subjects. The original plot is used with permission of the publisher. B) Flexibility plot generated by the template-based method. Here, the flexibility number in each time-window is the fraction of regions that change their affiliation from one time window to the next (i.e., the number of changed regions divided by the total number of nodes). The plots are generated using a subset, of size 331 subjects, from the same cohort as used in [Bra+15]. Note that in both plots a time window covers 15 EPI volumes with a TR of 2s, corresponding to a window length of 30s. The window was shifted with one volume at a time, allowing for 14 EPI volumes overlap between consecutive windows, which yielded 114 windows in total

3.1.4 *Complementary Integration Measure*

In some studies like [Bra+15], a complementary measure to study the level of integration/segregation of spatial meso-scale structures is used. To calculate the integration matrix R defined in [Bas+15] with elements $r_{k,l}$ which show the strength of co-activity between modules k and l, when there are N_{mod} modules $\{M_1, M_2, ...M_{N_{mod}}\}$, first the modular allegiance matrix T is calculated. Elements t_{ij} of matrix T indicate the fraction of times that nodes i and j have been assigned to the same community, in a predefined set of windows. Then the T elements with one end in module k and the other end in module l are used to calculate elements $i_{k,l}$ of intermodule connection matrix I, . It can be

written as:

$$i_{k,l} = \frac{\sum_{i \in M_k, j \in M_l} T_{i,j}}{|M_k||M_l|}, \tag{3.1}$$

where k and l are two modules and $|M_k|$ shows the size of module M_k. Then the elements of I are normalized with a division by internal connections of both modules and the resulting values, form integration matrix R elements as shown in equation 3.2:

$$r_{k,l} = \frac{i_{k,l}}{\sqrt{i_{k,k} i_{l,l}}}. \tag{3.2}$$

3.2 Results and Comparison

Figure 3.2.A shows the N-back flexibility pattern across all nodes from [Bra+15], while Figure 3.2.B shows the pattern generated by our method when applied to the same dataset (331/344 subjects of the same sample). Similar to Figure 3.2.A, the peaks illustrate maximum flexibility of the brain during performance of both the 0- and 2-back condition. In contrast, the transitions between the two task conditions coincide with troughs when applying our method, whereas [Bra+15] described additional, yet smaller peaks during these transition phases when using the generalized Louvain algorithm. On average, higher flexibility is observed during the 2-back than 0-back blocks, although the difference is relatively small ($t = -2.9, p = .03$).

In addition to calculating flexibility across all nodes, we can use the information captured in the fifth step to describe the affiliation changes of each individual node. This allows us to have a closer look at which nodes switch their affiliation over time most frequently, or at how often the a-priori constituents of each of the template networks switch their affiliation. Figure 3.3 illustrates how many times each node (Brainnetome regions in our analysis) switches its affiliation between two consecutive windows. Note that the number of switches was normalized to the number of switches performed by the node that switched most frequently, forcing the latter node to have a value of 1 and the other nodes to have a value between 0 and 1. Nodes within the prefrontal cortex predominantly show affiliation changes over time during execution of the N-back task. This is in agreement with the previous findings [Owe+05; Cao+14; Min+15; BGS15].

One level coarser and at the module level, we can look at the average switching ratio of template modules. The boxplots in Figure 3.4 demonstrate for each of the FIND lab template modules how often their a-priori defined constituent

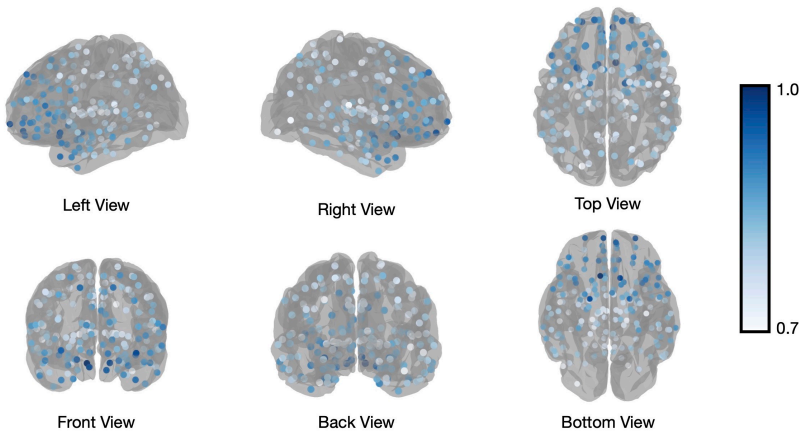

FIGURE 3.3. Brainnetome atlas brain regions switching Number of affiliation switches between consecutive windows for regions of the Brainnetome Atlas, averaged across all subjects and normalized to the most frequently switching node to yield values between 0 and 1. The visualized regions are those with values higher that 0.7.

nodes on average switch their modular affiliation over time across participants. Constituent nodes of the default mode network (DMN), salience network (SN), left and right executive control network (L/RECN), and language network seemingly switch their affiliation most often during execution of the N-back task.

It is possible with the sliding window approach, to separate the windows corresponding to each condition, 0-back and 2-back. We consider windows with minimum 80% of their time-points in one condition as the representers of that condition. We then calculate the modular allegiance T [see here: 3.1.4]and integration R of our 2 conditions. Figure 3.5 shows the result of this analysis. We observe a general increase in integration values in 2-back compared to 0-back expect for 3 modules. This overall increase in integration is in agreement with previous findings [Fin+20].

3.3 DISCUSSION

In this chapter an application and comparison of the flexibility measure was presented. We set out to compare our method against the currently most used data-driven method described in [Bra+15], in which the computationally more expensive generalized Louvain algorithm was applied to derive the modular structure of the data [Blo+08; Muc+10; Bas+11; Jeu+]. It was shown that our

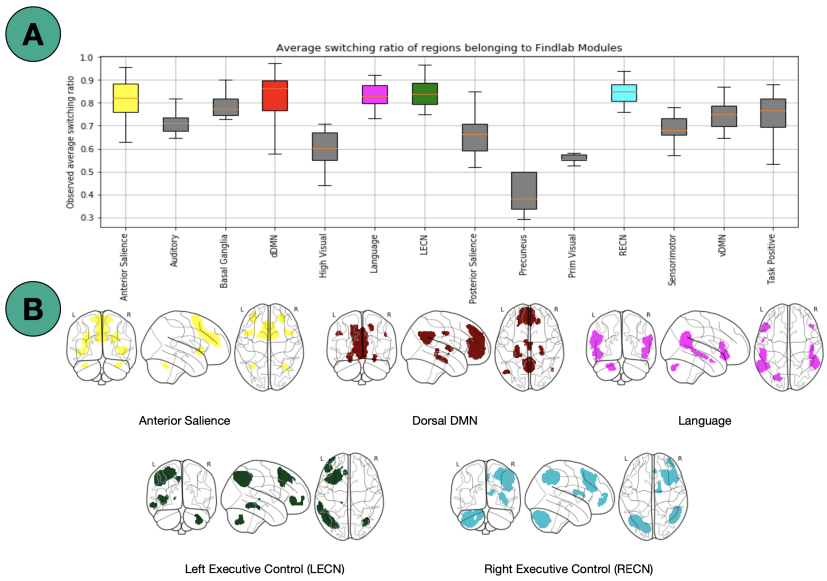

FIGURE 3.4. A) Average number of affiliation switches between consecutive windows for each FIND lab template network, averaged across all subjects. Abbreviations are listed in Table Table 3.1. B) Illustration of the four template networks for which its constituent nodes demonstrated the highest flexibility (http://findlab.stanford.edu/; [Shi+12]). [a]

[a] Python packages "nilearn", "scikit-learn" and "Matplotlib" are used for the visualizations [Ped+11; Hun07a]

template-based a-priori method is able to reveal a flexibility pattern during the N-back working memory task that is highly similar to the pattern found in [Bra+15]. The most notable difference between the results obtained with a-priori method and the Louvain algorithm was the absence of the small increase in flexibility during the transition of the 0- and 2-back blocks. Braun and colleagues [Bra+15] interpret this to reflect "dual-task" performance. We suggest an alternative explanation based on the current results: increased flexibility may be needed for switching tasks at the start of each new condition block (shown as a delayed peak in the middle of the marked blocks), while less flexibility may be needed during prolonged execution of the task in each block (shown as a delayed trough exactly in between blocks). As such, the periods of lower flexibility may show the preferred brain configuration for the execution of the task blocks. A further more theoretical analysis of a simulated BOLD signal with block induced inputs to help interpret the dual-task vs. no-dual-task dilemma is presented in Chapter 6.

As has been shown abundantly in the literature, the prefrontal cortex plays an important role in the performance of working-memory tasks [Owe+05;

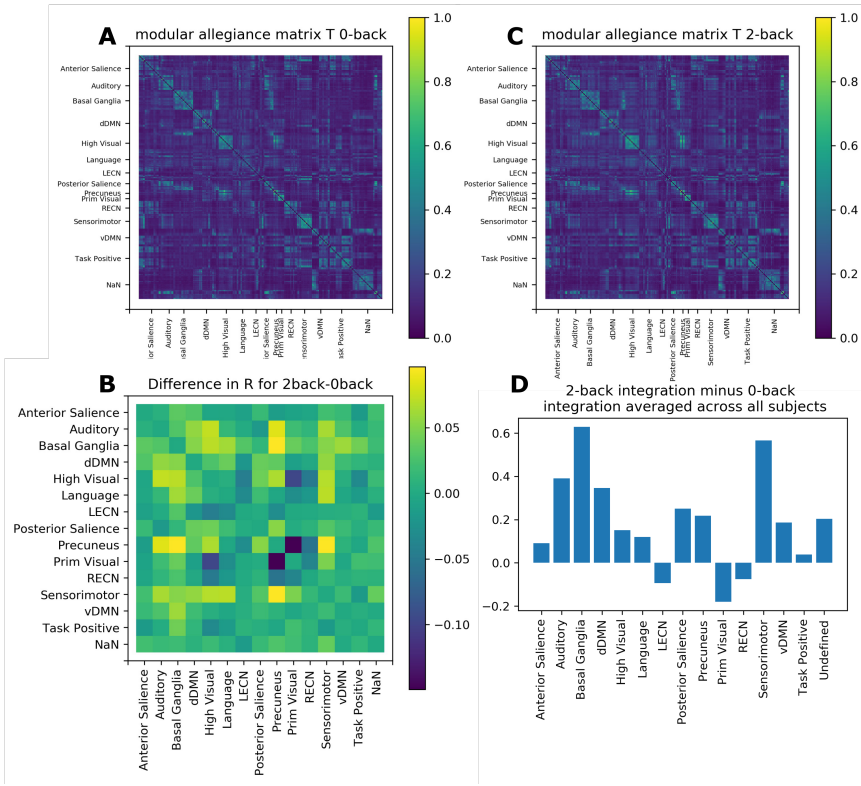

FIGURE 3.5. Modular allegiance and difference in integration. Diagonal elements of the matrices are set to be zero. A) Modular allegiance of 0-back condition and 0-back. B) Integration difference between 2-back and 0-back [$R_{2-back} - R_{0-back}$]. C) Modular allegiance of 2-back condition [to calculate a T matrix for one condition, only the windows with 80% of their time-points in that condition are used]. D) sum of rows (from C panel matrix) as each modules integration value.[a]

[a] Python packages "nilearn", "scikit-learn" and "Matplotlib" are used for the visualizations [Ped+11; Hun07a]

Cao+14; Min+15; BGS15]. Therefore, it is not surprising that we found nodes in the prefrontal cortex to show the most flexible behavior during execution of the N-back task. Moreover, at the modular level we see the highest flexibility in nodes that have an a-priori affiliation to the DMN, SN, L/RECN and language modules. The DMN is known to have an antagonistic relation with fronto-parietal networks, such as the L/RECN: when the latter is more active during cognitively demanding tasks (such as the N-back) the DMN is less active [Fox+05]. Interestingly, a key role has been assigned to the SN in allocating neural resources between more internally (DMN) or externally (ECN) oriented processes [Udd+11]. Taken together, we see these results as further proof of the a-priori method validity.

TABLE 3.2. Region a-priori Affiliation, columns marked "R" are region numbers and "M" columns are a-priori modular affiliations

R	M	R	M	R	M	R	M	R	M	R	M	R	M	R	M	R	M	R	M
1	1	26	11	51	6	76	2	101	15	126	13	151	9	176	4	201	5	226	3
2	1	27	7	52	11	77	1	102	15	127	13	152	9	177	9	202	5	227	3
3	7	28	11	53	12	78	8	103	13	128	14	153	4	178	4	203	5	228	3
4	11	29	14	54	12	79	2	104	13	129	14	154	4	179	4	204	5	229	3
5	4	30	14	55	12	80	6	105	5	130	14	155	12	180	1	205	5	230	3
6	4	31	14	56	12	81	7	106	5	131	8	156	12	181	13	206	5	231	3
7	1	32	11	57	12	82	15	107	14	132	8	157	2	182	13	207	9	232	3
8	1	33	6	58	12	83	6	108	14	133	14	158	2	183	1	208	9	233	3
9	1	34	11	59	12	84	15	109	15	134	14	159	14	184	1	209	14	234	3
10	1	35	6	60	12	85	6	110	15	135	13	160	14	185	4	210	14	235	8
11	1	36	6	61	2	86	6	111	13	136	13	161	12	186	4	211	15	236	8
12	1	37	1	62	2	87	6	112	13	137	7	162	12	187	4	212	15	237	4
13	4	38	1	63	14	88	6	113	13	138	11	163	8	188	4	213	15	238	4
14	4	39	6	64	14	89	15	114	13	139	14	164	15	189	5	214	15	239	8
15	1	40	1	65	13	90	15	115	15	140	14	165	1	190	5	215	4	240	3
16	11	41	4	66	8	91	14	116	15	141	8	166	1	191	10	216	4	241	4
17	7	42	4	67	12	92	14	117	15	142	11	167	1	192	10	217	4	242	3
18	11	43	6	68	12	93	15	118	15	143	6	168	1	193	5	218	4	243	3
19	1	44	11	69	15	94	15	119	13	144	6	169	8	194	10	219	3	244	3
20	1	45	15	70	15	95	7	120	15	145	8	170	8	195	10	220	3	245	3
21	1	46	15	71	2	96	15	121	6	146	8	171	15	196	5	221	3	246	3
22	11	47	4	72	2	97	14	122	6	147	13	172	15	197	10	222	3		
23	7	48	4	73	2	98	14	123	6	148	13	173	1	198	10	223	8		
24	11	49	4	74	2	99	7	124	6	149	13	174	1	199	5	224	15		
25	14	50	15	75	6	100	15	125	13	150	13	175	4	200	5	225	3		

Chapter 4: BRAIN FLEXIBILITY IN SCHIZOPHRENIA

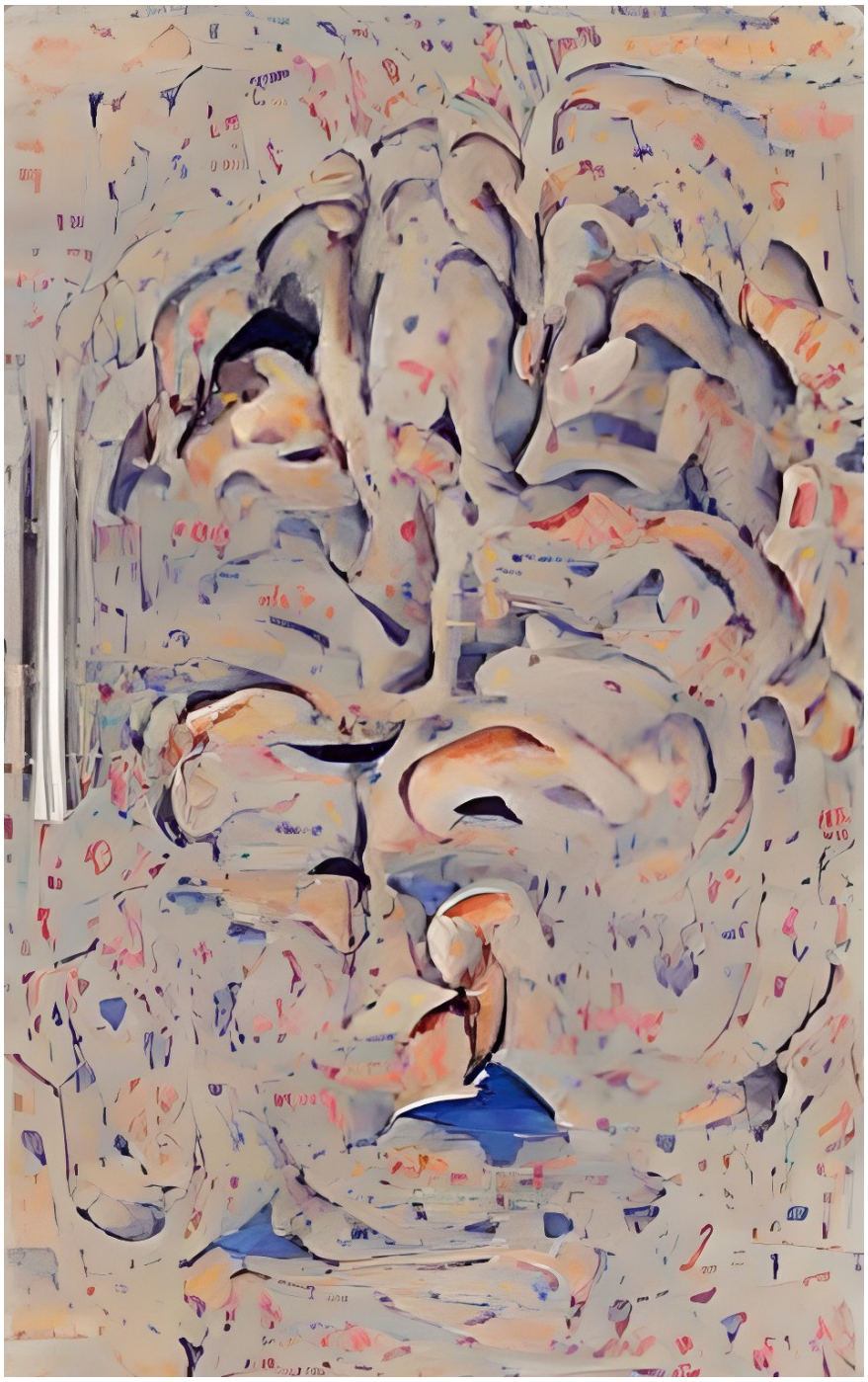

AI powered painting created by Wombo art [tea] using chapter 4 keywords.

Chapter 4

Brain Flexibility in Schizophrenia

"That's how the madness of the world tries to colonize you: from the outside in, forcing you to live in its reality."

- Jeff VanderMeer

The material discussed in this chapter has overlap with the content of the below mentioned extended abstract. Due to the differences in the nature of abstract and thesis, some topics and results are discussed more extensively here in the thesis.

Aberrant change in brain network flexibility during the performance of Theory of Mind task in schizophrenia patients

Narges Chinichian[1,2,3,*], Ahmad Ehyaei, Wladimir Tantchik[2], Pablo Reinhardt[2], Henrik Walter[2]

First published in: *Complex Networks 2022 Book of Abstracts* (2022).
DOI: 10.5281/zenodo.7183312

In the following chapter, an exploratory investigation of template-based brain flexibility measures (see chapters 2 and 3) is conducted on schizophrenia

[1]Institut for Theoretical Physics, Technical University of Berlin, Berlin, Germany. [2]Department of Psychiatriy and Psychotheray, CCM, Charité-Universitätsmedizin Berlin, corporate member of Freie Universität Berlin and Humboldt-Universität zu Berlin, Germany. [3]Bernstein Center for Computational Neuroscience, Berlin, Germany.

patients and healthy controls. During the performance of a Theory of Mind (ToM) task by both groups fMRI scans are collected. The analysis is performed on three distinct scales: the entire brain, groups of regions [modules], and individual regions. The results are then used to determine whether it is possible to accurately classify the subjects into the two groups of patients and controls using the flexibility-based features.

4.1 Theory of Mind (ToM)

Theory of Mind (ToM) is the ability to "see the others as intentional beings, to see their actions as motivated by mental states." and "the realization that the mental states of others may differ from one's own" [Tso18]. Or in other words, "the ability to infer intentions, dispositions, and beliefs of others"[Gre+08; Fri14; Bar+01].
Extreme social dysfunction may result from the inability to empathize with others and reflect on their mental state. Children between the ages of 3 and 5 begin developing the various components of theory of mind in different sequential orders depending on their culture, with the majority of studied cultures following this order[1] [WL04]:

1. Diverse Desires (DD): The understanding of existence of different desires, interests and motivations in others.

2. Diverse Beliefs (DB): The realization of existence of different beliefs about the same things in different people.

3. Knowledge Access (KA): The realization that other individuals can only know something if they have access to appropriate input/information. As an example, if Alice and Bob are in the same room with a chocolate bar on the table, and Alice leaves the room for a period of time while Bob places the chocolate in the drawer. In her return, Alice must be informed of this change in order to know it. Without observation or data, she will be unaware of the correct location of the chocolate bar.

4. False Beliefs (FB): Knowing that others can hold false beliefs and act based on them. In the above example, Alice can return and believe she can find a chocolate bar on the table.

5. Hidden Emotions (HE): The understanding that the emotion shown by people can differ from their real emotions.

1- The Chinese and Iranian children show faster KA and slower DB [Sha+11; Wel+06]

There are numerous paradigms designed to measure the theory of mind in children and adults that include stories, animations and games. Later in this chapter, a slide-based story is used to study ToM.

4.2 Schizophrenia

According to Diagnostic and Statistical Manual of Mental Disorders (DSM-5)[Ass+13], schizophrenia is diagnosed by the presence of at least two of the following criteria: "delusions", "hallucinations", "disorganized speech", "grossly disorganized or catatonic behavior", or what are known as "negative symptoms" (i.e. diminished emotional expression or avolition). At least one of these criteria must be from the first three, and they must persist for a significant portion of a 1-month period. For the non-clinical experts, these criteria can be explained in brief below:

- Delusion: Having firm beliefs that are not altered even when conflicting evidences are presented. The most common theme of delusion, called a "persecutory" delusion, is the belief that "one is going to be harmed, harassed and so forth by an individual, organization or other group".

- Hallucination: Perception of experience that occurs with no external stimulation. It can be with every sensory modality but DSM5 refers to the "auditory" hallucinations as the most common case in schizophrenia.

- Disorganized Thinking (Speech): Having severe disorganized, discontinued and incoherent speech (interpreted as the sign of disorganized and derailed thinking). Answering the questions with barely relevant or completely irrelevant statements and in rare cases, generating nearly incomprehensible speech ("word salad").

- Grossly Disorganized or Catatonic Behaviour: Showing abnormal motor behaviours ranging from "childlike silliness" to "unpredictable agitation" that can cause problems in the performance of various sorts of goal-directed daily activities. Catatonic behaviour can be defined as the decreased reactivity to the inputs from ones environment, it can be manifested in the forms of inappropriate, non-existing or excessive motor response to the situation.

- Negative Symptoms: Refer to decrease in normal motivation-related functions and behaviours [CS20]. The two prominent negative symptoms in schizophernia are the diminished emotional expression (reduced

emotional emphasis in speech, like not changing the intonation, not making eyes contact or showing body gestures in general) and avolition (lack of interest and motivation to initiate or follow purposeful activities).

A meta analysis by Sprong et al [Spr+07], which investigated 29 studies of mentalizing in schizophrenia (on a total number of 1518 participants) from publications between 1993 and 2006, found that the patients showed consistent significant deficit in their theory of mind. Even patients in remission still showed the deficits and IQ, gender and age did not significantly affect the mean effect size.

In the following sections, we investigate if the difference in brain reaction to a variation of ToM task between schizophrenia and control group is reflected in the flexibility of brain functional network detected by the template flexibility method introduced in chapters 2 and 3.

4.3 Subject Selection and Scanning

64 healthy controls and 64 schizophrenia patients were matched and selected from the IntegraMent (Integrated Understanding of Causes and Mechanisms of Mental Disorders) multi-centric study at Charité Universitätsklinikum Berlin and the Zentrum für Seelische Gesundheit in Mannheim. The subjects were recruited using both advertisements and psychiatric clinics recommendations and they all gave written informed consent for their participation. Local ethics committees approved the study. All of the schizophrenia patients were diagnosed (F20.x) according to ICD-10 by professional psychiatrists. In addition, to confirm the diagnosis, all patients went through a clinical interview for DSM-IV(SCID-I). The matching of subjects for sex and testing site was done by fuzzy extension for SPSS Version 22 (IBM Corp. Released 2013. IBM SPSS Statistics for Windows, Version 22.0. Armonk, NY: IBM Corp.). More detail on the selection of subset can be found in Tantchik et al [Tan+22].

4.3.1 Task and Preprocessing

The part of the multi-centric study data used in the present study contains Blood-oxygen-level dependent fMRI collected during the performance of the cartoon ToM paradigm first introduced by Schnell and colleagues and later used in several further studies [Sch+11; Wal+11; Moh+14; Moh+16]. Subjects were presented short cartoon stories of 3 images per trial and they were asked to evaluate either the change in the main character's affective state of mind (options: better/equal/worst) which is ToM condition or the number of living

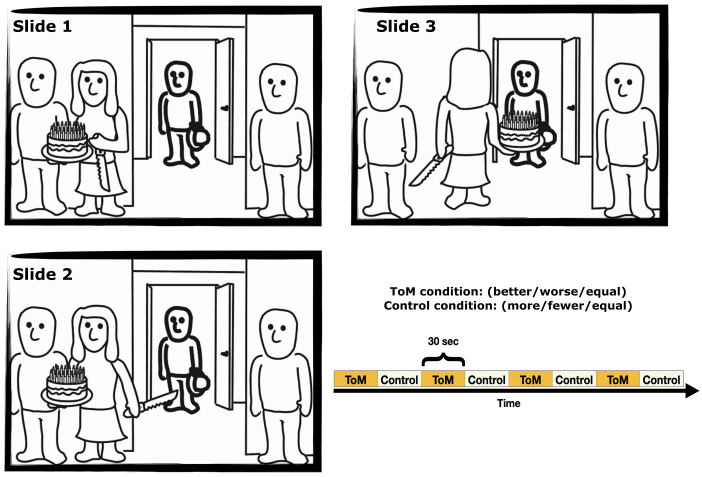

FIGURE 4.1. Sample cartoons from Theory of Mind (ToM) task
During ToM condition, The protagonist's (character in bold line) change in affective state should be described by participants as better, worse or equal. During the control condition, the number of living beings should be counted (more/fewer/equal). Each condition takes ~30 s including the instruction.

beings (options: more/equal/less) considered the control condition. See Figure 4.1 for an example of cartoons. The protagonist is marked with bold lines. The two conditions were presented in alternating blocks. Each condition contained 8 trials. Slides were presented each for 7.5 seconds (total of ~23 seconds) and a 6.5 seconds instruction slide was shown at the start of each block (adding up to the blocks of ~30 seconds).

Blood-oxygen-level dependent fMRI was performed using identical scanning protocols with Siemens Trio 3T MR scanners in Berlin and Mannheim. TR of 2sec. and TE 30ms, echoplanar imaging (EPI) with 240 volumes of 28 slices of 4mm thickness + 25% gap, flip angle 80° with FOV set to 192mm in descending slice order. Quality-control measurements were conducted at all sites on every day of data collection according to a multicenter quality-assurance protocol, revealing stable parameters over time. Preprocessing was done using a similar pipeline from Erk et al [Erk+17] in SPM8. It included realignment to mean image (movement parameters < 3mm and < 1.7 degrees between volumes), slice-time correction, normalization to the standard MNI (Montreal Neurological Institute) space with $3 \times 3 \times 3$ mm voxel size and Gaussian kernel smoothing with a 9 mm FWHM.

4.4 Dynamical Functional Network

Time series from 246 Brainnetome atlas [Fan+16] regions were then extracted from the preprocessed data using Python nilearn package [Ped+11]. Each Brainnetome region is referred to as a node and is affiliated to one of the modules (group of nodes, also referred to as “Networks” in the neuroscience literature. We avoid the potentially ambiguous usage of "Network" term to refer to modules in this work) of the brain introduced by Findlab [Shi+12] shown in table Table 4.1. Sliding windows of 15 time-points lengths (30 seconds) with an overlap of 14 time-points were used to observe the dynamics of the network. In each sliding window, pairwise Pearson correlation coefficients were calculated between the time series of each pair of nodes as a measure of cooperation between that pair of nodes.
A total of 237 time points (~7.5 minutes) were used to generate 222 sliding windows. These pairwise values form a matrix that is then treated as a weighted adjacency matrix of a network assigned to a window. The method for the calculation of flexibility introduced in chapter 2 is then applied. This method finds the deformation of a-priori modules in the brain by comparing the connection weights of the weighted adjacency matrix and pre-defined affiliation of the nodes. In each weighted adjacency matrix, the absolute value of functional connections between every single node and all the members of every module is calculated and then normalized to the size of each module. The resulting weights are compared to choose a “winner” affiliation. The winner affiliation can be the same or different from the a-priori affiliation. Assigning winner affiliations to every node, a new set of affiliations for all nodes in the window is achieved.

4.5 Whole-Brain Scale

By tracking the ratio of nodes that change their winner affiliation between the two consecutive windows a “whole-brain flexibility” (WBF) value between 0 and 1 is determined between every 2 consecutive windows. A WBF time serie of length 221 (from 222 windows) is therefore generated for each subject (resulting in 64 + 64 = 128 time series). Figure 4.3 shows these time series. A more detailed explanation of the method with the calculation steps is found in chapter 2. The python script for the calculation of these time series is available on the online thesis repository. For every time serie, the following values are calculated and saved as the features later used in the classifier:

I Average along the time axis.

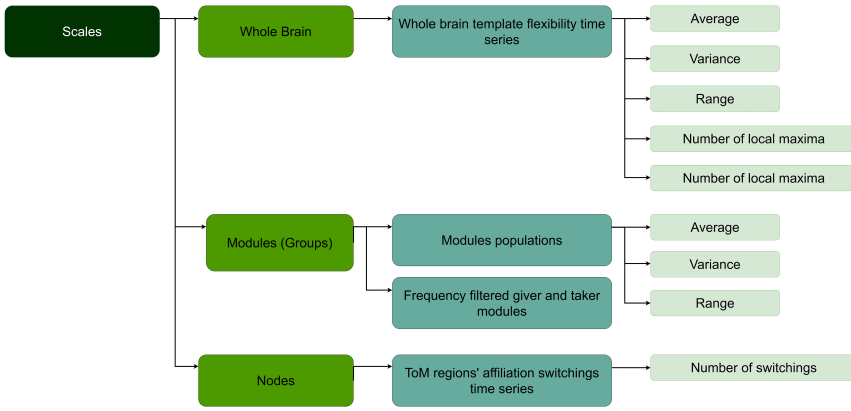

Figure 4.2. A summary of flexibility-based values calculated for each subject
On the whole brain scale, the WBF time series are calculated and average, variance, range, number of maxima and number of minima for each time serie are extracted and saved.
On the module scale, the population time series for all 15 Findlab modules are extracted and average, variance and range are calculated and saved. In addition, modules that had a dominant pattern of giving or taking members from or to other modules in the frequency associated with the task are marked and saved.
Finally, on node scale, 5 regions associated with ToM task are selected and the the number of affiliation-switching for each of them is counted.

II Variance along the time axis.

III Range (maximum - minimum along time axis).

IV Number of local minima.

V Number of local maxima.

4.6 Module Scale

4.6.1 Module Populations

The total number of nodes that belong to a single module at any given time can be regarded as the population of that module. The 15 Findlab modules listed in Table 4.1 have changing population during the performance of a cognitive task. Population for each module is calculated by counting the regions that had their winner affiliations to that module at any given window (see the averaged population dynamics plot averaged in each group in supplementary material Figure S1). For every time serie, similar to the previous measure, the average,

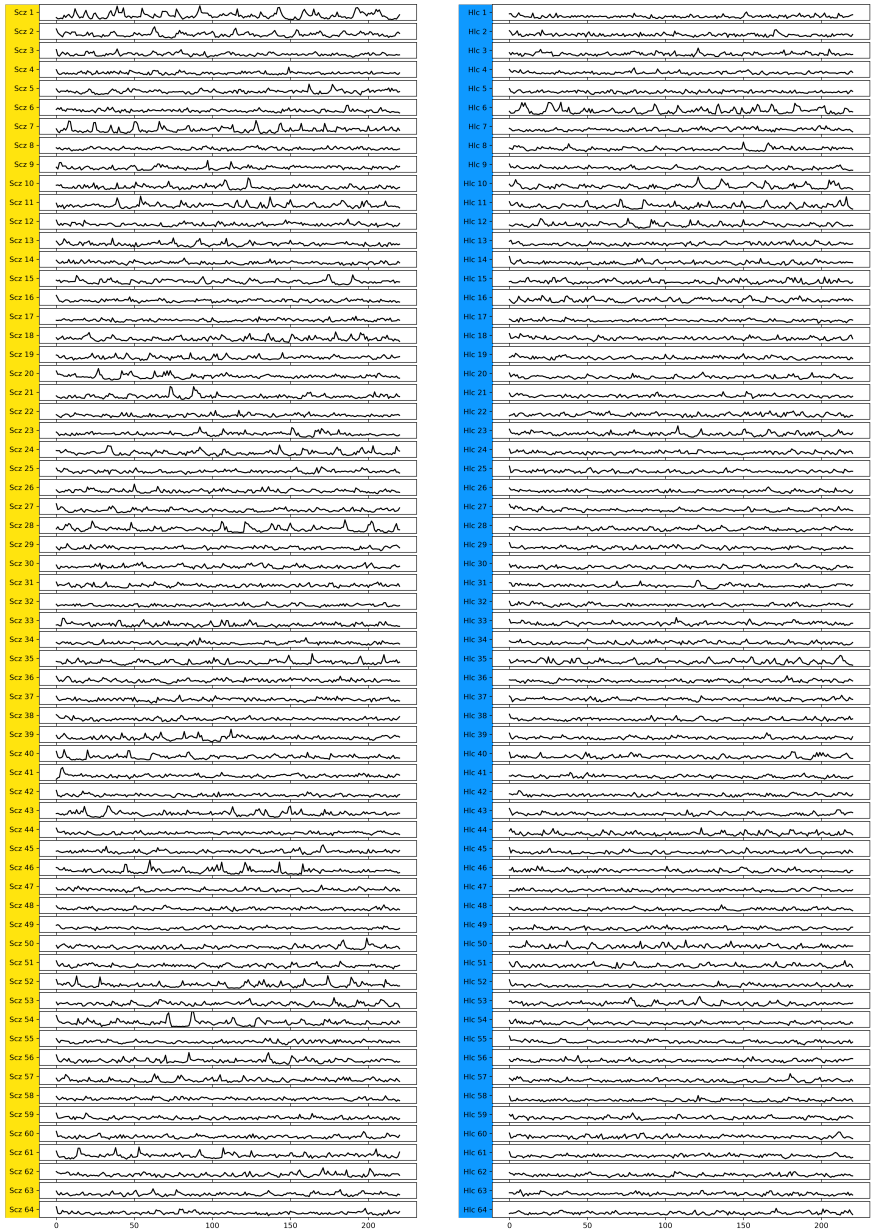

FIGURE 4.3. All whole-brain flexibility time series for schizophrenia patients and healthy controls
Right column shows all healthy controls and left column the schizophrenia patients. Y axis is template flexibility value for the whole brain (WBF) and x axis is time.

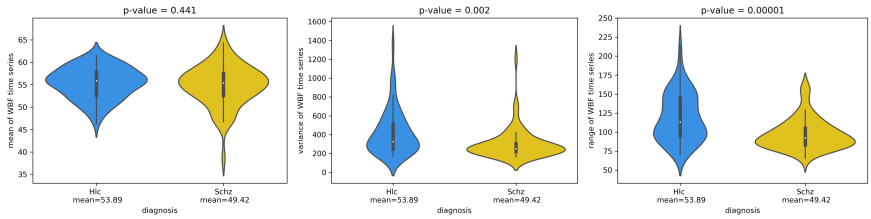

FIGURE 4.4. WBF (whole-brain flexibility) comparison
Average, variance and range of every WBF time serie is calculated and the 2 subject groups are compared based on these measures. Average, in contrast to the other two measures, is not showing a significant difference.

variance and range along the time axis were calculated and the results were saved for every module and participant.

4.6.2 *Frequency Filtered Give and Take*

When a node moves from one module to another between two consecutive time windows, one module loses a member and another gains one. We call these modules the "giver" [the module which loses a member] and "taker" [the module which gains a member] modules respectively. For each time step t between two windows, a 15×15 non-symmetric matrix called D_t with elements $D_{t,ij}$ showing the number of nodes that move from module i to module j in t is calculated. Extracting the information of a fixed i and j through time dimension, a time serie of giving-taking between module i and j is achieved. If this time

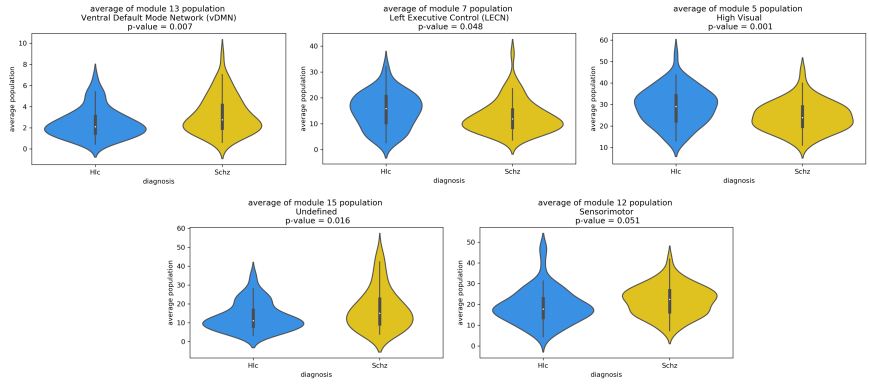

FIGURE 4.5. Significantly different module population averages
Blue and gold violin plots respectively show the control group and schizophrenia patients average module populations. The 5 modules (high visual, LECN, vDMN, sensorimotor and undefined [regions not associated with Findlab modules]) show considerably small p-values (=< 0.051).

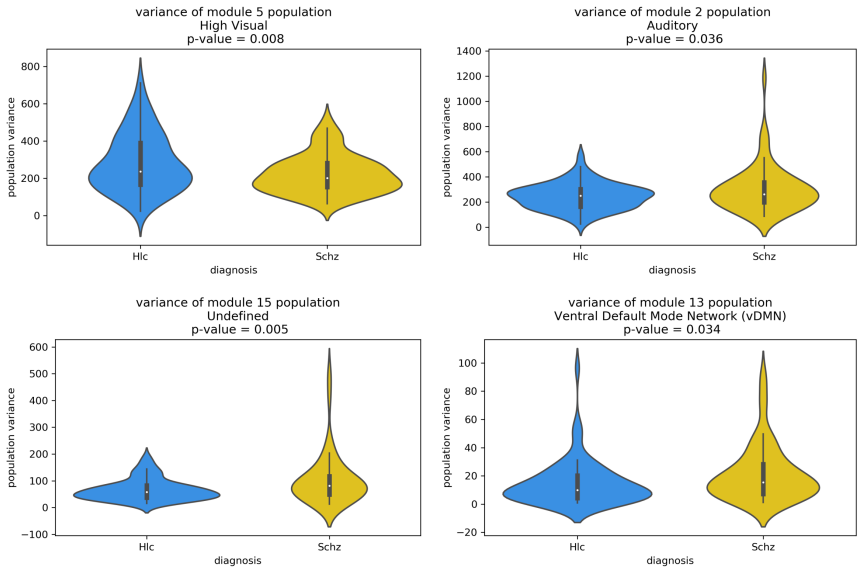

Figure 4.6. Significantly different module population variances
Blue and gold violin plots respectively show the control group and schizophrenia patients variance of module populations. The 4 modules (high visual, Auditory, vDMN, and undefined [regions not associated with Findlab modules]) show considerably small p-values (=< 0.036).

serie shows a peak in the frequency value close to our change of task conditions frequency, the giving-taking behaviour is associated with the performance of the ToM task. The task-associated giver and taker modules of each subject that show a repetitive behaviour in the range of +/-5 seconds from the task period were extracted and saved.

4.7 Node Scale

The vectors showing the affiliations of one single node over time could be extracted and studied individually. A mask of ToM-associated areas generated by Neurosynth† engine from 181 studies was overlaid by a Brainnetome atlas map of regions. Figure 4.9 shows Brainnetome regions and ToM associated area. Brainnetome regions with higher than 50% overlap with ToM areas were marked and selected to be investigated. These regions are the following five:

- Region 14: A10m, medial area 10 (SFG, Superior Frontal Gyrus, Frontal Lobe)

† https://neurosynth.org/

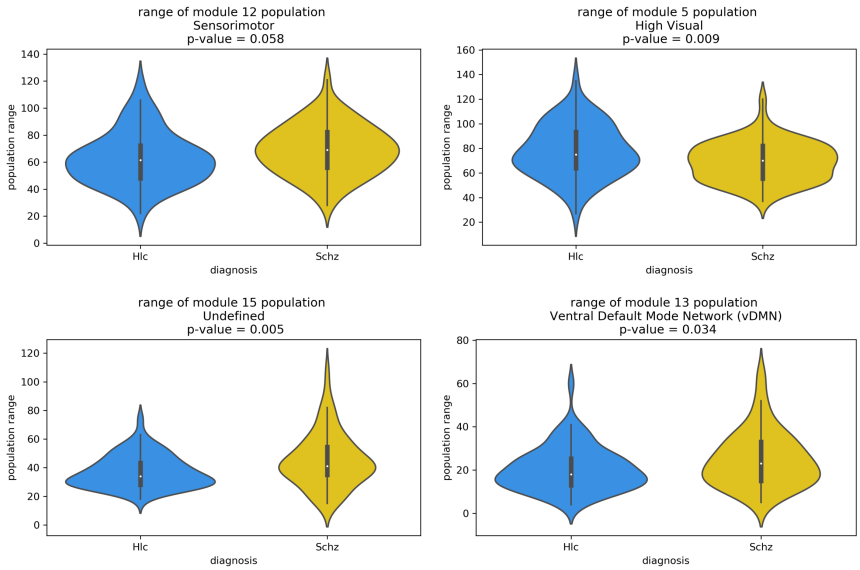

FIGURE 4.7. Significantly different module population ranges
Blue and gold violin plots respectively show the control group and schizophrenia patients range of module populations. The 4 modules (high visual, vDMN, sensorimotor and undefined [regions not associated with Findlab modules]) show considerably small p-values (=< 0.058).

- Region 83: Left A21r, rostral area 21 (MTG, Middle Temporal Gyrus, Temporal Lobe)
- Region 84: Right A21r, rostral area 21 (MTG, Middle Temporal Gyrus, Temporal Lobe)

TABLE 4.1. Number and Name of modules.

Module Number (Short Name)	Module Name
Module 1 (M1)	Anterior Salience
Module 2 (M2)	Auditory
Module 3 (M3)	Basal Ganglia
Module 4 (M4)	Dorsal Default Mode Network (dDMN)
Module 5 (M5)	High Visual
Module 6 (M6)	Language
Module 7 (M7)	Left Executive Control (LECN)
Module 8 (M8)	Posterior Salience
Module 9 (M9)	Precuneus
Module 10 (M10)	Primary Visual
Module 11 (M11)	Right Executive Control (RECN)
Module 12 (M12)	Sensorimotor
Module 13 (M13)	Ventral Default Mode Network (vDMN)
Module 14 (M14)	Task Positive
Module 15 (M15)	Undefined (untagged nodes listed in Figure 4.13)

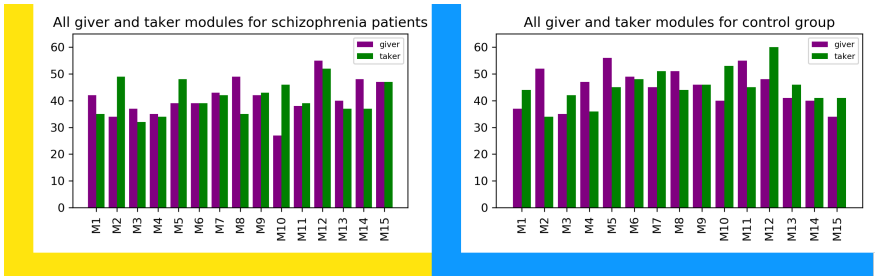

FIGURE 4.8. All non-unique giver and taker modules for both groups When a node moves from one module to another between two consecutive time windows, one module loses a member and another gains one. We call these modules the "giver" [the module which loses a member] and "taker" [the module which gains a member] modules respectively.
For each time step t between two windows, a 15×15 non-symmetric matrix called D_t with elements $D_{t,ij}$ showing the number of nodes that move from module i to module j in t is calculated.
Extracting the information of a fixed i and j through time dimension, a time serie of giving-taking between module i and j is achieved. If this time serie shows a peak in the frequency value close to our change of task conditions frequency, the giving-taking behaviour is associated with the performance of the ToM task.
The task-associated giver and taker modules of each subject that show a repetitive behaviour in the range of +/-5 seconds from the task period were extracted and and recorded to generate these plots. Each bar shows how many times a module was found as a giver (purpule) or taker(green)
Right plot shows healthy controls and left plot the schizophrenia patients.

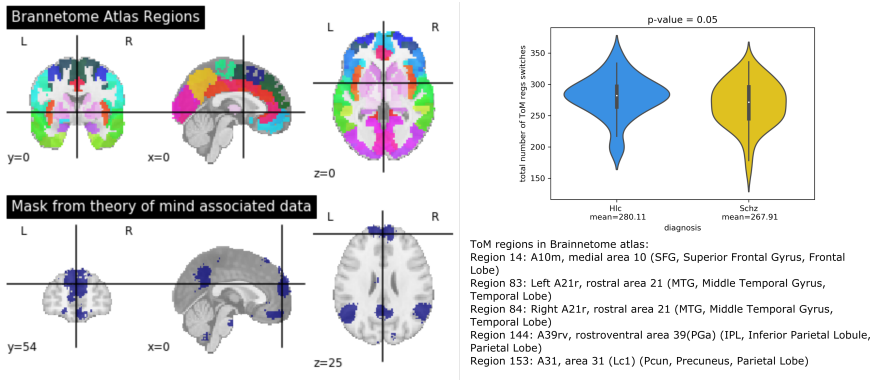

FIGURE 4.9. Brainnetome and ToM regions
There are 5 regions from Brainnetome atlas that have higher than 50% ovelap with ToM mask.

- Region 144: A39rv, rostroventral area 39(PGa) (IPL, Inferior Parietal Lobule, Parietal Lobe)
- Region 153: A31, area 31 (Lc1) (Pcun, Precuneus, Parietal Lobe)

For each of these regions, the number of affiliation-switches (see chapter 2)

was calculated.

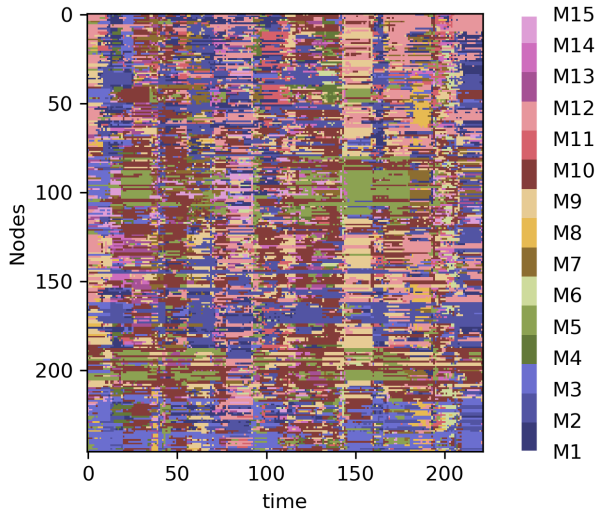

Figure 4.10. All 246 nodes affiliations over time for one sample subject
Visualization of affiliation change over time for all nodes in one subject.

4.8 Scales Results

Schizophrenia patients and healthy controls show significantly different variance and range in their WBF time series (see Figure 4.4) while their mean flexibilities are not significantly different. Looking at Figure 4.3, it can be observed that the schizophrenia group subjects are more likely to show an aberrant increase in their WBF at irregular times.

Our investigations on the module population dynamics suggests that there are significantly different behaviours in modules population dynamics of Auditory, High Visual, LECN, sensorimotor, vDMN and the 15th undefined module (see chapter 2 for the definition of this 15th module and Figure 4.13 for the list of regions in it). The differences are observed using the 3 measures (average, variance and range) on the module population time series (see Figure 4.5, Figure 4.6 and Figure 4.7). Abnormalities in the DMN and Executive Control Networks have been extensively reported in the resting state fMRI studies of schizophrenia patients [CEP09; Sal+10; Lit+15]. Our findings suggest that the different behaviours of DMN and ECN extend to the mentalizing tasks.

An overall decrease in give/take changes associated with the task time-pattern of ~30 s in schizophrenia is observed (height of all bars in Figure 4.8). This in turn agrees with the lower contrast between ToM and control conditions observed by several studies. The contrast is explained by either hypomentalization during ToM or hypermentalization during the control condition [Abu99; Fri04; LB08; Cia+15]. The results suggest that the schizophrenic brain distinguishes less between TOM and control stimuli than a healthy brain regardless of whether hyper- or hypo-mentalizing is the source of this change in the contrast.

In addition, some columns in Figure 4.8 show a different trend between the 2 groups. Module 2 [Auditory] and module 5 [High Visual], are dominantly giver modules in the control group while they act as stronger takers in the schizophrenia patients. This suggests that these modules are receiving reinforcement from other modules and expanding in a frequency corresponding to the task-blocks. Several schizophrenia studies in fact suggest that the deficits occurring at the stage of sensory processing and perception are the bottom-up reasons for the dysfunction in higher cognitive levels in patients suffering from schizophrenia [Jav09b; Jav09a; JS15; Bor+18].
The different trends observed by our method in the auditory, visual and sensorimotor modules could be interpreted as a further sign of perception-related abnormalities associated with schizophrenia.

4.9 Classification of Control Subjects and Schizophrenia Patients

A GLM model with L2 (ridge regression) penalties (alpha = 0), a gradient descent solver and logistic regression (binomial family) [Nyk+22] from h2o python package [H2O20] was used on a table with all the three level values (whole brain, modules and nodes) listed in Figure 4.2 as columns. The giver/taker columns were filtered to contain only columns with at least 10 non-zero values. The total number of columns after this filtering was 81. The mean accuracy in 10 fold for the classification was 0.74 (see Figure 4.11 for the cross-validation metrics summary). The relatively small dataset for training and test results in considerable fluctuation in accuracy (each prediction moves the accuracy by ~8%) within different folds but the classification distinguishes between the two groups with a significant margin. The contribution of columns as the coefficients in the classification are shown in Figure 4.12. The most influential five columns are:

The alpha parameter controls the distribution between the l1 (LASSO) and l2 (ridge regression) penalties. The penalty is defined as [Nyk+22]:

$$P(\alpha, \beta) = (1-\alpha)/2||\beta||_2^2 + \alpha||\beta||_1 = \Sigma_j[(1\alpha)/2\beta_j^2 + \alpha|\beta_j|]$$

	mean	sd	cv_1_valid	cv_2_valid	cv_3_valid	cv_4_valid	cv_5_valid	cv_6_valid	cv_7_valid	cv_8_valid	cv_9_valid	cv_10_valid
accuracy	0.742608	0.090405	0.666667	0.800000	0.875000	0.750000	0.583333	0.692308	0.666667	0.842105	0.750000	0.800000
auc	0.706121	0.115547	0.745455	0.777778	0.933333	0.666667	0.656250	0.650000	0.512500	0.769231	0.750000	0.600000
err	0.257392	0.090405	0.333333	0.200000	0.125000	0.250000	0.416667	0.307692	0.333333	0.157895	0.250000	0.200000
err_count	3.400000	2.065591	7.000000	3.000000	1.000000	1.000000	5.000000	4.000000	6.000000	3.000000	2.000000	2.000000
f0point5	0.699137	0.120361	0.642857	0.735294	0.862069	0.555556	0.500000	0.729167	0.625000	0.869565	0.714286	0.757576
f1	0.760537	0.103100	0.720000	0.769231	0.909091	0.666667	0.615385	0.777778	0.625000	0.888889	0.800000	0.833333
f2	0.842195	0.094967	0.818182	0.806452	0.961538	0.833333	0.800000	0.833333	0.625000	0.909091	0.909091	0.925926
lift_top_group	1.428654	1.084548	2.100000	2.500000	1.600000	0.000000	3.000000	1.625000	0.000000	1.461538	2.000000	0.000000
logloss	0.605597	0.122935	0.606646	0.565684	0.309346	0.720407	0.679225	0.692103	0.693523	0.567010	0.535866	0.686156
max_per_class_error	0.426768	0.133408	0.545455	0.222222	0.333333	0.333333	0.625000	0.600000	0.375000	0.333333	0.500000	0.400000
mcc	0.522010	0.149175	0.391965	0.600099	0.745356	0.577350	0.408248	0.317543	0.325000	0.622532	0.577350	0.654654
mean_per_class_accuracy	0.748187	0.075251	0.677273	0.805556	0.833333	0.833333	0.687500	0.637500	0.662500	0.794872	0.750000	0.800000
mean_per_class_error	0.251813	0.075251	0.322727	0.194444	0.166667	0.166667	0.312500	0.362500	0.337500	0.205128	0.250000	0.200000
mse	0.213540	0.047916	0.211321	0.192809	0.105944	0.263545	0.243125	0.249442	0.250165	0.190718	0.181579	0.246754
null_deviance	17.928375	7.712128	29.132708	20.964321	11.159250	5.610740	16.925781	18.187233	25.031984	27.318438	11.090355	13.862944
pr_auc	0.656512	0.198501	0.747247	0.702518	0.963536	0.306853	0.584491	0.739754	0.437974	0.848301	0.735552	0.498895
precision	0.665516	0.130398	0.600000	0.714286	0.833333	0.500000	0.444444	0.700000	0.625000	0.857143	0.666667	0.714286
r2	0.073469	0.252445	0.152796	0.196629	0.547974	-0.405572	-0.094060	-0.053894	-0.013169	0.117317	0.273684	0.012983
recall	0.915641	0.119620	0.900000	0.833333	1.000000	1.000000	1.000000	0.875000	0.625000	0.923077	1.000000	1.000000
residual_deviance	15.626870	7.392748	25.479120	16.970522	4.949533	5.763259	16.301400	17.994690	24.966812	21.546385	8.573858	13.723117

Figure 4.11. Cross-validation metrics summary
10 fold cross-validation metrics summary. For more information on how each value is calculated see [H2O]

1. Module 13 (ventral default mode) average population
2. Module 15 (un-tagged regions, listed in Figure 4.13) average population
3. WBF time serie variance
4. M7 (Left Executive Control) module sending members to M15 aligned with the task frequency
5. M2 (Auditory) module sending members to M7 aligned with the task frequency

4.9.1 Raw data classification

To further validate, that the flexibility-based measures improved the classification of subjects into controls and schizophrenia patients, we tested classification of raw data using an RNN+CNN neural network model from Tensorflow [Mar+15]. The highest accuracy achieved from the raw-data classification was 63%. This further confirms that the flexibility measures not only help in the reduction of data size but also introduce more interpretability to the results and improve the classification compared to the original fMRI time series.

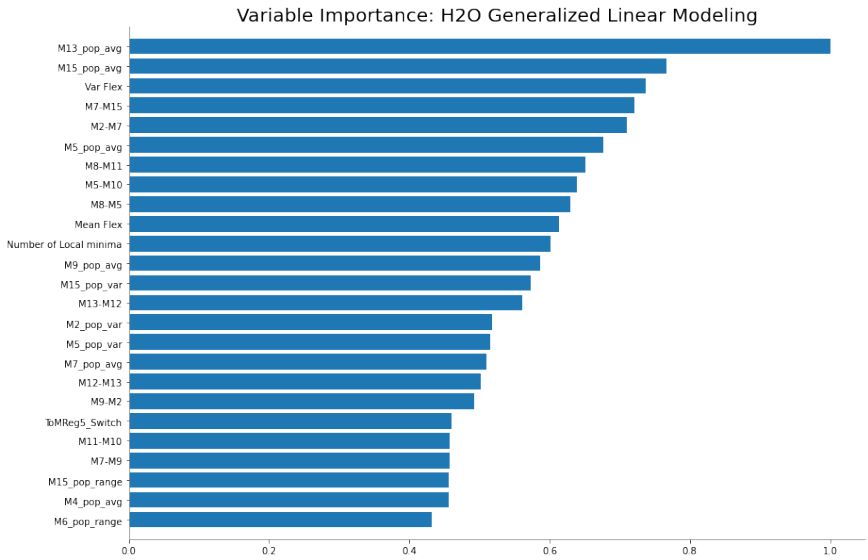

Figure 4.12. GLM variable importance
Variable coefficients sorted based on their importance in GLM model.

4.10 Discussion

Our exploratory research shows significant difference in the reconfiguration of functional [dynamical] brain networks between schizophrenia patients and healthy controls. The differences are observed on 3 scales of whole-brain, modules and nodes. A classification of subjects based on their flexibility-based measures succeeds in differentiating the 2 groups with a higher than 20% above chance accuracy. The significant differences found in the perception related modules including auditory, visual and sensorimotor support the bottom-up deficit hypothesis while the further distinguished behaviours in executive control and default mode modules are in line with the previous resting-state fMRI findings in schizophrenia patients.

Our findings show a rather small gap in the reconfiguration of the 5 selected ToM associated regions in the 2 groups. In fact, the first ToM region (5th region) to appear on the classification variable importance list (Figure 4.12) ranks 20th. There are several limitations to be addressed in this study. Our interpretations lack a bigger independent dataset validation. The relatively small dataset of only 128 subjects, is a serious limit to the interpretation of different findings. A further investigation on an independent dataset could help in a better training and validation process of our classifier.

Our flexibility method, though comprehensive and easy to calculate, is new and therefore not extensively available in the literature and the results could not be

compared one-to-one with similar studies due to the different approaches in the studies. The 15th module with regions listed in Figure 4.13, is not fitting a unified Findlab definition and therefore the differences between the two groups based on the behaviour of module 15 are not easily interpretable.

Despite all the limitations mentioned, we believe that the findings in this study could pave the way for the design of further experiments and if they are reproduced, they will provide us with a deeper understanding of the underlying mechanism in cognitive deficits of schizophrenia patients and the share of bottom-up or top-down deficits in the cognitive failures associated with severe cases of schizophrenia.

4.11 Chapter Summary

In this chapter, the flexibility-based measures of brain network obtained from fMRI data collected during the theory of mind (ToM) cognitive task for 2 groups of schizophrenia patients and healthy controls were calculated and compared. Based on these measures, the two groups could be distinguished with an average accuracy of 74% while the algorithm relied heavily on the information from population of modules 13 and 15 and variance of whole-brain flexibility together with the member exchange of modules 7 [Left Executive Control (LECN)] and 15 [Regions that were not tagged based on the Findlab atlas] and modules 2 [Auditory] and 7 [Left Executive Control (LECN)].

Lobe	Gyrus	Left and Right Hemisphere	Label ID.L	Label ID.R
Frontal Lobe	OrG, Orbital Gyrus	OrG_L(R)_6_3	45	46
		OrG_L(R)_6_5		50
Temporal Lobe	STG, Superior Temporal Gyrus	STG_L(R)_6_1	69	70
	MTG, Middle Temporal Gyrus	MTG_L(R)_4_1		82
		MTG_L(R)_4_2		84
	ITG, Inferior Temporal Gyrus	ITG_L(R)_7_1	89	90
		ITG_L(R)_7_3	93	94
		ITG_L(R)_7_4		96
		ITG_L(R)_7_6		100
		ITG_L(R)_7_7	101	102
	PhG, Parahippocampal Gyrus	PhG_L(R)_6_1	109	110
		PhG_L(R)_6_4	115	116
		PhG_L(R)_6_5	117	118
		PhG_L(R)_6_6		120
Insular Lobe	INS, Insular Gyrus	INS_L(R)_6_1		164
		INS_L(R)_6_5	171	172
Subcortical Nuclei	Amyg, Amygdala	Amyg_L(R)_2_1	211	212
		Amyg_L(R)_2_2	213	214
	BG, Basal Ganglia	BG_L(R)_6_3		224

Figure 4.13. Module 15 members
Regions in the 15th module and where they belong to.

Chapter 5: OTHER FUNCTIONAL MAGNETIC RESONANCE IMAGING (FMRI) STUDIES

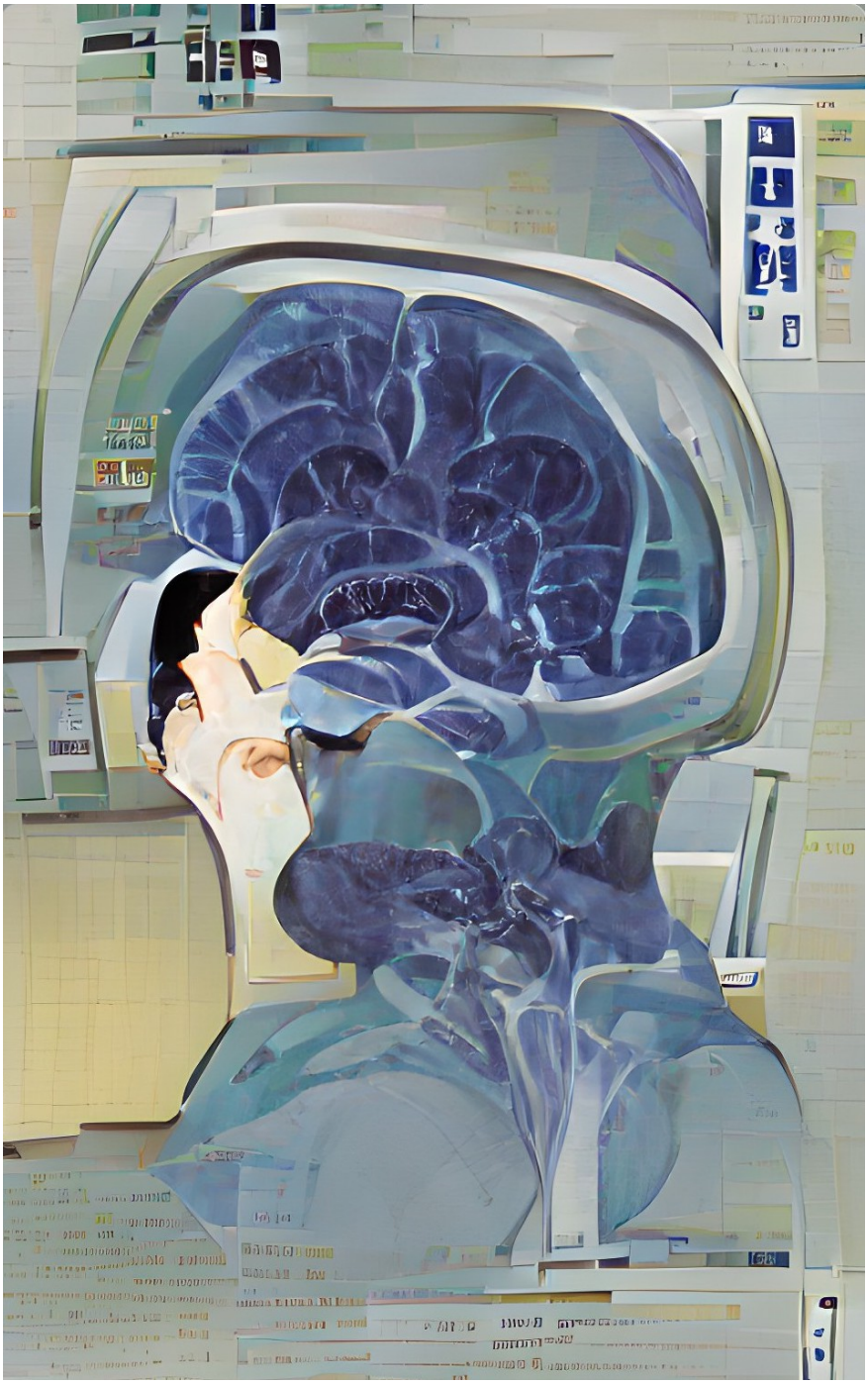

AI powered painting created by Wombo art [tea] using chapter 5 keywords.

Chapter 5

A Short Report on Another fMRI Study

"How are psychiatric and neurological disorders different? At the moment, the most obvious difference is the symptoms that patients experience. Neurological disorders tend to produce unusual behavior, or fragmentation of behavior into component parts, such as unusual movements of a person's head or arms, or loss of motor control. By contrast, the major psychiatric disorders are often characterized by exaggerations of everyday behavior. We all feel despondent occasionally, but this feeling is dramatically amplified in depression. We all experience euphoria when things go well, but that feeling goes into overdrive in the manic phase of bipolar disorder. Normal fear and pleasure seeking can spiral into severe anxiety states and addiction. Even certain hallucinations and delusions from schizophrenia bear some resemblance to events that occur in our dreams."

- Eric Kandel

The mini-chapter here is a short report on the findings from the collaborations with Justine Dickhoff and Marie-José van Tol from University of Groningen, in the Netherlands.

Time-averaged and dynamic resting-state functional connectivity characterizations in patients with suicide risk

Justine Dickhoff[1], Jan-Bernard C. Marsman[1], Narges Chinichian[2,3,4] , Ilya M. Veer[3,5], Esther M. Opmeer[6], Richard Dinga[5] , Nic J.A. van der Wee[7], Dick J. Veltman[8], André Aleman[1,9], Marie-José van Tol[1]

[1]University of Groningen, University Medical Center Groningen, Department of Biomedical Sciences

Manuscript in preparation (2022).

Narges Chinichian's Contribution:
The flexibility-based measures were primarily calculated by Narges Chinichian using the method from chapter 2 and the python codes presented in the online repository, in collaboration with the first author Justine Dickhoff and senior author of the chapter 2 method draft, Ilya Veer.

5.1 Flexibility and Suicidality

A total of 95 people who met the criteria for Major Depressive Disorder and/or common anxiety disorders were selected from the Netherlands Study of Depression and Anxiety (NESDA). Twenty-one had made at least one suicide attempt in the past, and 27 had ongoing suicidal ideation. Resting state 3T fMRI data was employed to investigate the suicidality and mood disorder effect on the connectivity and reconfiguration of brain network.

Using six of the template modules (Anterior and posterior cingulo-opercular (anterior/posterior salience), dorsal and ventral default mode (dDMN, vDMN) and left and right central executive-network (LECN and RECN), see chapter 3 for the full list of Findlab modules in table Table 3.1), data from the resting state was examined by a dual regression technique.
Two different comparison were made in the study:
1- A comparison between participants with (21 subjects) and without (74 subjects) a history of suicide attempt.
2- A comparison between individuals with (27 subjects) and without (68 subjects) suicidal ideation.
In total, 10 participants had both the history of suicide attempt and ongoing suicidal ideation.

Suicidal ideation and no ideation differed in whole-brain flexibility (i.e., the total change of network connections across time of all 246 nodes) ($F(1,81)= 5.33$, $p=.02$, $\eta^2 = .062$), but the other 2 groups (suicidal attempt and no attempt)

of Cells and Systems, Cognitive Neuroscience Center, Antonius Deusinglaan 1, 9713AV Groningen, the Netherlands. [2]Institut for Theoretical Physics, Technical University of Berlin, Berlin, Germany. [3]Department of Psychiatriy and Psychotheray, CCM, Charité-Universitätsmedizin Berlin, corporate member of Freie Universität Berlin and Humboldt-Universität zu Berlin, Germany. [4]Bernstein Center for Computational Neuroscience, Berlin, Germany. [5]Donders Institute for Brain, Cognition and Behavior, Nijmegen, the Netherlands; Radboud University Medical Center, Nijmegen, the Netherlands. [6]Applied University Windesheim, Department of Health and Welfare, Campus 2, 8017 CA Zwolle, the Netherlands. [7]Leiden Institute for Brain and Cognition (LIBC), Department of Psychiatry, Leiden University Medical Center, Albinusdreef 2, 2333 ZA Leiden, the Netherlands [8]Department of Psychiatry, VU University Medical Center, Academic Medical Center University of Amsterdam, Amsterdam, the Netherlands [9]University of Groningen, Department of Clinical Psychology and Experimental Psychopathology, Grote Kruisstraat 2/1, 9712TS Groningen, The Netherlands

showed no significant difference (F(1,81)=.10, p=.76, $\eta^2 = .001$). For the six a-priori modules in attempt vs no-attempt groups, no difference in network flexibility was detected at the given threshold ($\alpha = .00833$). Only the right central executive network showed a marginal difference between suicide attempt and no attempt (F(1,81)= 3.88, p=.05, $\eta^2 = .046$), suggesting that this network expanded and contracted more over time in people who attempted suicide. In participants with suicidal ideation vs no suicidal ideation, the 6 selected modules showed no significant difference.

The authors finally conclude that their findings, a lower whole brain flexibility for participants with suicidal ideation and mood disorder in comparison to those suffering from mood disorder but showing no suicidal ideation, might reflect the complex abnormalities including the deficits adapting to external and internal demands known to suicidal ideation symptom and suggest that the further suicidality research should include measures addressing the suicidal ideation to achieve a more profound result of network abnormalities.

Chapter 6: NUMERICAL SIMULATION OF BRAIN FLEXIBILITY

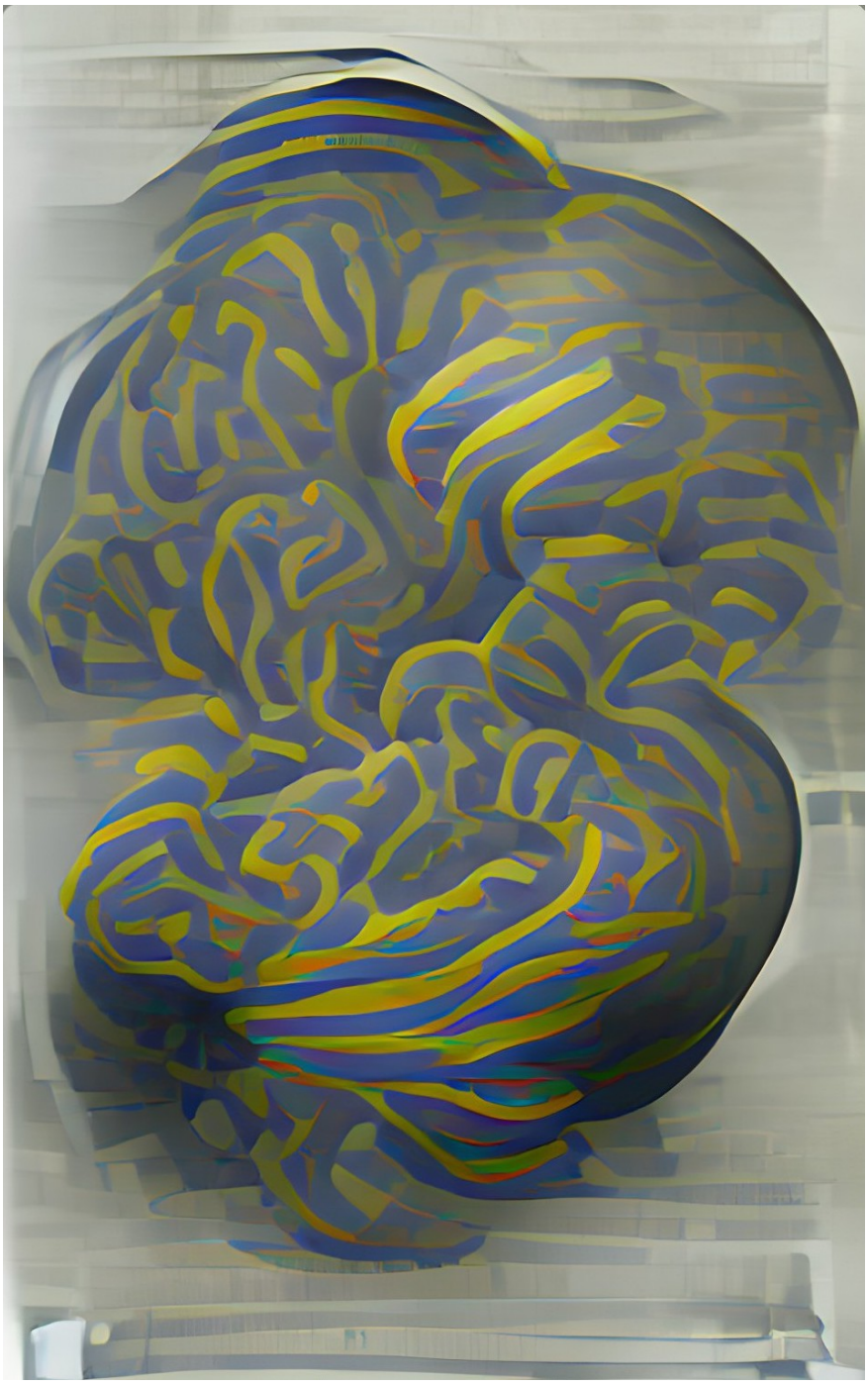

AI powered painting created by Wombo art [tea] using chapter 6 keywords.

Chapter 6

Numerical Simulation of Brain Flexibility

"Something that doesn't actually exist can still be useful."

- Ian Stewart

The material discussed in this chapter has overlap with the content of the below mentioned paper. Due to the differences in the nature of papers and thesis, some results are discussed more extensively here in the thesis.

Modeling brain flexibility in networks of coupled neural populations

Narges Chinichian[1,2,3,*], Michael Lindner[1,4], Serhiy Yanchuk[4,5], Tilo Schwalger[3,6], Eckehard Schöll[1,3,4], Rico Berner[1,7]

Manuscript in preparation (2022).

Understanding the brain and having an accurate model of it that can predict different functions, have been the dreams of generations of scientists from various fields of studies. From the estimated 1.019 billion euros "Human Brain Project"[1] to the "BRAIN Initiative" [2], many scientist around the world are actively working on computational models of the brain.

[1]Institut for Theoretical Physics, Technical University of Berlin, Berlin, Germany. [2]Department of Psychiatriy and Psychotheray, CCM, Charité-Universitätsmedizin Berlin, corporate member of Freie Universität Berlin and Humboldt-Universität zu Berlin, Germany. [3]Bernstein Center for Computational Neuroscience, Berlin, Germany. [4]Potsdam Institute for Climate Impact Research, Potsdam, Germany. [5]Institute of Mathematics, Humboldt Universität zu Berlin, Germany. [6]Institute of Mathematics, Technische Universität Berlin, Germany. [7]Department of Physics, Humboldt Universität zu Berlin, Germany.

1- https://www.humanbrainproject.eu/en/

2- https://braininitiative.nih.gov/

Computer simulations of the human brain are one of the new approaches used by scientists today. They not only help us to understand hidden aspects of mechanisms behind the function, but are also low cost test opportunities to examine hypotheses that might not be ethically or practically applicable on a real human brain.

With the help of simulations and computational models we can now explain the alterations in brain connectivity during progression of Alzheimer's disease [Dem+17], predict the optimal targets of deep brain stimulation [FDK22; Tre+20], explain epileptic seizures or find a patient-specific epileptogenicity of the brain regions to improve epilepsy surgeries at hospitals [Has+20; Ger+20; Olm+19; Pro+18].

In this chapter computer simulations of a simple dynamical model of the brain are presented. The model uses an empirical network structure obtained from Diffusion Tensor Imaging (DTI) data [see chapter 1] and generic dynamics on each node of the network. The model is employed to simulate brain flexibility patterns in order to have a way to assess the mechanism behind the flexibility measure [see chapter 2] in a simplified physics modeling sense and answer a few questions raised by the results of empirical brain data analysis in chapter 3. It was shown that during the performance of a working memory (WM) task the brains of healthy volunteers show the re-groupings that correspond to the block-designed task change. We will try to look at this flexibility phenomenon from a physics point of view and propose a meaningful yet simple dynamical model that helps us in the understanding of this phenomenon.

The questions investigated in this chapter are the following:
1- Is it possible to show the flexibility pattern as observed in the empirical data with all of the approximations and simplifications of a FitzHugh-Nagumo network model?
2- Is the brain specific network topology playing a role in the observed brain flexibility? What happens if we distort the structure and introduce randomness?
3- Does the selection of nodes in the brain, that are being associated with a task, have an effect on the flexibility observed?
4- Do the double-peaks [peaks both when the sliding window is capturing two tasks and when the window is capturing only one] previously not observed by our method in chapter 3 re-appear in an ideal simulation scheme?

The above questions were the motivation for the following brain simulations.

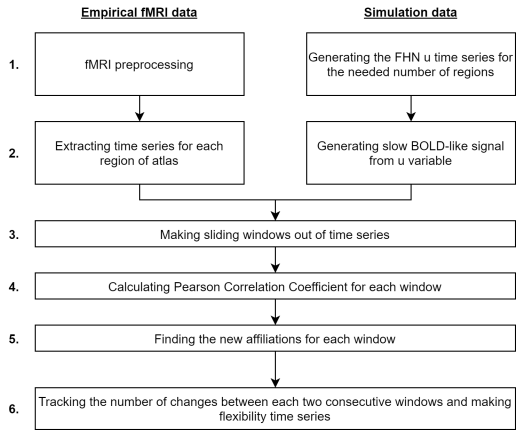

FIGURE 6.1. Empirical and Simulated Data Pipelines
Empirical data from participants is collected and preprocessed. Time series for all regions are extracted. Pearson correlation coefficients between time series in every sliding window are calculated. The flexibility time series are generated based on the changes of node affiliations between consecutive windows. For the simulated data the fMRI-like time series are produced using FitzHughNagumo (FHN) u-value time series and Balloon models slower oscillation conversion but then these time series are treated as their empirical counterparts.

6.1 BRAIN SIGNAL SIMULATION

The computer simulation in this chapter is aimed at generating artificial functional Magnetic Resonance Imaging time series that show similar behaviour to those recorded from real human subjects who performed the working memory task presented in chapter 3. These artificial time series can then be investigated in detail to answer the questions mentioned above.

6.1.1 *FitzHugh-Nagumo Model*

To simulate the neural activity, a specific type of FitzHugh-Nagumo oscillators [Fit61] is employed. The dynamics is similar to the one used by Ghosh et al [Gho+08]. The activator variable u_k and the inhibitor variable w_k of each oscillator k follow the dynamics shown in the equation below:

$$\frac{\mathrm{d}}{\mathrm{d}t}\begin{pmatrix}\epsilon u_k\\ w_k\end{pmatrix} = \begin{pmatrix}u_k - \frac{u_k^3}{3} - w_k + I_0\\ u_k + a - b w_k\end{pmatrix} - \sigma \sum_{l=1}^{N} g_{kl}\begin{pmatrix}u_l\\ 0\end{pmatrix} + \begin{pmatrix}I_k(t)\\ 0\end{pmatrix}, \tag{6.1}$$

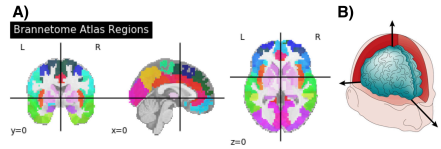

Figure 6.2. Brainnetome atlas regions
A) Brainnetome atlas[a] with 246 regions [Fan+16].B)Schematic figure for image axis. Reused by permission from [BJO02]

[a] https://atlas.brainnetome.org/

where u_k in the single neuron modeling represents the membrane potential and w_k is the slow recovery variable of the neuron. Index $k \in \{1, ..N\}$ refers to the k-th oscillator [of a total of N oscillators]. Parameters a and b are bifurcation parameters of the FitzHugh-Nagumo system. I_0 is an excitability parameter, an input given to the unit, same for every oscillator. The $\epsilon \ll 1$ is the time-scale ratio of the fast activator and the slow inhibitor variable. In our model, each Brainnetome brain region [see Figure 6.2] is seen as one single oscillator. The state variables u and w then describe the effective dynamics of that brain region. The coupling weight between oscillators k and l is given by the weighted adjacency matrix element g_{kl} multiplied by the overall coupling strength coefficient σ.
Finally, $I_k(t)$ is the input which is given specifically to oscillator k at time t. An appropriate input based on the phenomenon under investigation should be chosen.

A list of the parameters used in equation (6.1) [and later (6.3) to (6.9)] together with their meanings are presented in Table 6.1

The dynamics of the oscillators before they are coupled together is shown in Figure 6.3. Panels A and C show the oscillations of all the oscillators. With no coupling to connect the oscillators, each unit is only different in its initial condition. Panel B shows the nullclines and trajectory of one single oscillator. Panel D shows the u time serie for a longer period of time. Parameters b and a help tune the system for the simple case of one intersection point between the two nullclines and the move of intersection on the peak or trough of the u-nullcline based on the respective case. For a more detailed review on the behaviour of a FitzHugh-Nagumo oscillator, see chapter 3 of Gerstner's book [Ger+14] and the extensive dynamical visualizations with changing parameters offered in Scholarpedia by Izhikevich[†] .

[†] Izhikevich E. M. and FitzHugh R. (2006) FitzHugh-Nagumo model. Scholarpedia, 1(9):1349.

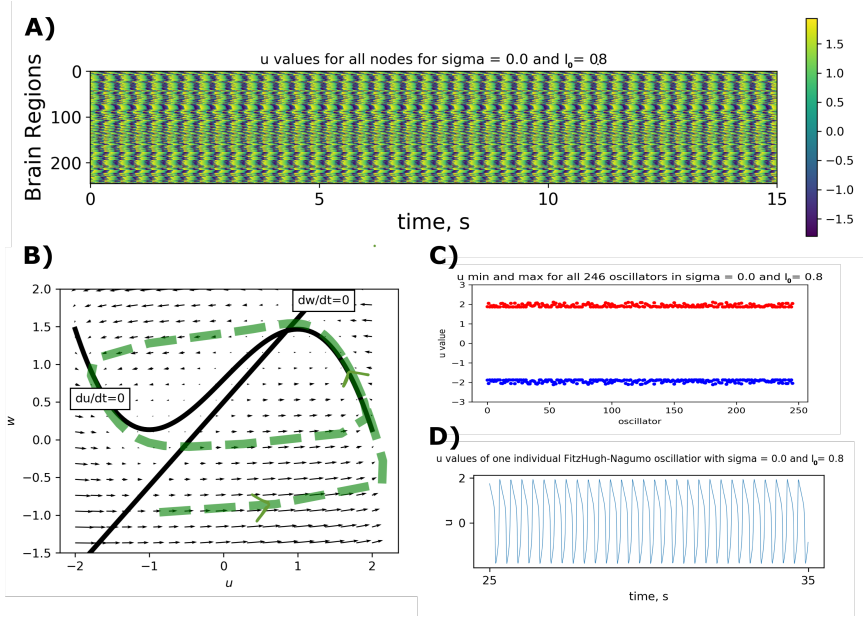

FIGURE 6.3. Oscillators behaviour when there is no coupling ($\sigma = 0$)
A) Space-time plot of all 246 oscillators vs time B) Phase portrait of one oscillator. C) minimum and maximum of u time series for all of the oscillators. Blue dots are minima and red dots are maxima D) Oscillation of one single oscillator for a longer time.

TABLE 6.1. Parameters used in the a FitzHugh-Nagumo model (6.1) and Balloon model (6.3) to (6.9).

Symbol	Meaning
$\sigma = 1.8$	overall coupling constant
$a = 0.45, b = 0.9$	bifurcation parameters of the FitzHugh-Nagumo system
$I_0 = 0.8$	excitability parameter
$\epsilon = 0.1$	controls time separation between fast activation and slow inhibition
$c = 3$	amplitude of the square-wave input I_k
$\tau_0 = 0.98$	mean transit time of venous compartment
$E_0 = 0.34$	capillary bed net oxygen extraction fraction
$V_0 = 0.02$	resting blood volume fraction
$\frac{1}{\alpha} = 0.32$	flow-volume relationship power
$\tau_s = 0.65$	time constant for signal decay
$\tau_f = 0.41$	time constant for auto-regulatory feedback from blood flow

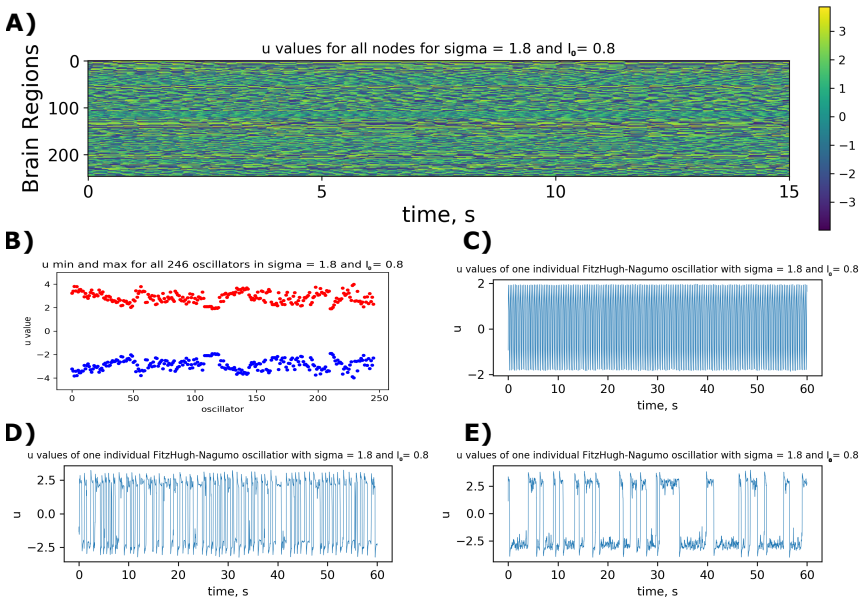

Figure 6.4. Oscillators behaviour with $\sigma = 1.8$, $I_0 = 0.8$ and no square-wave $I_k(t)$ input given to any region
A) Space-time plot of all 246 oscillators vs time. B) Minimum and maximum of u values for all of the oscillators. C) u values for the node with the lightest weighted connections to the other nodes. D) u values for the node with the median weighted connections to the other nodes. E) u values for the node with the heaviest weighted connections to the other nodes.

6.1.2 *Structural Connectivity Matrix G*

Diffusion Tensor Imaging (DTI) is a magnetic resonance imaging (MRI) technique to obtain the map of neural tracts in the brain. This method uses the ellipsoid-shaped diffusion of water in tissue, as opposed to a sphere, as an indicator of the presence of a tract that imposes certain boundary conditions on the diffusion. The neural tracts information can serve as a structural network of the brain. It can assign a weight to each two spatial regions of the brain based on the tracts connecting them (see chapter 1 for more information on DTI).
The structural connectivity weighted matrix G with elements g_{ij} in equation 6.1 is expected to show the weights of connections between regions in the brain. For this purpose a 246 × 246 averaged DTI matrix in Brainnetome atlas [Fan+16], obtained from 32 adults (mean age 31.5 years ± 8.6 SD and 14 female [Set+13]) who participated in Human Connectome Project (HCP) at Massachusetts General Hospital ("MGH HCP Adult Diffusion"), was used.

https://www.humanconnectome.org

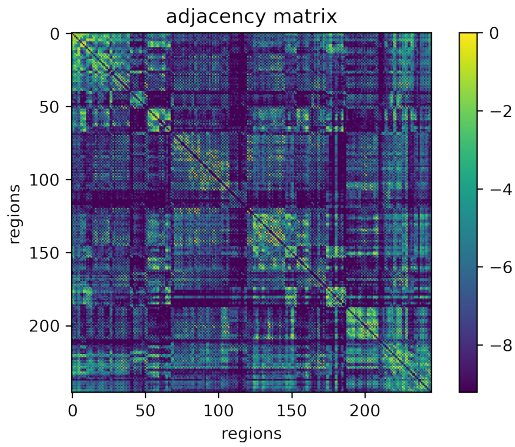

FIGURE 6.5. Average Diffusion Tensor Imaging (DTI) weighted adjacency matrix from 32 subjects of Human Connectome Project [a] [Set+13] calculated by Horn et al 2020 using Lead software [Hor+17; HK15; Hor+19]. For illustration purpose, $Log(g_{ij} + 10^{-}4)$ is plotted. [b]

[a] https://www.humanconnectome.org
[b] Used plotting tool [Hun07b]

The averaged DTI was calculated using Lead group softwares. [Hor+17; HK15; Hor+19]. Figure 6.5 shows this G. A coupling coefficient σ is multiplied by G so that the oscillation can be tuned.

6.1.3 *Input*

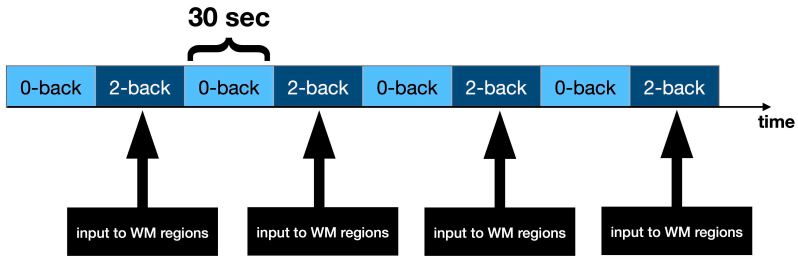

FIGURE 6.6. Alternating blocks of working memory task
N-back working memory task design.

The N-back memory task in chapter 3 was consisted of 30-second blocks of 0-back followed by 30 seconds of 2-back. 0-back serves as baseline in this task (see Figure 6.6). The baseline provides all the activities (for example looking at the slides, making decisions and choosing) minus the working memory part that is being measured in the experiment. To mimic the block-design of our memory task in a simplified way, we use a square-wave input that can be written as:

$$I_k(t) = -c(2\lfloor ft \rfloor) - \lfloor 2ft \rfloor)), \tag{6.2}$$

where coefficient c regulates the amplitude, $f = \frac{1}{T}$ is the frequency and T = 60 seconds [for empirical reason of having 30-sec blocks for each condition]. See Figure 6.12 panel A and Figure 6.6 for plot and schematic of this input.

To select the regions which should receive the input we used a map of "working memory" associated areas from Neurosynth [1] which is shown in Figure 6.7 and calculated the overlap of Brainnetome regions [also presented in Figure 6.7] with Working Memory (WM) areas. The regions with over 50% overlap were then selected as target regions to receive the input introduced in equation 6.2. The total number of regions was six

6.1.4 Balloon-Windkessel Model

The high frequency activator outputs u from FitzHugh-Nagumo oscillators go through the Balloon-Windkessel model [Fri+00] to form a slower BOLD-like (Blood-oxygen-level-dependent) signal, which represents the measured signal during brain scans in the fMRI (functional Magnetic Resonance Imaging) machines [BHV21].

The Balloon model [Fri+00; Man+99; Cak20] is a hemodynamic model that mediates between synaptic activity and measured BOLD (Blood-oxygen-level-dependent imaging) signals. This model uses normalized venous volume v, normalized total deoxyhemoglobin voxel content q and resting net oxygen extraction fraction by the capillary bed E_0 to generate BOLD-like signal $y(t)$ as defined by:

$$y(t) = \lambda(v, q, E_0) = V_0(k_1(1-q) + k_2(1-\frac{q}{v}) + k_3(1-v)), \tag{6.3}$$

where $k_1 = 7E_0$ and $k_2 = 2$ and $k_3 = 2E_0 - 0.2$ and V_0 is the resting blood volume fraction. A list of parameters in Balloon-Windkessel model together with their meanings are summarized in Table 6.1

The changing rate of volume is defined by:

$$\dot{v} = \frac{1}{\tau_0}(f_{in} - f_{out}) \tag{6.4}$$

which is dependent on the difference of in-flow f_{in} and out-flow f_{out} of the venous compartment multiplied by a time constant τ_0 that represents the

1- Neurosynth is a platform for large-scale, automated synthesis of functional magnetic resonance imaging (fMRI) data. A set of 1091 studies related to "Working Memory" were used to generate the association map. See here: https://neurosynth.org/analyses/terms/working%20memory/

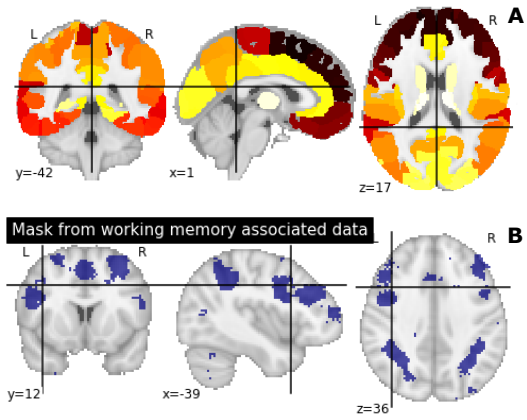

FIGURE 6.7. Brain regions to be stimulated
A) Brainnetome regions from Brainnetome atlas[a], 246 regions in total [Fan+16] B) Working Memory associated areas extracted from Neurosynth engine [b]. [c]. The Brainnetome regions with bigger than 50% overlap are listed below:

- Regions 25 and 26: A6vl, ventrolateral area 6 from Middle Frontal Gyrus
- Region 29: A44d, dorsal area 44 from IFG from Inferior Frontal Gyrus
- Region 63: A6cvl, caudal ventrolateral area 6 from Precentral Gyrus
- Region 127: A7c, caudal area 7 from SPL from Superior Parietal Lobule
- Region 211: mAmyg, medial amygdala from Amygdala

The list of all Brainnetome regions can be found in the Supplementary Material

[a] https://atlas.brainnetome.org/
[b] https://neurosynth.org/
[c] Brain plots are made using nilearn package in Python [Ped+11]. The x,y,z values show the plotting coordinates

average transit time (time to pass the venous compartment). The Windkessel model [1] [Man+99] suggests that f_{out} is dependent on the volume and can be written as

$$f_{out} = v^{1/\alpha}, \tag{6.5}$$

where α, determined empirically, relates to the flow regime and the ratio of capacitance to compliance in balloon.
The dynamics of state variable q then reflects the difference of out-flow and in-flow of deoxyhemoglobin in the venous compartment.

$$\dot{q} = \frac{1}{\tau_0}\left(\frac{E(f_{in}, E_0)}{E_0} - f_{out}(v)\frac{q}{v}\right), \tag{6.6}$$

1-"wind- kessel" means leather bag

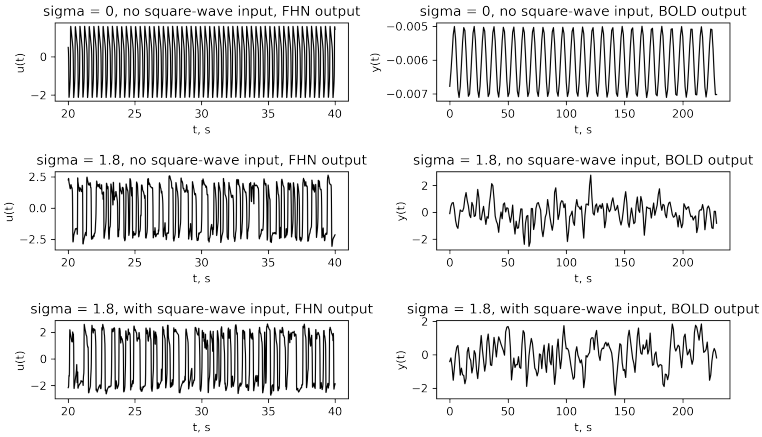

FIGURE 6.8. Fitzhugh-Nagumo and Balloon models outputs
An example plot for the outputs of FHN and Balloon models for a region in the middle of the sorted list of weighted connections [a] for the 3 cases; Top: $\sigma = 0$ and no square-wave input to any region. Middle: $\sigma = 1.8$ and no square-wave input to any region. Bottom: $\sigma = 1.8$ and square-wave input of $I_k(t) = -3(2\lfloor ft \rfloor) - \lfloor 2ft \rfloor))$ given to the 6 selected working memory regions.
See supplementary material for the least connected node (115), most connected node (230) and a node that is directly receiving input (63).

[a] Region 148 from Brainnetome

where $E(f_{in}, E_0)$ shows the ratio of oxygen extracted from the inflow to the delivered amount and is assumed to depend on oxygen arriving with the in-flow:

$$E(f_{in}, E_0) = 1 - (1 - E_0)^{\frac{1}{f_{in}}} \tag{6.7}$$

The in-flow, f_{in} changes based on the induced signal that depends on the fast neuronal activity $u_k(t)$ which comes from FitzHugh-Nagumo oscillators in our study.

$$\dot{f_{in}} = s \tag{6.8}$$

and

$$\dot{s} = \epsilon_B u_k(t) - \frac{s}{\tau_s} - \frac{(f_{in} - 1)}{\tau_f} \tag{6.9}$$

where ϵ_B,τ_s and τ_f are parameters that determine the dynamics of s. They respectively represent:

- ϵ_B: Efficacy with which neuronal activity causes an increase in signal

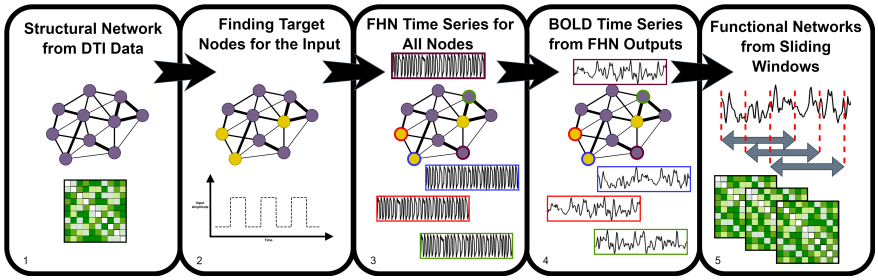

FIGURE 6.9. Schematic View of Simulation Steps
1) Structural network is based on white matter Diffusion Tensor Imaging (DTI) data. 2) Nodes that receive the input are marked and the shape of the input is decided. 3) FitzHughNagumo (FHN) time series are generated using the dynamics introduced in equation 6.1. 4) FHN u time series are passed to Balloon model to produce slower Blood Oxygen Level Dependent (BOLD)-like signals. 5) The slow signals are treated like the empirical data. Sliding windows Pearson's correlation coefficients are calculated between each pair of nodes and used as functional networks.

- τ_s: Time constant for signal decay
- τ_f: Time constant for auto-regulatory feedback from blood flow

Having equations 6.4,6.6,6.8 and 6.9 we are able to calculate the desired $y(t)$ which has the nature of slower BOLD (Blood-oxygen-level-dependent) signals we needed.
The parameters used for the simulation purposes are presented in Table 6.1 .

6.2 SUMMARY OF SIMULATION STEPS

The FitzHugh-Nagumo time series with parameters given in Table 6.1 and the time-dependent input introduced in 6.2 given to regions in 6.1.3 were generated on the nodes of matrix G in 6.1.2. The standardized [with z-score [1]] output was then fed to the Balloon model introduced in section 6.1.4 and the result was treated as a single subject fMRI brain signal. The simulation was repeated 300 times with different random initial conditions to account for the effect of initial condition and random fluctuations.

6.3 FLEXIBILITY AND PEARSON CORRELATION DISTANCE OF CONSECUTIVE WINDOWS WEIGHTED ADJACENCY MATRICES

In addition to the flexibility measure introduced in chapter 2 another more straight-forward measure for comparison between the empirical and simulated

1- For variable X from a time serie with mean μ and standard deviation σ, the z-score is: $z = \frac{X-\mu}{\sigma}$

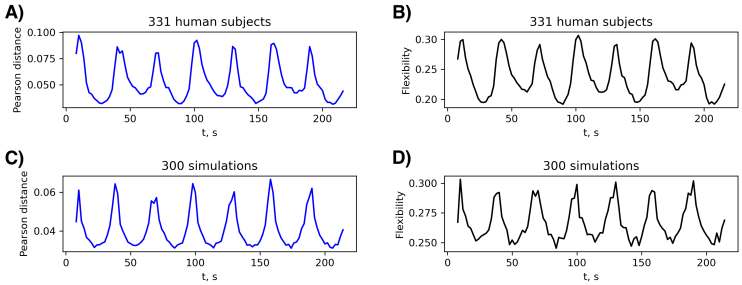

FIGURE 6.10. Comparing empirical and simulation cases
Correlations of consecutive windows weighted adjacency matrices on the left column and template flexibilities on the right column in empirical data (first row, A and B panels) and simulated data (second row, C and D panels). Pearson correlation coefficient for the two flexibility time series is 0.85 and for the two Pearson distances is 0.87 (with mean absolute error (MAE) of 0.01 and 0.03 respectively). A "subject" in empirical data means one participant and a "simulation" in simulated data means a single run with a random initial condition [empirical data: averaged over 331 participants and simulated data averaged over 300 random initial conditions]. Calculating the flexibility time serie is explained in details in chapter 3. Each sliding time window is covering 30 seconds and two consecutive time windows have 28 seconds overlap.

data, which is independent of our choice of template modules, can be defined. For the calculation of this measure, the same procedure as in chapter 2 until step 2 is followed. At this step a weighted adjacency matrix (A_{win}, we have to avoid using w,s and t indices for less confusion) see Chapter 2) is calculated for each sliding time window from the empirical or simulated BOLD time series. Then these weighted adjacency matrices are flattened (we denote the flattened A_{win} by Δ_{win}) and the Pearson correlation distance $1 - r_{(win-1,win)}$ between each two consecutive flattened windows arrays is calculated again using the Pearson correlation coefficient r and Pearson's distance $1 - r$ formula below:

$$1 - r_{(win-1,win)} = 1 - \frac{\sum_{\eta=1}^{N^2}(\Delta_{(win,\eta)} - \overline{\Delta}_{(win)})(\Delta_{(win-1,\eta)} - \overline{\Delta}_{(win-1)})}{\sqrt{\sum_{\eta=1}^{N^2}(\Delta_{(win,\eta)} - \overline{\Delta}_{(win)})^2}\sqrt{\sum_{\eta=1}^{N^2}(\Delta_{(win-1,\eta)} - \overline{\Delta}_{(win-1)})^2}} \tag{6.10}$$

where η is a counter over array elements. N^2 is the size of flattened array. Overline shows the mean (e.g $\overline{\Delta}$ is the average of the elements in Δ) and a time series of "$1 - r$" can be calculated between all consecutive windows.
In other words, using 1 time Pearson correlation and 1 time Pearson distance will result in this measure.
This measure is closely related to the template flexibility because if the two consecutive weighted adjacency matrices are very similar the correlation is high [note that it does not necessarily hold the other way around, very different matrices (by element values) can still have big correlation coefficients] and at

the same time there is less switching in affiliations. On the other hand, when the two consecutive weighted adjacency matrices are dissimilar, the chance of switching is high and in many cases the correlation coefficient is also small. There are mathematical cases where the two measures are not showing similar patterns [see Figure 6.11 as an example of the measures deviating] but they are defined in a related way. Figure 6.10, shows the dynamics of the two measures, flexibility and correlation of weighted adjacency matrices in empirical and simulated data. The simulated case shows a similar pattern to the empirical data.

6.4 Results

Reproducing Flexibility Pattern

The first question in this study is if the simulation based on our highly simplified oscillator model and connection assumptions can reproduce a similar pattern to that observed in the empirical data. The differences in steps to generate the flexibility time series in empirical vs simulated data are shown in figure Figure 6.1. The simulated data generation pipeline is shown in schematic figure Figure 6.9 and explained in more details in the method section. Structural network is based on an averaged white matter Diffusion Tensor Imaging (DTI) matrix. Nodes, that receive the input, are found by overlaying a mask of Working Memory associated regions with our selected parcellation for regions. The shape of the input is decided to be a simple square wave matching the block design of empirical task. FitzHughNagumo (FHN) time series are generated for every node using the dynamics introduced in the methods section. FHN activator time series are then passed to Balloon model to produce slower Blood Oxygen Level Dependent (BOLD)-like signals. Finally these slow signals are treated like the empirical BOLD signals from human participants.

Figure Figure 6.10 shows the plots for the two cases, empirical and simulated data. The two template a-priori flexibility time series [calculated using the method introduced in previous study by Chinichian et al [Chi+22]] for empirical data vs simulated data on the right column and the two simplified correlation distance time series of weighted adjacency matrices introduced in method section of this study on the left column. The averaged simulated case shows a similar pattern to the averaged empirical data. The Pearson correlation coefficient for the two flexibility time series equal to 0.85 and for the two Pearson distances 0.87 (with mean absolute error (MAE) of 0.01 and 0.03 respectively). During the performance of each block of tasks, the brain stays in a specific configuration which is then changed by moving to the next block. To

have a comparable smoothing and count for the initial condition differences, the simulation is repeated for 300 times with the same parameters and random initial conditions and then averaged across all runs. The empirical data is smoothed as a result of averaging across 331 participants.

6.4.1 *Effect of Structure*

The structure of brain networks and its importance in human cognitive abilities has been a topic of great interest in the network neuroscience community but is this structure playing any role in the mesoscale flexibility behaviour observed during the cognitive task? To test for the effect of the specific DTI structure (called G in this study) without increasing or decreasing the weights associated to the network links (edges), we use a randomly reshuffled version of the empirical DTI matrix (and call it G'. We keep the upper triangle of the matrix and shuffle the weights (and then use the upper triangle to build a symmetric lower triangle). An ensemble (of size 50) of simulations with the same model parameters but different structural matrices (G and G') were performed.

As shown in figure Figure 6.11, the simulations on random network topology do not show the same regular oscillatory Pearson distance and template flexibility measure patterns as seen in the previous case. The Pearson correlation coefficient for the two flexibility time series is 0.64 and for the two Pearson distances is 0.42 (with mean absolute error (MAE) of 0.01 for both cases). Both shown cases ("Baseline" and "Reshuffled DTI") had the same ensemble size (runs with different random initial conditions) of 50. The result suggests that the structure of network is an inseparable part of the flexibility pattern in the brain. The disturbance in the regular oscillatory pattern shows that the regular input (the square wave) alone can not be the source of strong oscillatory pattern observed.

6.4.2 *Effect of Node Selection*

The third question of this study on the role of node selection for input can be answered with the investigation of flexibility pattern when the input in equation 6.2 is given to regions other than those marked as Working Memory (WM) associated. The working memory (WM) regions in 6.1.3 are the following regions from Brainnetome atlas:

- Regions 25 and 26: A6vl, ventrolateral area 6 from Middle Frontal Gyrus
- Region 29: A44d, dorsal area 44 from IFG from Inferior Frontal Gyrus

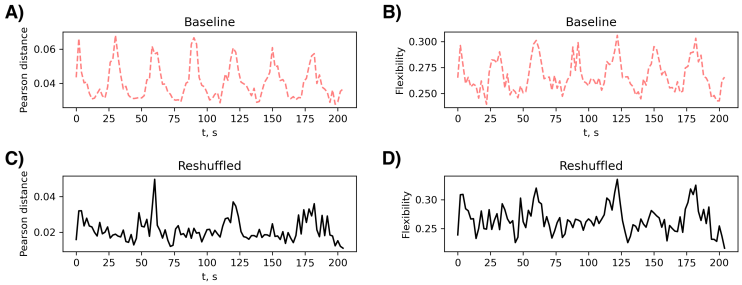

FIGURE 6.11. Randomly reshuffled G simulation
Comparing the two case with a normal DTI-based G and a randomly reshuffled G with the same weight distribution. Panels A and B are from simulations on G (averaged DTI matrix) while panels C and D are from simulation on G' (reshuffled G). All other simulation parameters were kept the same (equal to those in Figure 6.10). In both cases, the ensemble size averaged is 50 (50 simulations with different random initial conditions). Pearson correlation coefficient for the two flexibility time series is 0.64 and for the two Pearson distances is 0.42 (with mean absolute error (MAE) of 0.01 for both cases)

- Region 63: A6cvl, caudal ventrolateral area 6 from Precentral Gyrus
- Region 127: A7c, caudal area 7 from SPL from Superior Parietal Lobule
- Region 211: mAmyg, medial amygdala from Amygdala

Figure 6.12.B shows the weighted degree distribution of the DTI matrix. The WM nodes fall mainly in the middle part of this histogram. If we sort the nodes in the DTI matrix (light to heavy i.e., low weighted degree to hight weighted degree) based on their weighted degrees, the following list of indices is achieved:

115, 117, 211, 212, 116, 119, 213, 118, 49, 238, 109, 120, 111, 114, 113, 110, 112, 187, 50, 42, 168, 188, 41, 214, 184, 174, 166, 69, 180, 195, 70, 165, 102, 47, 246, 179, 100, 96, 158, 172, 46, 183, 236, 167, 48, 242, 164, 62, 94, 92, 157, 61, 196, 171, 90, 78, 43, 231, 45, 122, 44, 40, 77, 234, 101, 232, 84, 124, 235, 215, 244, 237, 38, 37, 74, 72, 73, 189, 217, 34, 80, 163, 216, 52, 89, 98, 32, 108, 20, 153, 240, 30, 106, 51, 82, 39, 54, 105, 67, 19, 185, 76, 177, 33, 93, 147, 219, 28, 64, 103, 191, 31, 36, 228, 14, 154, 27, 245, 91, 11, **35, 173, 159, 148, 202, 146**, 79, 83, 65, 133, 192, 123, 104, 16, 178, 156, 218, 197, 13, 190, 241, 155, 88, 160, 15, 18, 95, 200, 71, 170, 149, 127, 29, 86, 24, 4, 129, 23, 151, 63, 22, 125, 220, 97, 145, 198, 66, 68, 26, 25, 204, 206, 193, 12, 134, 130, 239, 139, 194, 186, 243, 144, 21, 121, 137, 58, 128, 99, 131, 53, 201, 75, 107, 233, 87, 209, 55, 9, 132, 81, 227, 210, 181, 207, 175, 150, 1, 59, 152, 142, 85, 203, 10, 205, 135, 126, 56, 222, 223, 162, 141, 17, 8, 136, 60, 140, 199, 6, 208, 226, 161, 138, 7, 169, 224, 176, 57, 3, 2, 143, **5, 182, 221, 225, 229, 230**

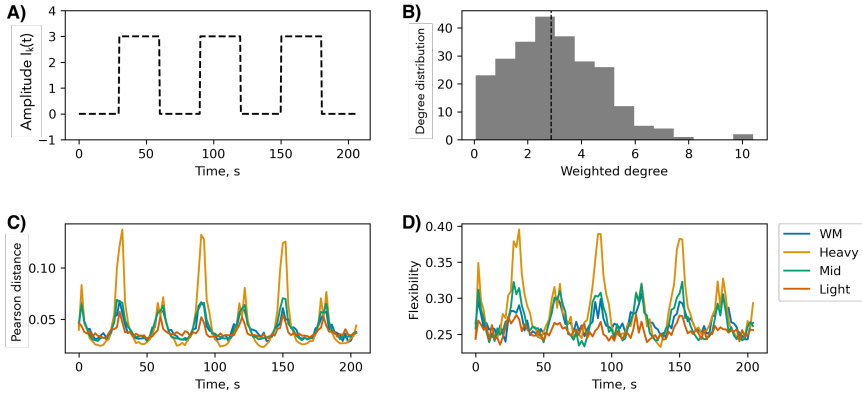

FIGURE 6.12. Node selection scenarios
A) Shape of square-wave time dependent input given to the 6 selected nodes. B) Histogram of weighted degrees for all 246 nodes in the DTI matrix. The dashed line shows the median value of weighted degrees. C) Comparison between Pearson distance measure for the 4 simulation scenarios of Working Memory (WM), Heavy, Middle and Light nodes being stimulated by $I_k(t)$. D) Comparison of template flexibility time series for the 4 scenarios.

where the working memory (WM) regions are underlined. We test 3 scenarios:
1- Stimulating the least connected nodes (Light scenario)
2- Stimulating the middle connected nodes (Mid scenario)
3- Stimulating the most connected nodes (Heavy scenario)
These three artificially chosen groups of high, intermediate, and low degree (marked heavy, mid, light, respectively, in Figure 6.12) are marked in boldface on our above list.

The results of our 3 simulation scenarios together with the WM case are presented in figure Figure 6.12 panels C and D. The FitzHugh-Nagumo u time series for the three scenario are also shown in figures Figure 6.13, Figure 6.14 and Figure 6.15. The "Light" scenario shows a visibly weaker oscillatory pattern. This was to be expected as the lightest nodes are not well connected to the rest of the network and the input would not strongly affect the neighboring nodes through the couplings. The "Mid" scenario, has the most similar pattern to the WM area. Indeed, checking the distribution of WM nodes in the weighted degree list, the "Mid" scenario is the closest to it. The most notable result of this simulation is the "Heavy" scenario, when the input is given to the heavily connected nodes, the symmetry between the blocks is broken and the start of 2-back task is marked by deeper troughs and the bigger flexibility is observed for the 2-back reconfiguration. In the empirical data, marginally higher flexibility

was observed during the 2-back compared to 0-back blocks (t = 2.9, p = .03). This might suggest that the working memory regions are empirically well-connected but they are not the main weight hubs of the brain network.

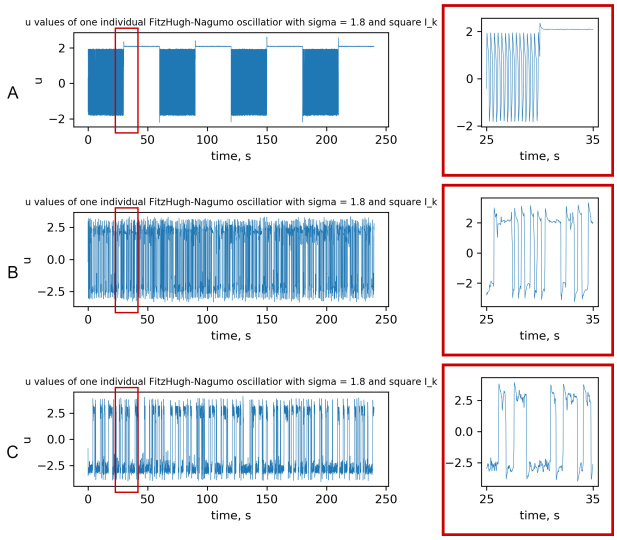

FIGURE 6.13. Light scenario FHN timeseries
In the left column, u time series for three different nodes (from start or low weighted degree (A), middle or intermediate weighted degree (B) and end or high weighted degree (C) of the sorted weighted degree list) are shown when 6 nodes with lightest weighted degrees (Light) are stimulated by $I_k(t)$. In the right column, a 10 seconds period with red borders is magnified.

6.4.3 *Middle-peaks*

Our observations in the empirical data was consistently showing one single peak per block. Some researcher suggest that the middle of each block and the dual condition windows (the windows that have half of their time-points in one condition (e.g. 0-back) and the other half in the other condition (e.g. 2-back) should each introduce one peak in the meso-scale reconfiguration of the brain [BGS15] adding up to 2 peaks per block. There was no observation of double peaks in any of our simulations.

We added an investigation of the effect of contrast size between 2 conditions (reflected in c coefficient of I_k) on the number of extrema per block to observe if the increased contrast between the two conditions will introduce a change in the number of extrema in flexibility or Pearson measures (to more than one

t-value and p-value from statistical hypothesis testing

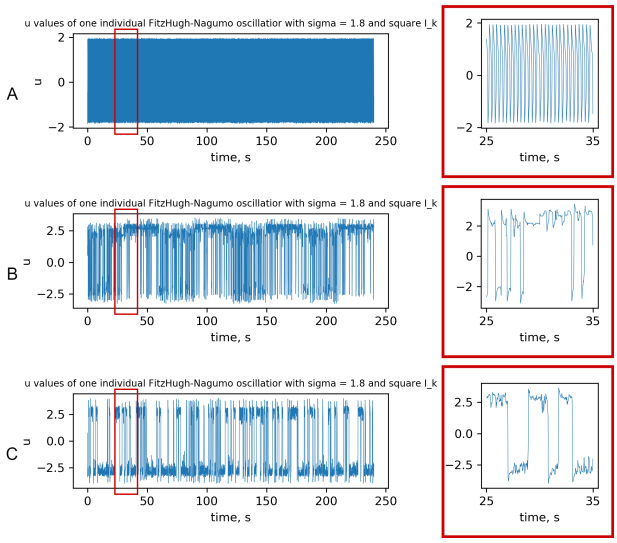

FIGURE 6.14. Intermediate degree (Mid) scenario FHN time series $u_i(t)$
In the left column, u time series for three different nodes (from start or low weighted degree (A), middle or intermediate weighted degree (B) and end or high weighted degree (C) of the sorted weighted degree list) are shown when 6 nodes with intermediate degree (Mid) are stimulated by $I_k(t)$. In the right column, a 10 seconds period with red borders is magnified.

maximum/minimum per condition). A set of simulations with different input amplitude c were performed but no clear middle-peak was observed in the range investigated. Figure 6.16 shows a part of the time series for 3 of the investigated inputs. The smaller indents observed are not consistently present in every case and can best be described with step-like decays leaning towards one of the peaks (with the sliding windows moving to new intervals sometimes causing a small indent) than a singular middle-peak. These simulations are not sufficient for the rejection of middle-peaks in the reconfiguration of brain modules hypothesis but they suggest no double peak per condition can be observed with tuning the two blocks contrast in our approximations. Further investigations can be designed with more complex input functions and wider range of inputs.

6.5 CHAPTER SUMMARY AND FURTHER INVESTIGATION

Using a computational dynamical model a simplified simulated version of flexibility was built in this chapter. This reconstruction allowed for a more thorough examination of the impact of characteristics such as brain structure. The connectivity structure of the brain network plays a significant role in the

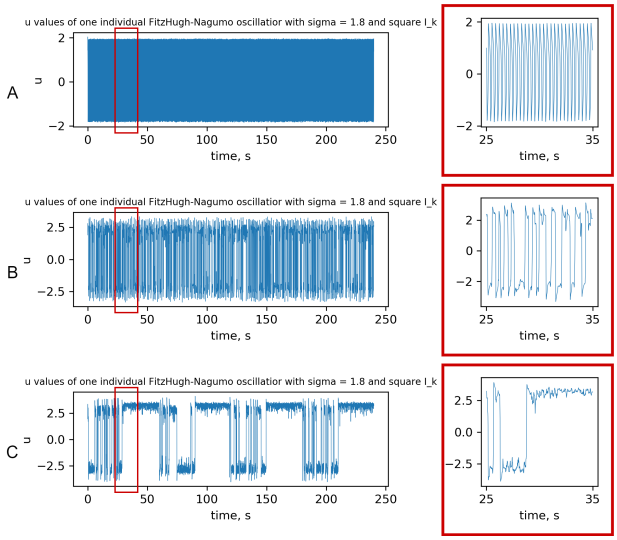

FIGURE 6.15. Heavy scenario FHN timeseries
In the left column, u time series for three different nodes (from start or low weighted degree (A), middle or intermediate weighted degree (B) and end or high weighted degree (C) of the sorted weighted degree list) are shown when 6 nodes with highest weighted degrees (Heavy) are stimulated by $I_k(t)$. In the right column, a 10 seconds period with red borders is magnified.

cooperation of brain areas and the execution of cognitive tasks. A random reshuffling of network weights can result in the expected oscillatory behavior no longer being observed anymore. Additionally, the regions stimulated during the execution of a cognitive task influence the patterns. Changes in the task-stimulated areas can result in distinct patterns being observed. If highly interconnected nodes in the system are stimulated, the difference between task blocks with and without input becomes more significant. In conclusion, the observed flexibility pattern in the brain is the result of a complex interaction between the connectivity structure of the brain and the activation of cognitively relevant regions during the execution of each task. An extended study of the flexibility measure capacity in classification of Schizophrenia patients performing "theory of mind" task is in preparation by the author [Chi22] on the basis of findings in chapter 4. Future research that follows a simulation phase with tuning structural and functional elements of the model in accordance with the available literature on schizophrenia aids in replicating and explaining the greater variation in patients relative to the control group.

Despite the success in reconstructing the flexibility pattern, our model has severe simplification and limitations. Part of this comes from the n-back task nature. Although the n-back task is a well-studied manipulation of working-memory, the task's structure makes it difficult to differentiate the cognitive

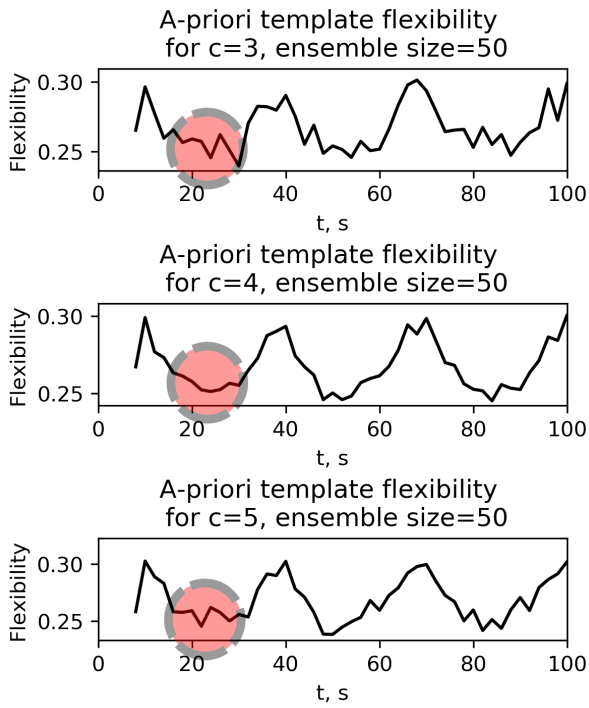

Figure 6.16. Effect of contrast of input step function upon middle-peak of flexibility response Three different I_k input amplitude c simulations. Fluctuations are observed in the flexibility pattern (calculated using the template flexibility method in chapter 2) but there is no consistent significant middle-peak effect in the highlighted zones [in the middle of two bigger peaks]. Ensemble size refers to number of runs with different random initial conditions.

processes of working-memory maintenance from information manipulation [Bra+15; Kri+05]. Our study was simplified by taking 0-back as the baseline and associating input only with the 2-back condition blocks. Although this follows the idea of task design (stimulating all elements of cognition in the baseline condition except for the aspect being researched), it is a very rough estimation of the cognitive process. Another limitation is the ability of a single Fitzhugh-Nagumo oscillator to simulate each brain area as large as a few cubic centimeters. The choice of region size has a substantial impact on our spatial resolution. Therefore, we overlook the critical fine-scale diversity in the complexity of human brain function.

Yet even with all simplifications and limitations, we believe that this simulations sheds some light on the possibility of simulating brain reconfiguration and the significance of brain structure in the reconfiguration process.

Supplementary Online Material: The Python and Julia scripts for our simulations together with some videos of the dynamical systems' behavior are accessible online here.

Chapter 7: CONCLUSION

AI powered painting created by Wombo art [tea] using chapter 7 keywords.

Chapter 7

Conclusion

"There is no real ending. It's just the place where you stop the story"

- Frank Herbert

This thesis was focused on a deeper investigation of meso-scale reconfigurations in human brain network extracted empirically from fMRI scans or artificially from computer simulations. A simple schematic of the subprojects in this thesis is shown in figure Figure 7.1

Chapter 1, gave a quick overview of essential concepts to the reader. Graphs, their adjacency matrices, weights, and representations were introduced in that chapter. A few different imaging techniques were briefly discussed the procedures used to gather them were mentioned. The broad method to building a network based on brain data was explained. The scales often used to study brain networks were discussed. The terms "functional" and "structural" brain networks were clarified and finally a few measures to investigate networks were introduced. The final sections were dedicated to the advantages of brain simulations to equip the reader with basic ideas behind this work.

The second chapter revisited brain flexibility as a meso-scale dynamical measure of brain network performance. This measure focuses on how the groups/clusters/modules formed by nodes in a network change over time as a result of gaining or losing members. The standard variation of this measure in the literature is based on heuristic algorithms like Louvain, the clusters that result from running the algorithm on the same adjacency matrix may differ each time. As a result, brain modules demonstrate diversity within and between people. This can be solved by running the algorithm as many times as we obtain a consensus on the modular structure. Nevertheless, it can be a computationally

intensive procedure, and the found modules may have little biological plausibility or cannot be interpreted easily. Our motivation to propose our novel "template/a-priori flexibility" measure in chapter 2 was to improve three main aspects: i) Reducing computation time by not needing a consensus for each matrix. ii) Improving replicability with keeping the same template in different subjects and samples. iii) Allowing researchers to select the most appropriate or biologically relevant module templates for each study. In our method, an apriori set of modules is adopted based on our knowledge of human brain [consider an example of all countries in the world map with people being nodes of a network located on this map]. At the first level, every node is assigned an a-priori affiliation [in our map example, every human being can be assigned a nationality based on their location]. On the second level, the correlation of time series from pair of brain nodes is regarded as a layer of information that can change the affiliation of that node, if the heaviest normalized sum of connections between a node and members of another module is stronger than the a-priori module of that node, the node is re-tagged as a member of the new dominant module [in our country example, imagine we check each individual's social media and if their number of friends in a country other than the one they are located in (normalized by the size of different countries) is bigger than their pre-assumed country, we assign them a new nationality based on the dominant nationality of their friends]. With this process, we find a deformed list of affiliations for nodes in each matrix or window of time. We then count the number of nodes that changed their affiliations between two consecutive windows [relative to all nodes] and interpret it as a measure of network flexibility [in our country exmaple, this measure can be an indicative of international mobility].
The study of flexibility gives us the opportunity to observe how the performance of a cognitively demanding task effects the structure and cooperation in the brain. Flexibility, with its broader definition of nodes reconfiguring in the brain as a result of function, has been found to associate with executive function [Bra+15], mentalization [Chi22], mood, fatigue and novelty of experience [Bet+16], aging [Bet+15] and learning [SB16].

Like all the proposed solutions to measure brain flexibility, there are limitations to our proposed method. The feasibility of modules depends heavily on the meaningful choice of a-priori modules. The reliability of normalization to the size of modules is reduced if the a-priori modules vary in size significantly. Our modules are separated by hard clustering, meaning a node can only belong to one single group, this can in turn result in overlooking the finer patterns of affiliation specially if a node has close to uniform weighted connection distribution to different modules.

Finally, we argue that our proposed a-priori method merits consideration due to its computational efficiency and promotion of replicability across dif-

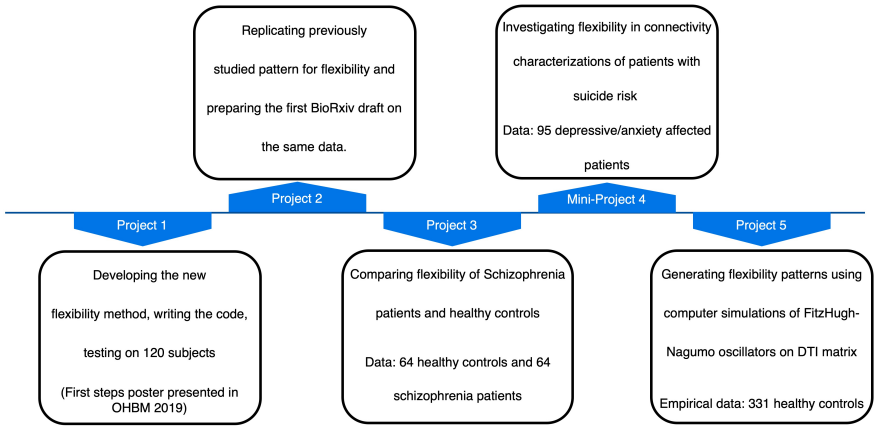

Figure 7.1. Overview of subprojects collected in this thesis
The 5 projects and their datasets are shown above. After developing the method and testing it on healthy control data, we implemented the techniques for the study of patients data. Finally, a first attempt to simulate the flexibility pattern as seen in the empirical data using a simplified model was made.

ferent samples and studies via the use of physiologically plausible template modules. We believe that the method can be a viable option for researchers wishing to examine dynamical reconfiguration at varying scales of the brain, including nodes, modules, and the whole brain.

In chapter 3, we apply the flexibility method developed in chapter 2 [originally developed and tested on a sample of 120 fMRI recordings from both healthy controls and patients before the OHBM (Organization for Human Brain Mapping) conference in 2019 where the initial poster of the idea was presented] to an fMRI dataset of 331 healthy subjects. The fMRI scans were acquired during the performance of the n-back working memory task, which was designed with alternating blocks of 2-back and 0-back. The reason to choose this dataset was the previous study by Braun et al [Bra+15] on it (we in fact only included 331 of their 344 patients. Thirteen subjects were excluded due to insufficient image quality, scanning artefacts or exceeding movement). Their study included an extensive Louvain-based flexibility analysis that could be used as a comparison basis for our investigation. We demonstrate that our method is capable of identifying a pattern of flexibility during the N-back working memory task that is highly similar to that found in Beaun et al [Bra+15]. The prefrontal cortex has a crucial role in the execution of working-memory tasks, as has been extensively demonstrated in the literature [BGS15; Cao+14; Min+15; Owe+05]. Thus, it is not unexpected that nodes in the prefrontal cortex demonstrated the most flexible behaviour during N-back task performance. Besides that, at the modular level, the most adaptable nodes are those with an a-prori affilia-

tion to the DMN, SN, L/RECN, and language modules. When fronto-parietal networks, such as the L/RECN, are more active during cognitively demanding tasks (such as the N-back), the DMN is less active [Fox+05]. Finally, the SN has a crucial role in allocating brain resources between more internally (DMN) and outwardly (ECN) focused functions [Udd+11]. We regard these findings as evidences that our flexibility method is able to capture reasonable aspects of the cognitive function. At this point, a curious mind might ask if this patterns of flexibility could be a basis for distinguishing patients from controls. With this in mind, we moved to the fourth chapter of this thesis.

Chapter 4 extended the use of flexibility-based measurements to patients, after having been tested on healthy participants in Chapter 3. The brain template flexibility of 64 schizophrenia patients and 64 healthy controls was compared on the three [topological axis] scales of nodes, modules, and whole-brain during the performance of a "Theory of Mind" task. Schizophrenia patients and healthy controls have significantly different variance and range in their whole brain flexibility time series [no significantly different mean]. Subjects in the schizophrenia group are more likely to have aberrant changes in whole brain flexibility at non-task-related intervals.

According to our investigation on module population dynamics, the Auditory, High Visual, LECN, sensorimotor, vDMN, and the 15th non-tagged module exhibit significantly different behaviors between the two groups. On the module population time series, the differences are observed using three measures (average, variance, and range). In resting state fMRI studies of schizophrenia patients, abnormalities in the DMN and Executive Control Networks have been extensively reported [CEP09; Sal+10; Lit+15]. Our findings suggest that the differences in DMN and ECN behavior extend to mentalizing tasks.

In schizophrenia patients, there is an overall decrease in give/take [of member nodes] changes associated with the task time-pattern of 30s. This is consistent with the lower contrast observed in several studies between ToM and control conditions. This difference can be explained by hypomentalization during ToM or hypermentalization during the control condition [Abu99; Fri04; LB08; Cia+15]. The findings suggest that the schizophrenic brain distinguishes less between TOM and control stimuli than the healthy brain, regardless of whether this difference is caused by hyper- or hypo-mentalizing.

Furthermore, some give/take measures show a distinct trend between the two groups. In the control group, Module 2 [Auditory] and Module 5 [High Visual] are dominant giver modules, whereas in the schizophrenia patients, they are stronger takers. This implies that these modules are receiving reinforcement from other modules and expanding at the task-block frequency. Several schizophrenia studies suggest that deficits in sensory processing and perception

are the root causes of dysfunction in higher cognitive levels in patients suffering from schizophrenia [Jav09b; Jav09a; JS15; Bor+18]. The different trends observed by our method in the auditory, visual, and sensorimotor modules could be interpreted as another hint towards schizophrenia perception-related abnormalities.
Finally, feeding the measures from the three scales of flexibility study to a simple GLM classifier, an average accuracy of 0.74 was achieved. This means that the flexibility measures increase the chance of classifying patients and controls in their correct corresponding groups to a significant degree.

Mini-chapter 5 was a brief report on the results of a group of our collaborators who explored the impact of suicidality on the brain network utilizing our template flexibility method as a tool. The author of this thesis was responsible for implementing the method on their data set. The fundamental difference between this application and our Schizophrenia chapter is that the data in the study desinged by Dickhoff et al was resting state fMRI. A resting state scan means that the subjects lay inside the scanner without being asked to perform a specific cognitive task. Methods based on the reconfigurations therefore might fail in capturing significant differences without synchronized instructed task being performed by the participants. Two major comparisons were performed in that study. One comparison was between participants with and without a history of suicide attempt. The other between participants with and without suicidal ideation. In the comparison of suicidal ideation vs no suicidal ideation, the two groups differed in accumulated whole-brain flexibility (i.e., the total change of network connections across time for all 246 nodes) ($F(1,81)= 5.33$, $p=.02$, $\eta^2 = .062$). In the other comparison, only on the module level, the right central executive network (RECN) demonstrated a small difference between suicide attempt and no attempt ($F(1,81)=.388$, $p=.05$, $\eta 2=.046$), indicating that this network expanded and contracted more in those who attempted suicide.

In the sixth chapter, a simplified oscillator model in physics was used to replicate the flexibility pattern found in the N-back empirical data. This simulation was built on an averaged empirical brain structural network based on DTI data, the nodes showed a dynamics following a form of the FitzHughNagumo (FHN) oscillator equations. Six nodes that associate with working memory were given a square-wave input in the blocks resembling 2-back. The output from FHN oscillators was then fed to the Balloon model in order to generate fMRI-like signals. Although this simulation was an extremely simplified first attempt to regenerate the flexibility pattern, the results were showing some potentials for further research. The simulated reconstruction allows for a more in-depth evaluation of the effects of factors such as brain structure. The network structure of the brain has a substantial impact on the collaboration of

brain regions and the performance of cognitive tasks. This network did not exhibit the expected oscillating flexibility behavior when it underwent random reshuffling. Moreover, the patterns were influenced by the selection of regions that were stimulated during the execution of our artificial cognitive task. Changes in the task-activated regions could result in the observation of significantly different patterns. When the heaviest (in terms of weighted connections) nodes of the network were receiving the square-wave input, the start of 0-back and 2-back blocks were not showing the considerably similar peak heights they showed in middle and light nodes stimulation scenarios. We can carefully conclude that the observed pattern of brain flexibility is the consequence of a complex interaction between the structure of the brain and the activation of cognitively important regions during the performance of each task though further more accurate simulations with more details are always needed to have a better chance of uncovering the exact mechanism behind the complex brain behaviour.

Anyway, we still need a Hari Seldon of the twenty-first century Earth to mathematically prove that the complexity of the human brain can be captured by things less complex than the human brain.

"Well then, we know that some comparatively simple things are easy to simulate and as things grow more and more complex they become harder to simulate until finally they become impossible to simulate. But at what level of complexity does simulation cease to be possible? Well, what I have shown, making use of a mathematical technique first invented in this past century and barely usable even if one employs a large and very fast computer, our Galactic society falls short of that mark. It can be represented by a simulation simpler than itself. And I went on to show that this would result in the ability to predict future events in a statistical fashion-that is, by stating the probability for alternate sets of events, rather than flatly predicting that one set will take place."*

* From "Prelude to Foundation" by Isaac Asimov. Conversation between Hari Seldon, the mathematician and Hummin, the reporter.

Bibliography

[Abu99] Ahmad Abu-Akel. "Impaired theory of mind in schizophrenia". In: *Pragmatics & cognition* 7.2 (1999), pp. 247–282.

[Ade+87] George Adelman et al. *Encyclopedia of neuroscience*. Birkhäuser, 1987.

[Ala+15] Mohsen Alavash et al. "Persistency and flexibility of complex brain networks underlie dual-task interference". In: *Human brain mapping* 36.9 (2015), pp. 3542–3562.

[Ass+13] American Psychiatric Association et al. *Diagnostic and statistical manual of mental disorders (DSM-5®)*. American Psychiatric Pub, 2013.

[Bad92] Alan Baddeley. "Working memory". In: *Science* 255.5044 (1992), pp. 556–559.

[Ban20] Peter A Bandettini. *Fmri*. MIT Press, 2020.

[Bar+01] Simon Baron-Cohen et al. "The "Reading the Mind in the Eyes" Test revised version: a study with normal adults, and adults with Asperger syndrome or high-functioning autism". In: *The Journal of Child Psychology and Psychiatry and Allied Disciplines* 42.2 (2001), pp. 241–251.

[Bas+11] Danielle S Bassett et al. "Dynamic reconfiguration of human brain networks during learning". In: *Proceedings of the National Academy of Sciences* 108.18 (2011), pp. 7641–7646.

[Bas+15] Danielle S Bassett et al. "Learning-induced autonomy of sensorimotor systems". In: *Nature neuroscience* 18.5 (2015), pp. 744–751.

[Baz+16] Marya Bazzi et al. "Community detection in temporal multilayer networks, with an application to correlation networks". In: *Multiscale Modeling & Simulation* 14.1 (2016), pp. 1–41.

[BB17a] Richard F Betzel and Danielle S Bassett. "Multi-scale brain networks". In: *Neuroimage* 160 (2017), pp. 73–83.

[BB17b] Richard F Betzel and Danielle S Bassett. "Multi-scale brain networks". In: *Neuroimage* 160 (2017), pp. 73–83.

[Bet+15] Richard F Betzel et al. "Functional brain modules reconfigure at multiple scales across the human lifespan". In: *arXiv preprint arXiv:1510.08045* (2015).

[Bet+16] Richard F Betzel et al. "A positive mood, a flexible brain". In: *arXiv preprint arXiv:1601.07881* (2016).

[Bey+13] Johanna Beyer et al. "Exploring the connectome: Petascale volume visualization of microscopy data streams". In: *IEEE computer graphics and applications* 33.4 (2013), pp. 50–61.

[BGS15] Kurt Braunlich, Javier Gomez-Lavin, and Carol A Seger. "Frontoparietal networks involved in categorization and item working memory". In: *NeuroImage* 107 (2015), pp. 146–162.

[BHV21] Şeyma Bayrak, Philipp Hövel, and Vesna Vuksanović. "Modeling functional connectivity on empirical and randomized structural brain networks". In: *Differential Equations and Dynamical Systems* 29.4 (2021), pp. 789–805.

[BJO02] Matthew Brett, Ingrid S Johnsrude, and Adrian M Owen. "The problem of functional localization in the human brain". In: *Nature reviews neuroscience* 3.3 (2002), pp. 243–249.

[Blo+08] Vincent D Blondel et al. "Fast unfolding of communities in large networks". In: *Journal of statistical mechanics: theory and experiment* 2008.10 (2008), p. 10008.

[BM+76] John Adrian Bondy, Uppaluri Siva Ramachandra Murty, et al. *Graph theory with applications*. Vol. 290. Macmillan London, 1976.

[BM08] J A Bondy and U S R Murty. "Graph Theory, 6 Springer". In: *Grad. Texts in Math* 244 (2008).

[Boc+14] Stefano Boccaletti et al. "The structure and dynamics of multilayer networks". In: *Physics reports* 544.1 (2014), pp. 1–122.

[Bor+10] Elena Borra et al. "Cortical connections to area TE in monkey: hybrid modular and distributed organization". In: *Cerebral cortex* 20.2 (2010), pp. 257–270.

[Bor+18] Cécile Bordier et al. "Disrupted modular organization of primary sensory brain areas in schizophrenia". In: *NeuroImage: Clinical* 18 (2018), pp. 682–693.

[Bra+15] Urs Braun et al. "Dynamic reconfiguration of frontal brain networks during executive cognition in humans". In: *Proceedings of the National Academy of Sciences* 112.37 (2015), pp. 11678–11683.

[Bri+14] Matthew R. Brier et al. "Functional connectivity and graph theory in preclinical Alzheimer's disease". In: *Neurobiology of Aging* 35.4 (2014), pp. 757–768. issn: 0197-4580.

[Buc+09] Randy L Buckner et al. "Cortical hubs revealed by intrinsic functional connectivity: mapping, assessment of stability, and relation to Alzheimer's disease". In: *Journal of neuroscience* 29.6 (2009), pp. 1860–1873.

[Buz04] György Buzsáki. "Large-scale recording of neuronal ensembles". In: *Nature neuroscience* 7.5 (2004), pp. 446–451.

[CAA18] Wen Jia Chai, Aini Ismafairus Abd Hamid, and Jafri Malin Abdullah. "Working memory from the psychological and neurosciences perspectives: a review". In: *Frontiers in psychology* 9 (2018), p. 401.

[Cak20] Yuksel Cakir. "Hybrid modeling of alpha rhythm and the amplitude of low-frequency fluctuations abnormalities in the thalamocortical region and basal ganglia in Alzheimer's disease". In: *European Journal of Neuroscience* 52.2 (2020), pp. 2944–2961.

[Cal+14] Vince D Calhoun et al. "The chronnectome: time-varying connectivity networks as the next frontier in fMRI data discovery". In: *Neuron* 84.2 (2014), pp. 262–274.

[Cao+14] Hengyi Cao et al. "Test–retest reliability of fMRI-based graph theoretical properties during working memory, emotion processing, and resting state". In: *Neuroimage* 84 (2014), pp. 888–900.

[CEP09] Vince D Calhoun, Tom Eichele, and Godfrey Pearlson. "Functional brain networks in schizophrenia: a review". In: *Frontiers in human neuroscience* 3 (2009), p. 17.

[Cha+10] Mario Chavez et al. "Functional modularity of background activities in normal and epileptic brain networks". In: *Physical review letters* 104.11 (2010), p. 118701.

[Chi+22] Narges Chinichian et al. "A Fast and Intuitive Method for Calculating Dynamic Network Reconfiguration and Node Flexibility". In: *bioRxiv* (2022).

[Chi22] Narges et al Chinichian. "Aberrant change in brain network flexibility during the performance of Theory of Mind task in schizophrenia patients". In: *in preparation, extended abstract in Complex Networks 2022 conference book of abstracts* (2022).

[Cia+15] Angela Ciaramidaro et al. "Schizophrenia and autism as contrasting minds: neural evidence for the hypo-hyper-intentionality hypothesis". In: *Schizophrenia bulletin* 41.1 (2015), pp. 171–179.

[Coc+22] Carrisa Cocuzza et al. "CDistributed network processes account for the majority of variance in localized visual category selectivity". In: *BioRxiv Preprint* (2022). doi: https://doi.org/10.1101/2022.02.19.481103.

[CS20] Christoph U Correll and Nina R Schooler. "Negative symptoms in schizophrenia: A review and clinical guide for recognition, assessment, and treatment." In: *Neuropsychiatric disease and treatment* (2020).

[Dem+17] Murat Demirtaş et al. "A whole-brain computational modeling approach to explain the alterations in resting-state functional connectivity during progression of Alzheimer's disease". In: *NeuroImage: Clinical* 16 (2017), pp. 343–354.

[Dow+01] Paul E Downing et al. "A cortical area selective for visual processing of the human body". In: *Science* 293.5539 (2001), pp. 2470–2473.

[Egu+05] Victor M Eguiluz et al. "Scale-free brain functional networks". In: *Physical review letters* 94.1 (2005), p. 018102.

[Erk+17] S Erk et al. "Functional neuroimaging effects of recently discovered genetic risk loci for schizophrenia and polygenic risk profile in five RDoC subdomains". In: *Translational psychiatry* 7.1 (2017), e997–e997.

[Ess+09] Christine Esslinger et al. "Neural mechanisms of a genome-wide supported psychosis variant". In: *Science* 324.5927 (2009), pp. 605–605.

[Eul41] Leonhard Euler. "Solutio problematis ad geometriam situs pertinentis". In: *Commentarii academiae scientiarum Petropolitanae* (1741), pp. 128–140.

[Fai+09] Damien A Fair et al. "Functional brain networks develop from a "local to distributed" organization". In: *PLoS comput biol* 5.5 (2009), e1000381.

[Fan+16] Lingzhong Fan et al. "The human brainnetome atlas: a new brain atlas based on connectional architecture". In: *Cerebral cortex* 26.8 (2016), pp. 3508–3526.

[FDK22] Henrique M Fernandes, Gustavo Deco, and Morten L Kringelbach. "Whole-brain modeling to predict optimal deep brain stimulation targeting". In: *Connectomic Deep Brain Stimulation*. Elsevier, 2022, pp. 543–559.

[Fin+20] Karolina Finc et al. "Dynamic reconfiguration of functional brain networks during working memory training". In: *Nature communications* 11.1 (2020), pp. 1–15.

[Fit61] Richard FitzHugh. "Impulses and physiological states in theoretical models of nerve membrane". In: *Biophysical journal* 1.6 (1961), pp. 445–466.

[FKL19] Farzad V Farahani, Waldemar Karwowski, and Nichole R Lighthall. "Application of graph theory for identifying connectivity patterns in human brain networks: a systematic review". In: *frontiers in Neuroscience* 13 (2019), p. 585.

[For10] S. Fortunato. "Community detection in graphs". In: *Phys. Rep.-Rev. Sec. Phys. Lett.* 486 (2010), pp. 75–174.

[Fox+05] Michael D Fox et al. "The human brain is intrinsically organized into dynamic, anticorrelated functional networks". In: *Proceedings of the National Academy of Sciences* 102.27 (2005), pp. 9673–9678.

[Fri+00] Karl J Friston et al. "Nonlinear responses in fMRI: the Balloon model, Volterra kernels, and other hemodynamics". In: *NeuroImage* 12.4 (2000), pp. 466–477.

[Fri04] Christopher D Frith. "Schizophrenia and theory of mind". In: *Psychological medicine* 34.3 (2004), pp. 385–389.

[Fri11] Karl J Friston. "Functional and effective connectivity: a review". In: *Brain connectivity* 1.1 (2011), pp. 13–36.

[Fri14] Christopher Donald Frith. *The cognitive neuropsychology of schizophrenia*. Psychology press, 2014.

[FZB16] Alex Fornito, Andrew Zalesky, and Edward Bullmore. *Fundamentals of brain network analysis*. Academic Press, 2016.

[Gal+20] Riccardo Gallotti et al. "Assessing the risks of 'infodemics' in response to COVID-19 epidemics". In: *Nature human behaviour* 4.12 (2020), pp. 1285–1293.

[Ger+14] Wulfram Gerstner et al. *Neuronal dynamics: From single neurons to networks and models of cognition*. Cambridge University Press, 2014.

[Ger+20] Moritz Gerster et al. "FitzHugh–Nagumo oscillators on complex networks mimic epileptic-seizure-related synchronization phenomena<? A3B2 show [editpick]?>" In: *Chaos: An Interdisciplinary Journal of Nonlinear Science* 30.12 (2020), p. 123130.

[Gho+08] Anandamohan Ghosh et al. "Noise during rest enables the exploration of the brain's dynamic repertoire". In: *PLoS Comput Biol* 4.10 (2008), e1000196.

[Gog+04] Nitin Gogtay et al. "Dynamic mapping of human cortical development during childhood through early adulthood". In: *Proceedings of the National Academy of Sciences* 101.21 (2004), pp. 8174–8179.

[Gol96] Patricia S Goldman-Rakic. "The prefrontal landscape: implications of functional architecture for understanding human mentation and the central executive". In: *Philosophical Transactions of the Royal Society of London. Series B: Biological Sciences* 351.1346 (1996), pp. 1445–1453.

[Gre+08] Michael F Green et al. "Social cognition in schizophrenia: an NIMH workshop on definitions, assessment, and research opportunities". In: *Schizophrenia bulletin* 34.6 (2008), pp. 1211–1220.

[H2O] H2O.ai. *Source code h2o model metrics base*. Accessed: 2022-04-11. url: shorturl.at/evJ05.

[H2O20] H2O.ai. *h2o: Python Interface for H2O*. Python package version 3.36.0.4. 2020. url: https://github.com/h2oai/h2o-3.

[Har+19] Vatika Harlalka et al. "Atypical flexibility in dynamic functional connectivity quantifies the severity in autism spectrum disorder". In: *Frontiers in human neuroscience* 13 (2019), p. 6.

[Has+20] Meysam Hashemi et al. "The Bayesian Virtual Epileptic Patient: A probabilistic framework designed to infer the spatial map of epileptogenicity in a personalized large-scale brain model of epilepsy spread". In: *NeuroImage* 217 (2020), p. 116839.

[He+09] Yong He et al. "Uncovering intrinsic modular organization of spontaneous brain activity in humans". In: *PloS one* 4.4 (2009), e5226.

[HH18] Michael N Hallquist and Frank G Hillary. "Graph theory approaches to functional network organization in brain disorders: A critique for a brave new small-world". In: *Network Neuroscience* 3.1 (2018), pp. 1–26.

[HK15] Andreas Horn and Andrea A Kühn. "Lead-DBS: a toolbox for deep brain stimulation electrode localizations and visualizations". In: *Neuroimage* 107 (2015), pp. 127–135.

[Hor+17] Andreas Horn et al. "Probabilistic conversion of neurosurgical DBS electrode coordinates into MNI space". In: *Neuroimage* 150 (2017), pp. 395–404.

[Hor+19] Andreas Horn et al. "Lead-DBS v2: Towards a comprehensive pipeline for deep brain stimulation imaging". In: *Neuroimage* 184 (2019), pp. 293–316.

[HP85] U Halsband and RE Passingham. "Premotor cortex and the conditions for movement in monkeys (Macaca fascicularis)". In: *Behavioural brain research* 18.3 (1985), pp. 269–277.

[Huf03] Carl Huffman. "Alcmaeon". In: (2003).

[Hun07a] J. D. Hunter. "Matplotlib: A 2D graphics environment". In: *Computing in Science & Engineering* 9.3 (2007), pp. 90–95. doi: 10.1109/MCSE.2007.55.

[Hun07b] John D Hunter. "Matplotlib: A 2D graphics environment". In: *Computing in science & engineering* 9.3 (2007), pp. 90–95.

[Iid14] Tetsuya Iidaka. "Role of the fusiform gyrus and superior temporal sulcus in face perception and recognition: An empirical review". In: *Japanese Psychological Research* 56.1 (2014), pp. 33–45.

[IT20] Hiroyasu Inoue and Yasuyuki Todo. "The propagation of economic impacts through supply chains: The case of a mega-city lockdown to prevent the spread of COVID-19". In: *PloS one* 15.9 (2020), e0239251.

[Jav09a] Daniel C Javitt. "Sensory processing in schizophrenia: neither simple nor intact". In: *Schizophrenia bulletin* 35.6 (2009), pp. 1059–1064.

[Jav09b] Daniel C Javitt. "When doors of perception close: bottom-up models of disrupted cognition in schizophrenia". In: *Annual review of clinical psychology* 5 (2009), pp. 249–275.

[Jeu+] Lucas Jeub et al. *A generalized Louvain method for community detection implemented in MATLAB*. url: https://github.com/GenLouvain/GenLouvain.

[JS15] Daniel C Javitt and Robert A Sweet. "Auditory dysfunction in schizophrenia: integrating clinical and basic features". In: *Nature Reviews Neuroscience* 16.9 (2015), pp. 535–550.

[Kan10] Nancy Kanwisher. "Functional specificity in the human brain: a window into the functional architecture of the mind". In: *Proceedings of the National Academy of Sciences* 107.25 (2010), pp. 11163–11170.

[Kir58] Wayne K Kirchner. "Age differences in short-term retention of rapidly changing information." In: *Journal of experimental psychology* 55.4 (1958), p. 352.

[KKG18] Petra Klepac, Stephen Kissler, and Julia Gog. "Contagion! the bbc four pandemic–the model behind the documentary". In: *Epidemics* 24 (2018), pp. 49–59.

[KMC97] Nancy Kanwisher, Josh McDermott, and Marvin M Chun. "The fusiform face area: a module in human extrastriate cortex specialized for face perception". In: *Journal of neuroscience* 17.11 (1997), pp. 4302–4311.

[Kri+05] Stephan Krieger et al. "Executive function and cognitive subprocesses in first-episode, drug-naive schizophrenia: an analysis of N-back performance". In: *American Journal of Psychiatry* 162.6 (2005), pp. 1206–1208.

[Kru09] Leah Krubitzer. "In search of a unifying theory of complex brain evolution". In: *Annals of the New York Academy of Sciences* 1156.1 (2009), pp. 44–67.

[KVL19] Waldemar Karwowski, Farzad Vasheghani Farahani, and Nichole Lighthall. "Application of graph theory for identifying connectivity patterns in human brain networks: a systematic review". In: *frontiers in Neuroscience* 13 (2019), p. 585.

[KY06] Nancy Kanwisher and Galit Yovel. "The fusiform face area: a cortical region specialized for the perception of faces". In: *Philosophical Transactions of the Royal Society B: Biological Sciences* 361.1476 (2006), pp. 2109–2128.

[LB08] Robyn Langdon and Jon Brock. "Hypo-or hyper-mentalizing: It all depends upon what one means by "mentalizing"". In: *Behavioral and Brain Sciences* 31.3 (2008), pp. 274–275.

[Lew11] Ted G Lewis. *Network science: Theory and applications*. John Wiley & Sons, 2011.

[LF12] Andrea Lancichinetti and Santo Fortunato. "Consensus clustering in complex networks". In: *Scientific reports* 2.1 (2012), pp. 1–7.

[Lia+12] Xia Liang et al. "Effects of different correlation metrics and preprocessing factors on small-world brain functional networks: a resting-state functional MRI study". In: *PloS one* 7.3 (2012), e32766.

[LIS78] Niels A Lassen, David H Ingvar, and Erik Skinhøj. "Brain function and blood flow". In: *Scientific American* 239.4 (1978), pp. 62–71.

[Lit+15] Harri Littow et al. "Aberrant functional connectivity in the default mode and central executive networks in subjects with schizophrenia–a whole-brain resting-state ICA study". In: *Frontiers in psychiatry* 6 (2015), p. 26.

[Liu+08] Yong Liu et al. "Disrupted small-world networks in schizophrenia". In: *Brain* 131.4 (2008), pp. 945–961.

[Lop18] Silvia Lope-Piedrafita. "Diffusion tensor imaging (DTI)". In: *Preclinical MRI*. Springer, 2018, pp. 103–116.

[LV15] Nora Leonardi and Dimitri Van De Ville. "On spurious and real fluctuations of dynamic functional connectivity during rest". In: *Neuroimage* 104 (2015), pp. 430–436.

[Ma+20] Qing Ma et al. "Transdiagnostic dysfunctions in brain modules across patients with schizophrenia, bipolar disorder, and major depressive disorder: a connectome-based study". In: *Schizophrenia bulletin* 46.3 (2020), pp. 699–712.

[Man+99] Joseph B Mandeville et al. "Evidence of a cerebrovascular postarteriole windkessel with delayed compliance". In: *Journal of Cerebral Blood Flow & Metabolism* 19.6 (1999), pp. 679–689.

[MBK09] Marieke Mur, Peter A Bandettini, and Nikolaus Kriegeskorte. "Revealing representational content with pattern-information fMRI—an introductory guide". In: *Social cognitive and affective neuroscience* 4.1 (2009), pp. 101–109.

[Meu+09] David Meunier et al. "Age-related changes in modular organization of human brain functional networks". In: *Neuroimage* 44.3 (2009), pp. 715–723.

[Min+15] Takehiro Minamoto et al. "The rostral prefrontal cortex underlies individual differences in working memory capacity: An approach from the hierarchical model of the cognitive control". In: *Cortex* 71 (2015), pp. 277–290.

[MLB10] David Meunier, Renaud Lambiotte, and Edward T Bullmore. "Modular and hierarchically modular organization of brain networks". In: *Frontiers in neuroscience* 4 (2010), p. 200.

[Moh+14] Sebastian Mohnke et al. "Further evidence for the impact of a genome-wide-supported psychosis risk variant in ZNF804A on the Theory of Mind Network". In: *Neuropsychopharmacology* 39.5 (2014), pp. 1196–1205.

[Moh+16] Sebastian Mohnke et al. "Theory of mind network activity is altered in subjects with familial liability for schizophrenia". In: *Social cognitive and affective neuroscience* 11.2 (2016), pp. 299–307.

[Mos81] Angelo Mosso. "Concerning the circulation of the blood in the human brain". In: *Leipzig: Verlag von Viet & Company* (1881).

[MPJ18] Rogier B Mars, Richard E Passingham, and Saad Jbabdi. "Connectivity fingerprints: from areal descriptions to abstract spaces". In: *Trends in cognitive sciences* 22.11 (2018), pp. 1026–1037.

[MS99] Akira Miyake and Priti Shah. *Models of working memory: Mechanisms of active maintenance and executive control*. Cambridge University Press, 1999.

[Muc+10] Peter J Mucha et al. "Community structure in time-dependent, multiscale, and multiplex networks". In: *science* 328.5980 (2010), pp. 876–878.

[MUM83] Mortimer Mishkin, Leslie G Ungerleider, and Kathleen A Macko. "Object vision and spatial vision: two cortical pathways". In: *Trends in neurosciences* 6 (1983), pp. 414–417.

[New+09] Karl M Newell et al. "Adaptation and learning: Characteristic time scales of performance dynamics". In: *Human movement science* 28.6 (2009), pp. 655–687.

[New06] Mark EJ Newman. "Modularity and community structure in networks". In: *Proceedings of the national academy of sciences* 103.23 (2006), pp. 8577–8582.

[New10] Mark Newman. *Networks*. Oxford university press, 2010.

[NHB09] Toru Nakamura, Frank G Hillary, and Bharat B Biswal. "Resting network plasticity following brain injury". In: *PloS one* 4.12 (2009), e8220.

[NS04] Robert A Novelline and Lucy Frank Squire. *Squire's fundamentals of radiology*. La Editorial, UPR, 2004.

[NS05] Ernst Niedermeyer and FH Lopes da Silva. *Electroencephalography: basic principles, clinical applications, and related fields*. Lippincott Williams & Wilkins, 2005.

[Nyk+22] T. Nykodym et al. *Generalized Linear Modeling with H2O*. Mar. 2022. url: https://docs.h2o.ai/h2o/latest-stable/h2o-docs/booklets/GLMBooklet.pdf.

[OHK08] Hans P Op de Beeck, Johannes Haushofer, and Nancy G Kanwisher. "Interpreting fMRI data: maps, modules and dimensions". In: *Nature Reviews Neuroscience* 9.2 (2008), pp. 123–135.

[Ole18] Michał Oleksowicz. "Aristotle on the Heart and Brain". In: *European Journal of Science and Theology* 14.3 (2018), pp. 77–94.

[Olm+19] Simona Olmi et al. "Controlling seizure propagation in large-scale brain networks". In: *PLoS computational biology* 15.2 (2019), e1006805.

[OP09] Tore Opsahl and Pietro Panzarasa. "Clustering in weighted networks". In: *Social networks* 31.2 (2009), pp. 155–163.

[Owe+05] Adrian M Owen et al. "N-back working memory paradigm: A meta-analysis of normative functional neuroimaging studies". In: *Human brain mapping* 25.1 (2005), pp. 46–59.

[Pas85] RE Passingham. "Premotor cortex: sensory cues and movement". In: *Behavioural brain research* 18.2 (1985), pp. 175–185.

[PBV07] Gergely Palla, Albert-László Barabási, and Tamás Vicsek. "Quantifying social group evolution". In: *Nature* 446.7136 (2007), pp. 664–667.

[PC09] Soojin Park and Marvin M Chun. "Different roles of the parahippocampal place area (PPA) and retrosplenial cortex (RSC) in panoramic scene perception". In: *Neuroimage* 47.4 (2009), pp. 1747–1756.

[Ped+11] F. Pedregosa et al. "Scikit-learn: Machine Learning in Python". In: *Journal of Machine Learning Research* 12 (2011), pp. 2825–2830.

[Pen+11] William D Penny et al. *Statistical parametric mapping: the analysis of functional brain images*. Elsevier, 2011.

[Per+19] Alistair Perry et al. "Connectomics of bipolar disorder: a critical review, and evidence for dynamic instabilities within interoceptive networks". In: *Molecular psychiatry* 24.9 (2019), pp. 1296–1318.

[Pow+10] Jonathan D Power et al. "The development of human functional brain networks". In: *Neuron* 67.5 (2010), pp. 735–748.

[PQB05] Ernesto Pereda, Rodrigo Quian Quiroga, and Joydeep Bhattacharya. "Nonlinear multivariate analysis of neurophysiological signals". In: *Progress in neurobiology* 77.1-2 (2005), pp. 1–37.

[Pro+18] Timothée Proix et al. "Predicting the spatiotemporal diversity of seizure propagation and termination in human focal epilepsy". In: *Nature communications* 9.1 (2018), pp. 1–15.

[PSK02] Richard E Passingham, Klaas E Stephan, and Rolf Kötter. "The anatomical basis of functional localization in the cortex". In: *Nature Reviews Neuroscience* 3.8 (2002), pp. 606–616.

[RS10] Mikail Rubinov and Olaf Sporns. "Complex network measures of brain connectivity: uses and interpretations". In: *Neuroimage* 52.3 (2010), pp. 1059–1069.

[Sal+10] Raymond Salvador et al. "Overall brain connectivity maps show cortico-subcortical abnormalities in schizophrenia". In: *Human brain mapping* 31.12 (2010), pp. 2003–2014.

[San+14] Stefano Sandrone et al. "Weighing brain activity with the balance: Angelo Mosso's original manuscripts come to light". In: *Brain* 137.2 (2014), pp. 621–633.

[SB16] Olaf Sporns and Richard F Betzel. "Modular brain networks". In: *Annual review of psychology* 67 (2016), pp. 613–640.

[Sch+11] Knut Schnell et al. "Functional relations of empathy and mentalizing: an fMRI study on the neural basis of cognitive empathy". In: *Neuroimage* 54.2 (2011), pp. 1743–1754.

[Sch+17] Gerwin Schalk et al. "Facephenes and rainbows: Causal evidence for functional and anatomical specificity of face and color processing in the human brain". In: *Proceedings of the National Academy of Sciences* 114.46 (2017), pp. 12285–12290.

[Sha+11] Ameneh Shahaeian et al. "Culture and the sequence of steps in theory of mind development." In: *Developmental psychology* 47.5 (2011), p. 1239.

[Shi+12] William R Shirer et al. "Decoding subject-driven cognitive states with whole-brain connectivity patterns". In: *Cerebral cortex* 22.1 (2012), pp. 158–165.

[SMD04] Felice T Sun, Lee M Miller, and Mark D'esposito. "Measuring interregional functional connectivity using coherence and partial coherence analyses of fMRI data". In: *Neuroimage* 21.2 (2004), pp. 647–658.

[Smi+06] Stephen M Smith et al. "Tract-based spatial statistics: voxelwise analysis of multi-subject diffusion data". In: *Neuroimage* 31.4 (2006), pp. 1487–1505.

[Smi+11] Stephen M Smith et al. "Network modelling methods for FMRI". In: *Neuroimage* 54.2 (2011), pp. 875–891.

[Spo10] Olaf Sporns. *Networks of the Brain*. MIT press, 2010.

[Spo12] Olaf Sporns. "From simple graphs to the connectome: networks in neuroimaging". In: *Neuroimage* 62.2 (2012), pp. 881–886.

[Spr+07] Mirjam Sprong et al. "Theory of mind in schizophrenia: meta-analysis". In: *The British journal of psychiatry* 191.1 (2007), pp. 5–13.

[Syl78] James Joseph Sylvester. "Chemistry and algebra". In: *Nature* 17.432 (1878), p. 284.

[Tan+22] Wladimir Tantchik et al. "Investigating the neural correlates of affective mentalizing and their association with general intelligence in patients with schizophrenia". In: *In submission* (2022).

[tea] Wombo team. *Wombo Art wombo.ai*. https://www.wombo.ai/. Accessed: 2021.

[Tre+20] Svenja Treu et al. "Deep brain stimulation: imaging on a group level". In: *Neuroimage* 219 (2020), p. 117018.

[Tso18] Ioannis Tsoukalas. "Theory of mind: towards an evolutionary theory". In: *Evolutionary Psychological Science* 4.1 (2018), pp. 38–66.

[TTT05] Mario Tudor, Lorainne Tudor, and Katarina Ivana Tudor. "Hans Berger (1873-1941)–the history of electroencephalography". In: *Acta medica Croatica: casopis Hravatske akademije medicinskih znanosti* 59.4 (2005), pp. 307–313.

[TWD07] John C Taylor, Alison J Wiggett, and Paul E Downing. "Functional MRI analysis of body and body part representations in the extrastriate and fusiform body areas". In: *Journal of neurophysiology* 98.3 (2007), pp. 1626–1633.

[Udd+11] Lucina Q Uddin et al. "Dynamic reconfiguration of structural and functional connectivity across core neurocognitive brain networks with development". In: *Journal of Neuroscience* 31.50 (2011), pp. 18578–18589.

[Vir+20] Pauli Virtanen et al. "SciPy 1.0: Fundamental Algorithms for Scientific Computing in Python". In: *Nature Methods* 17 (2020), pp. 261–272. doi: 10.1038/s41592-019-0686-2.

[VM18] Michael Vaiana and Sarah Feldt Muldoon. "Multilayer brain networks". In: *Journal of Nonlinear Science* (2018), pp. 1–23.

[Wal+11] Henrik Walter et al. "Effects of a genome-wide supported psychosis risk variant on neural activation during a theory-of-mind task". In: *Molecular psychiatry* 16.4 (2011), pp. 462–470.

[Wan+09] Jinhui Wang et al. "Parcellation-dependent small-world brain functional networks: A resting-state fMRI study". In: *Human brain mapping* 30.5 (2009), pp. 1511–1523.

[Wei+18] Kevin S Weiner et al. "Defining the most probable location of the parahippocampal place area using cortex-based alignment and cross-validation". In: *Neuroimage* 170 (2018), pp. 373–384.

[Wel+06] Henry M Wellman et al. "Scaling of theory-of-mind understandings in Chinese children". In: *Psychological science* 17.12 (2006), pp. 1075–1081.

[Win22] H Richard Winn. *Youmans and Winn Neurological Surgery E-Book*. Elsevier Health Sciences, 2022.

[WL04] Henry M Wellman and David Liu. "Scaling of theory-of-mind tasks". In: *Child development* 75.2 (2004), pp. 523–541.

[XT15] Dongkuan Xu and Yingjie Tian. "A comprehensive survey of clustering algorithms". In: *Annals of Data Science* 2.2 (2015), pp. 165–193.

[Yue+17] Qiuhai Yue et al. "Brain modularity mediates the relation between task complexity and performance". In: *Journal of cognitive neuroscience* 29.9 (2017), pp. 1532–1546.

[Zha+11] Junran Zhang et al. "Disrupted brain connectivity networks in drug-naive, first-episode major depressive disorder". In: *Biological psychiatry* 70.4 (2011), pp. 334–342.

[ZY15] Xiaoyan Zhan and Rongjun Yu. "A window into the brain: advances in psychiatric fMRI". In: *BioMed research international* 2015 (2015).

Appendix A

Supporting information

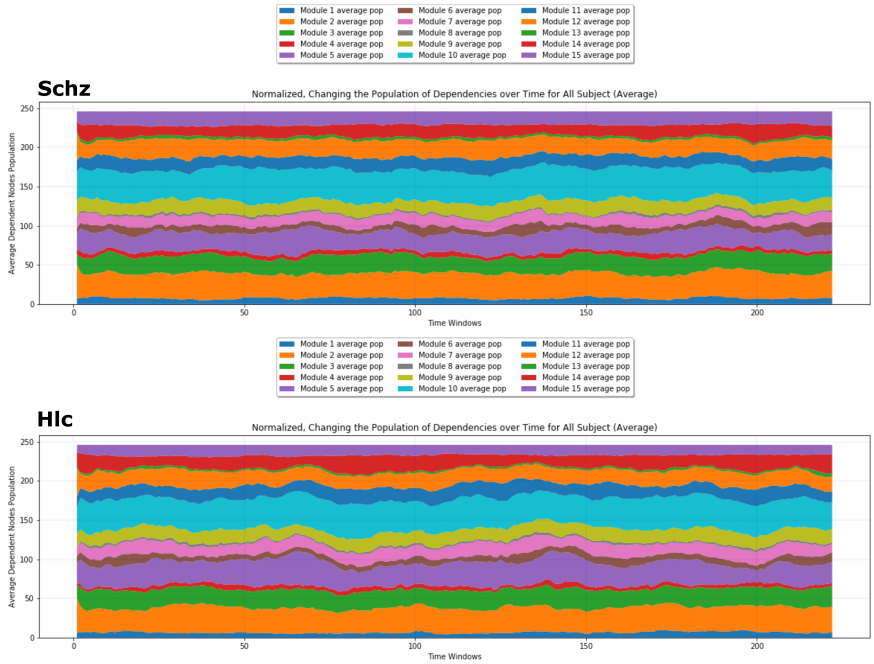

Figure S1. Chapter 4: Average population of all modules averaged for each group
Top: schizophrenia patients. Bottom: healthy controls

Lobe	Gyrus	Label ID.L	Label ID.R	
Frontal Lobe	SFG, Superior Frontal Gyrus	1	2	A8m, medial area 8
		3	4	A8dl, dorsolateral area 8
		5	6	A9l, lateral area 9
		7	8	A6dl, dorsolateral area 6
		9	10	A6m, medial area 6
		11	12	A9m,medial area 9
		13	14	A10m, medial area 10
	MFG, Middle Frontal Gyrus	15	16	A9/46d, dorsal area 9/46
		17	18	IFJ, inferior frontal junction
		19	20	A46, area 46
		21	22	A9/46v, ventral area 9/46
		23	24	A8vl, ventrolateral area 8
		25	26	A6vl, ventrolateral area 6
		27	28	A10l, lateral area10
	IFG, Inferior Frontal Gyrus	29	30	A44d,dorsal area 44
		31	32	IFS, inferior frontal sulcus
		33	34	A45c, caudal area 45
		35	36	A45r, rostral area 45
		37	38	A44op, opercular area 44
		39	40	A44v, ventral area 44
	OrG, Orbital Gyrus	41	42	A14m, medial area 14
		43	44	A12/47o, orbital area 12/47
		45	46	A11l, lateral area 11
		47	48	A11m, medial area 11
		49	50	A13, area 13
		51	52	A12/47l, lateral area 12/47
	PrG, Precentral Gyrus	53	54	A4hf, area 4(head and face region)
		55	56	A6cdl, caudal dorsolateral area 6
		57	58	A4ul, area 4(upper limb region)
		59	60	A4t, area 4(trunk region)
		61	62	A4tl, area 4(tongue and larynx region)
		63	64	A6cvl, caudal ventrolateral area 6
	PCL, Paracentral Lobule	65	66	A1/2/3ll, area1/2/3 (lower limb region)
		67	68	A4ll, area 4, (lower limb region)
Temporal Lobe	STG, Superior Temporal Gyrus	69	70	A38m, medial area 38
		71	72	A41/42, area 41/42
		73	74	TE1.0 and TE1.2
		75	76	A22c, caudal area 22
		77	78	A38l, lateral area 38
		79	80	A22r, rostral area 22
	MTG, Middle Temporal Gyrus	81	82	A21c, caudal area 21
		83	84	A21r, rostral area 21
		85	86	A37dl, dorsolateral area37
		87	88	aSTS, anterior superior temporal sulcus
	ITG, Inferior Temporal Gyrus	89	90	A20iv, intermediate ventral area 20
		91	92	A37elv, extreme lateroventral area37
		93	94	A20r, rostral area 20
		95	96	A20il, intermediate lateral area 20
		97	98	A37vl, ventrolateral area 37
		99	100	A20cl, caudolateral of area 20
		101	102	A20cv, caudoventral of area 20
	FuG, Fusiform Gyrus	103	104	A20rv, rostroventral area 20
		105	106	A37mv, medioventral area37
		107	108	A37lv, lateroventral area37
	PhG, Parahippocampal Gyrus	109	110	A35/36r, rostral area 35/36
		111	112	A35/36c, caudal area 35/36
		113	114	TL, area TL (lateral PPHC, posterior parahippocampal gyrus)
		115	116	A28/34, area 28/34 (EC, entorhinal cortex)
		117	118	TI, area TI(temporal agranular insular cortex)
		119	120	TH, area TH (medial PPHC)
	pSTS, posterior Superior Temporal Sulcus	121	122	rpSTS, rostroposterior superior temporal sulcus
		123	124	cpSTS, caudoposterior superior temporal sulcus

Parietal Lobe	SPL, Superior Parietal Lobule	125	126	A7r, rostral area 7
		127	128	A7c, caudal area 7
		129	130	A5l, lateral area 5
		131	132	A7pc, postcentral area 7
		133	134	A7ip, intraparietal area 7(hIP3)
	IPL, Inferior Parietal Lobule	135	136	A39c, caudal area 39(PGp)
		137	138	A39rd, rostrodorsal area 39(Hip3)
		139	140	A40rd, rostrodorsal area 40(PFt)
		141	142	A40c, caudal area 40(PFm)
		143	144	A39rv, rostroventral area 39(PGa)
		145	146	A40rv, rostroventral area 40(PFop)
	Pcun, Precuneus	147	148	A7m, medial area 7(PEp)
		149	150	A5m, medial area 5(PEm)
		151	152	dmPOS, dorsomedial parietooccipital sulcus(PEr)
		153	154	A31, area 31 (Lc1)
	PoG, Postcentral Gyrus	155	156	A1/2/3ulhf, area 1/2/3(upper limb, head and face region)
		157	158	A1/2/3tonla, area 1/2/3(tongue and larynx region)
		159	160	A2, area 2
		161	162	A1/2/3tru, area1/2/3(trunk region)
Insular Lobe	INS, Insular Gyrus	163	164	G, hypergranular insula
		165	166	vIa, ventral agranular insula
		167	168	dIa, dorsal agranular insula
		169	170	vId/vIg, ventral dysgranular and granular insula
		171	172	dIg, dorsal granular insula
		173	174	dId, dorsal dysgranular insula
Limbic Lobe	CG, Cingulate Gyrus	175	176	A23d, dorsal area 23
		177	178	A24rv, rostroventral area 24
		179	180	A32p, pregenual area 32
		181	182	A23v, ventral area 23
		183	184	A24cd, caudodorsal area 24
		185	186	A23c, caudal area 23
		187	188	A32sg, subgenual area 32
Occipital Lobe	MVOcC, MedioVentral Occipital Cortex	189	190	cLinG, caudal lingual gyrus
		191	192	rCunG, rostral cuneus gyrus
		193	194	cCunG, caudal cuneus gyrus
		195	196	rLinG, rostral lingual gyrus
		197	198	vmPOS,ventromedial parietooccipital sulcus
	LOcC, lateral Occipital Cortex	199	200	mOccG, middle occipital gyrus
		201	202	V5/MT+, area V5/MT+
		203	204	OPC, occipital polar cortex
		205	206	iOccG, inferior occipital gyrus
		207	208	msOccG, medial superior occipital gyrus
		209	210	lsOccG, lateral superior occipital gyrus
Subcortical Nuclei	Amyg, Amygdala	211	212	mAmyg, medial amygdala
		213	214	lAmyg, lateral amygdala
	Hipp, Hippocampus	215	216	rHipp, rostral hippocampus
		217	218	cHipp, caudal hippocampus
	BG, Basal Ganglia	219	220	vCa, ventral caudate
		221	222	GP, globus pallidus
		223	224	NAC, nucleus accumbens
		225	226	vmPu, ventromedial putamen
		227	228	dCa, dorsal caudate
		229	230	dlPu, dorsolateral putamen
	Tha, Thalamus	231	232	mPFtha, medial pre-frontal thalamus
		233	234	mPMtha, pre-motor thalamus
		235	236	Stha, sensory thalamus
		237	238	rTtha, rostral temporal thalamus
		239	240	PPtha, posterior parietal thalamus
		241	242	Otha, occipital thalamus
		243	244	cTtha, caudal temporal thalamus
		245	246	lPFtha, lateral pre-frontal thalamus

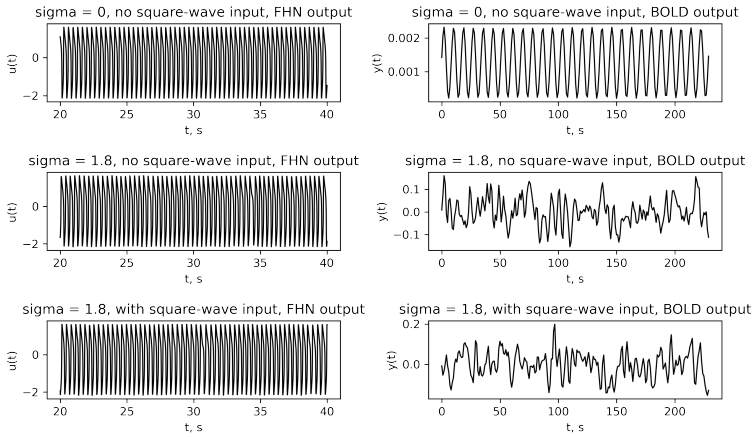

FIGURE S2. Chapter 6: Fitzhugh-Nagumo and Balloon models outputs
An example plot for the outputs of FHN and Balloon models for a region at the start of the sorted list of weighted connections [a] for the 3 cases; Top: $\sigma = 0$ and no square-wave input to any region. Middle: $\sigma = 1.8$ and no square-wave input to any region. Bottom: $\sigma = 1.8$ and square-wave input of $I_k(t) = -3(2\lfloor ft \rfloor) - \lfloor 2ft \rfloor))$ given to the 6 selected working memory regions.

[a] Region 115 from Brainnetome

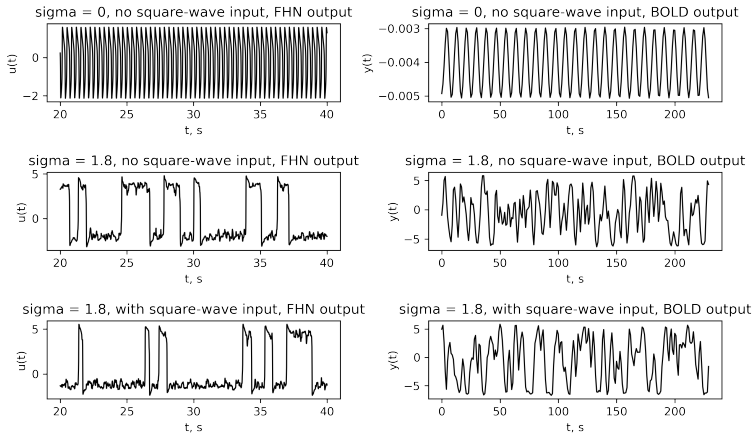

FIGURE S3. Chapter 6: Fitzhugh-Nagumo and Balloon models outputs
An example plot for the outputs of FHN and Balloon models for a region at the end of the sorted list of weighted connections [a] for the 3 cases; Top: $\sigma = 0$ and no square-wave input to any region. Middle: $\sigma = 1.8$ and no square-wave input to any region. Bottom: $\sigma = 1.8$ and square-wave input of $I_k(t) = -3(2\lfloor ft \rfloor) - \lfloor 2ft \rfloor))$ given to the 6 selected working memory regions.

[a] Region 230 from Brainnetome

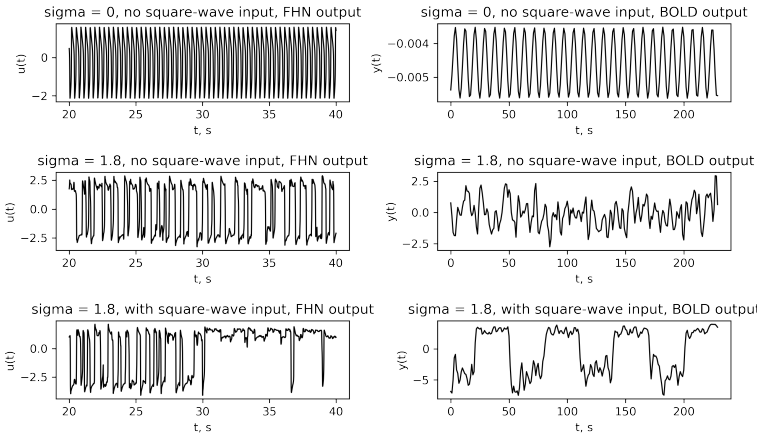

FIGURE S4. Chapter 6: Fitzhugh-Nagumo and Balloon models outputs
An example plot for the outputs of FHN and Balloon models for a region which is receiving the input I_k directly [a] for the 3 cases; Top: $\sigma = 0$ and no square-wave input to any region. Middle: $\sigma = 1.8$ and no square-wave input to any region. Bottom: $\sigma = 1.8$ and square-wave input of $I_k(t) = -3(2\lfloor ft \rfloor) - \lfloor 2ft \rfloor))$ given to the 6 selected working memory regions.

[a] Region 63 from Brainnetome

سخن از نیمه بُریدم که نگه کردم و دیدم

که به پایان رِسَدَم عمر و به پایان نرسانم

«سعدی»